UNIVERSIDADE D
COIMBRA

Guilherme Cruto Ala da Costa

DIGITALLY PRINTED STRETCHABLE SILVER-GALLIUM BATTERIES

Thesis submitted to the University of Coimbra in fulfilment of the requirements for the Master's Degree in Engineering Physics under the scientific supervision of Ph.D. Mahmoud Tavakoli.

October 2021

· U C ·
FCTUC FACULDADE DE CIÊNCIAS
E TECNOLOGIA
UNIVERSIDADE DE COIMBRA

Guilherme Cruto Ala da Costa

Digitally Printed Stretchable Silver-Gallium Battery

Thesis submitted to the University of Coimbra for the degree of Master in Engineering Physics

Supervisor:
Prof. Dr. Mahmoud Tavakoli

Coimbra, October 2021

This work was developed in collaboration with:

FACULDADE DE CIÊNCIAS E TECNOLOGIA
UNIVERSIDADE D COIMBRA

This work was founded by the Foundation of Science and Technology (FCT) of Portugal through the CMU-Portugal project WoW (Reference Nr: 45913), and Dermotronics (PTDC/EEIROB/31784/2017), financed by the EU structural and investment Funds (FEEI) through operational program of the center region.

Agradecimentos

Em primeiro lugar, gostaria de agradecer à minha família, especialmente à minha mãe e ao meu pai, por todo o apoio que me deram ao longo da minha vida. Estiveram lá comigo nos melhores momentos e, talvez ainda mais importante, nos momentos que estive mais em baixo. Formaram-me na pessoa que sou hoje e estou eternamente grato por isso.

Queria também agradecer ao professor Mahmoud Tavakoli pela orientação, apoio e por todos os ensinamentos, estando sempre disponível ao longo deste ano, além de todos os materiais disponibilizados.

Deixo também agradecimento ao Pedro Lopes, André Silva, Afasaneh LaSanati, Alexandre Chambel e a todos os restantes colegas de laboratório do Soft Printed Microelectronics pela ajuda que me deram ao longo deste ano. Todos foram uma parte indispensável deste projeto e para a sua realização da melhor forma possível.

De mencionar também os meus colegas (e irmãos) de curso José Adriano, João Tremoço, Luís Martins, Nuno Sousa, Xavier Pinheiro, Francisco Cidade e Rodrigo Simões, que fizeram do meu percurso por Coimbra, nas noites de estudo e boémia, uma aventura que levarei para a vida.

Também quero agradecer aos meus amigos João Cardoso, Maria Inês Costa, António Sanches, José Martinho, ao José Chichorro e à Mariana Chichorro que já há muito me aturam e que sempre me ajudaram e estiveram lá para mim.

Por fim, queria também deixar um agradecimento à Secção de Fado da Associação Académica de Coimbra, em particular, aos membros do Grupo de Fado Capas ao Luar, ao Espanhol, ao Pedro, ao Anão e ao Nholas, por me terem mostrado o que é verdadeiramente a vida de um estudante de Coimbra, e por me terem permitido fazer parte da história da academia.

A todos vós e a muitos que não mencionei individualmente, por falta de espaço na página,

Muito Obrigado!

"Levo amigos e memórias
O Fado que me embala
A Torre em sua glória
A Guitarra que se cala"

Balada de Despedida 2021 - Grupo de Fado Capas ao Luar

Resumo

O rápido progresso nos campos da Internet das Coisas (IoT), Internet das Coisas Médicas (IoMT), biomonitorização wearable, e tecidos electrónicos, leva a uma maior procura de baterias de película fina de próxima geração. É desejável que estas baterias sejam extensíveis, de modo a suportar uma quantidade adequada de ciclos de tensão quando integradas num e-têxtil adaptável ao corpo, e quando usadas pelos utilizadores. Além disso, ao desenvolver materiais e métodos que permitem o fabrico das baterias através da impressão digital, damos um passo em direção ao fabrico autónomo de baterias extensíveis que podem ser facilmente feitas à medida, consoante a aplicação desejada.

Nesta dissertação, introduzimos, pela primeira vez, uma bateria extensível de Gálio-Prata totalmente impressa digitalmente, que pode ser esticada mais de 130%. Foram testados dois métodos distintos de fabrico: impressão a stencil e extrusão digital. Os dispositivos impressos a stencil apresentam uma capacidade média de armazenamento de energia de 6.5 mAh/cm^2 enquanto os dispositivos impressos digitalmente exibem valores médios de 19.22 mAh/cm^2. Tanto o valor máximo de tensão como a capacidade de armazenamento por unidade de área são valores recordes no campo das baterias extensíveis.

Isto é concretizado através da impressão subsequente de quatro materiais: um Metal Liquido (LM) de Gálio Índio Eutético (EGaIn) e um composto à base de prata dentro de uma matriz elastomérica de Polystyrene – block – Polyisoprene – block – Polystyrene (SIS), EGaIn-Ag-SIS, como primeiro colector de corrente; um composto de Carbono (CB)-SIS como segunda camada colectora de corrente e protetora; um composto Ag_2O-SIS como cátodo; e uma nova camada Ga-CB-SIS como anodo. Todos os quatro materiais são optimizados para impressão digital, e não requerem qualquer sinterização térmica, ótica ou mecânica, tornando-os compatíveis com substratos sensíveis ao calor. Mostramos que a bateria Ag-Ga é uma excelente alternativa às baterias Ag-Zn, apresentando maior capacidade de armazenamento de energia e maior elasticidade.

Ao contrário das baterias impressas anteriormente, que utilizam deposição manual e impressão a stencil dos colectores actuais, esta bateria é impressa digitalmente na sua totalidade, permitindo a personalização da bateria relativamente ao tamanho desejado, e geometria para cada aplicação, sem a necessidade de recorrer à criação de stencils.

Também realizamos a caracterização das baterias através de múltiplos estudos de ciclagem electroquímica. Além disso, estudamos também o seu comportamento sob tensão mecânica. As nossas descobertas relacionadas com a microestrutura dos eléctrodos são apresentadas, através de microscopia e análise elementar via SEM

(Scanning Electron Microscopy) e EDS (Energy Dispersive X-Ray Spectroscopy).

Como exemplo de uma aplicação, mostramos baterias multi-células impressas digitalmente. Os vários componentes dos dispositivos, juntamente com os seus traços de interligação, são todos impressos digitalmente. Devido a este facto, tanto os traços como as baterias podem ser personalizados numa forma específica, a fim de fornecer a tensão e corrente de saída desejadas. Também fabricamos uma versão e-textile das baterias impressas, integramo-la numa cinta e-textile de monitorização wearable e demonstramos a sua aplicação para monitorização por Electrocardiograma (ECG). A bateria impressa na cinta mostra uma autonomia energética de 22 horas.

Palavras-Chave: Cinto vestível de tecido eletrónico para monitorização; Gálio-Carbono-SIS; EGaIn-Ag-SIS; Bateria impressa digitalmente; Bateria extensível.

Abstract

The rapid progress in the fields of Internet of Things (IoT), Internet of Medical Things (IoMT), wearable biomonitoring, and e-textiles, leads to the higher demand for the next generation of thin-film batteries. It is desired that these batteries are stretchable, in order to withstand an adequate amount of strain cycles when integrated into a body-conformable e-textile, and worn by the users. In addition, by developing materials and methods that allow fabrication of the batteries via digital printing, we move a step towards autonomous fabrication of stretchable batteries that can be easily tailor-made for each application.

In this dissertation, we introduce, for the first time, a fully digitally printed stretchable silver-gallium battery that can be strained over 130%. Two distinct fabrication methods were tested: stencil and digital extrusion printing. The stencil printed devices present an average energy storage capacity of 6.5 mAh/cm^2 whereas digitally printed devices exhibit 19.22 mAh/cm^2. Both the maximum strain value and the areal storage capacitance are record-breaking values in the field of stretchable batteries.

This is achieved through subsequent printing of four materials: an Eutectic Gallium Indium (EGaIn) Liquid Metal (LM) and silver based composite within a elastomeric matrix of Polystyrene – block – Polyisoprene – block – Polystyrene (SIS), EGaIn-Ag-SIS, as the first current collector; a Carbon Black(CB)-SIS composite as the second and protective current collector layer; an Ag_2O-SIS composite as the cathode electrode; and a novel Ga-CB-SIS layer as the anode electrode. All four materials are optimized for digitally printing, and do not require any thermal, optical, or mechanical sintering, making them compatible with heat sensitive substrates. We show that the Ag-Ga battery is an excellent alternative to Ag-Zn batteries, presenting higher energy storage and stretchability.

Unlike the previous printed batteries, that use manual deposition and stencil printing of the current collectors, this battery is digitally printed in its entirely, allowing customization of the battery regarding the desired size, and geometry for each application, without the need for creation of stencils.

We also perform the characterization of the batteries via multiple electrochemical cycling studies. In addition, we also study their behavior under mechanical strain. Moreover, our findings related with the microstructure of the electrodes are presented, through microscopy and elemental analysis via SEM (Scanning Electron Microscopy) and EDS (Energy Dispersive X-Ray Spectroscopy).

As an example of an application, we show digitally printed multi-cell batteries. The several components of the devices, along with its interconnecting traces, are all digitally printed. Due to this fact, both the traces and the batteries are able to

be customized into a specific shape in order to provide the desired output voltage and current. In addition, we fabricate an e-textile version of the printed batteries, integrate it in a wearable monitoring e-textile belt, and demonstrate its application for Electrocardiogram monitoring (ECG). The printed battery on the belt shows an energy autonomy of 22 hours.

Keywords: Wearable monitoring e-textile belt; Gallium-Carbon-SIS;EGaIn-Ag-SIS; Digitally Printed Battery; Stretchable Battery

List of Acronyms

ADC Analog to Digital Converter

CC Current Collector

CNTs Carbon NanoTubes

ECG Electrocardiogram

EGaIn Eutetic Indium Gallium

FHE Flexible Hybrid Electronics

IoT Internet of Things

ISR Instituto de Sistemas e Robótica

KOH Potassium Hydroxide

NPs NanoParticles

NWs NanoWires

PC polycarbonate

PCB Printed Circuit Board

PDMS Poly-dimethly Syloxane

PET Polyethylene terephthalate

PGSTAT Potentiostat/Galvanostat

PVA polyvinyl alcohol

SC Supercapacitor

SEM Scanning Electron Microscopy

SIS Polystyrene – block – Polyisoprene – block – Polystyrene

SOTA State of the Art

TPU Thermoplastic PolyUrethane

TTP Transfer Tatoo Papper

UV UltraViolet

List of Figures

List of Tables

Contents

Chapter 1

Introduction

In recent years, significant advances in Flexible Electronics have been made. New discoveries of materials, systems, fabrication methods and applications, have lured engineers and researchers into exploring this field. This led to an increase in the demand for Flexible Hybride Electronics (FHE). According to [1], an article from IDTechEx, this market is expected to reach a value of over 3 billion dollars in the year 2030.

Today, not only electrical interconnects can be printed, but also sensors, antennas, resistors, capacitors, batteries, Supercapacitors (SCs), and even transistors. The printing technologies of these several elements are in different levels of maturity. While some of them, such as Radio Frequency Identification (RFID), antennas and Near Field Communication (NFC) coils are already being printed at high scales (billion unit quantities) [2] [3], others, such as transistors, are still in the research and development phase.

Flexible and Hybrid Electronics have a wide range of applications. This includes printed touch panels in the home appliances, battery-free sensors, tags used in electronics keys, credit cards, security tags, and printed temperature, gas, and pressure sensors [4]. Usually, the properties of different materials are explored in order to develop several types of sensing elements. Examples include gas sensitive materials, such as graphene-based composites and metal oxides, or piezo electric-based sensors for sensing pressure. Therefore, the field of flexible electronics includes research and investigation into the physical and chemical properties of materials, and also engineering methods for their synthesis, deposition and application. A review on flexible electronics and its applications can be found in [5].

In addition, daily tracking of sport activities through fitness trackers is becoming a very accessible technology, even for non-professional athletes. The new commercial Fitbit Flex is a good example of wearable technology used nowadays for fitness tracking (see figure 1.1). It is able to monitor calories, steps, among other features.

High demands on smart packaging is another factor driving the growth of this market. Smart packaging helps easier object tracking, facilitates the management of the logistics and stock managements. In the food industry, it can help to track the temperature of the aliments from the time of packaging, until reaching to the client [6]. Printed sensors on smart packaging, can be used to determine signs of food devastation as well.

Printed sensors can also be applied to collect information from plant facilities, like pipelines and tanks, or from infrastructures like roads, bridges and tunnels. Yokogawa is a company that has been developing and applying this technology.

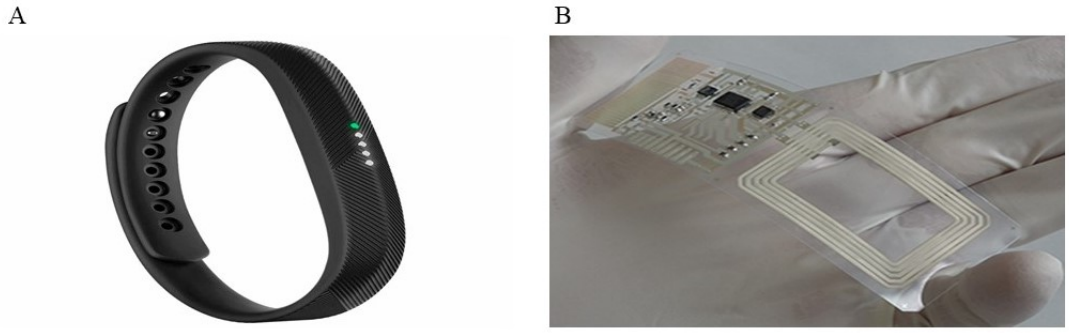

Figure 1.1: a) The Fitbit Flex; b) Printed Sensor by Yokogawa Electric Corporation

1.1 Wearable Biomonitoring and IoT

One field of interest for printed electronics has been wearable biomonitoring. This can come in the form of biomonitoring patches [7], wearable e-textiles [8], and "electronic tattoos" [9], that can interface the human skin, to obtain clinical grade data.

Unlike smart watches, which are mainly used for fitness tracking systems and can have certain tolerance to data errors, in the health sector the accuracy and reliability of data acquisition and transmission are very important. As such, there is a demand for more accurate solutions that reliably attach to the human skin for continuous acquisition of clinically relevant data. In this case, the electronic systems should not be only flexible, but also stretchable, in order to withstand the body movement, and the dynamic morphology of the human skin, without losing their functionality [10]. Wearable monitoring can reduce significantly staying time at the hospitals, thus reducing the hospital costs [7], while improving the clinical outcomes, due to better health tracking [11]. It is an important step toward domiciliary hospitalization [7], and digital health [12].

The Internet of Things (IoT) or, when referring to IoT applied directly to medical systems, IoMT, is gaining more attention regarding this field, as it can be used along with wearables to facilitate the communications with medical facilities and reduce the load in the health care system [13] [7]. Figure 1.2 presents a schematic of this application.

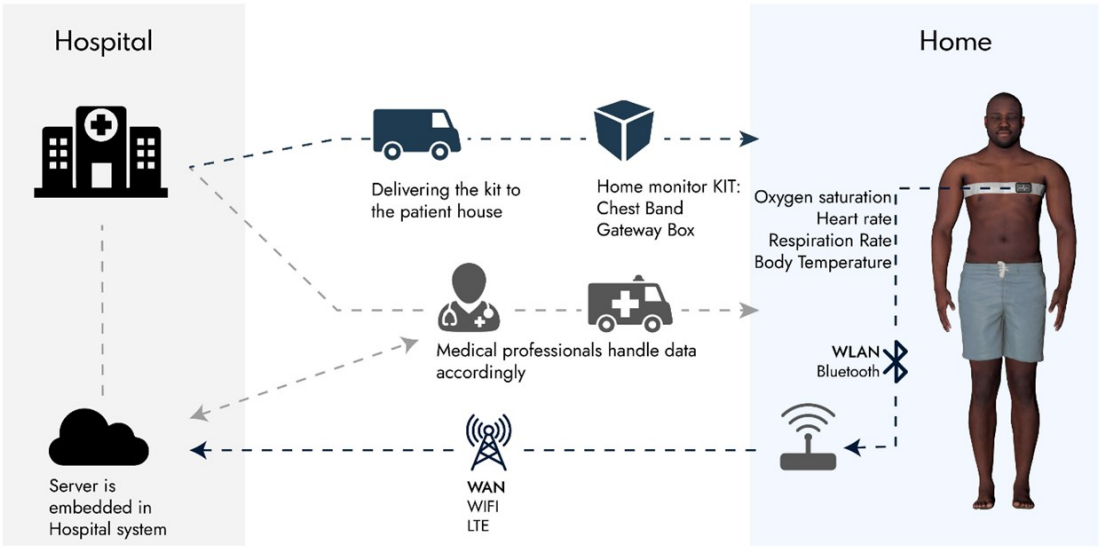

Figure 1.2: Schematics of an IoMT system with a biomonitoring layer, connecting the patient to the medical facilities [14]

The data acquired includes biological acquisitions as Electrocardiogram (ECG) [15], ElectroEncephalogram (EEG) [16], ElectroMyogram (EMG) [17] and Galvanic Skin Response (GVR) [18]. These require complex circuits and devices, in which further development of wearable technology proves to be useful. However, most of the previous implementation are tethered to an external power supply, or use a battery, which is the bulkiest rigid component of the patch.

Naturally, these devices are not only applied in medical scenarios. The Muse headband, for instance, is a wearable device that records EEG data. A recent article, [19], conducted a study on the applications of this tool, along with other recent commercially available wearable devices, on attention building.

As previously mentioned, wearables have the necessity of conforming them with the shape of the human skin, in order to be integrated in real-life situations. Our skin is a fantastic organ that protects the vital parts of our body, while possessing, at the same time, neural sensing capacities for detecting pressure, temperature changes and many others stimulus, exhibiting also stretchability. Therefore, conventional materials used for traditional rigid electronics, like tin or copper, represent sources

of limitations in terms of the end usages required from wearables. As such, to afford the dynamic morphology of the skin, new materials needed to be studied that could be used as replacement.

1.2 Stretchable Electronics

As the term suggests, stretchable electronics uses different materials, ultra-thin layers, bio-sensing electrodes, energy storage devices and chips integrated with interconnects to adapt to different forms and shapes, allowing the performance of movements as stretching and bending. The main types of materials used are the following:

- **Liquid Metals**, like Eutetic Indium Gallium (EGaIn), which are metals that are liquid at room temperature. These are normally used as interconnects due to their high conductivity and stretchable properties. They are usually mixed with silver to form printable inks [20]. EGaIn is commonly preferred to other metals, like mercury for example, due to its low toxicity;
- **Conductive composites**, like carbon, silver or gold, that are mixed with polymers to provide them with stretchability. These composites are normally used in the forms of NanoTubes or small particles. Polymers commonly used include Poly-dimethly Syloxane (PDMS) and Polystyrene – block – Polyisoprene – block – Polystyrene (SIS) [21].

In order to develop electronic circuits and stretchable devices, different fabrication methods are usually applied. Some of these include ink-jet printing [22]; stencil lithography [23]; contact printing [24]; laser patterning [25], spray and aerosol printing [26], and high-density soft matter electronics [27]. Recently, there has been an increasing interest in rapid fabrication of customized advanced electronics, IoT stickers, e-textile, and biomonitoring patches via digital printing. Digital printing eliminates the need for fabrication of stencils, and manual deposition, and permits autonomous fabrication of customized systems. This process demands for novel digitally printable materials for fabrication of complex soft, thin, and stretchable circuits with printed interconnects, sensors, and energy storage devices.

Other possible application for stretchable electronics, besides health monitoring and wearables, is related to electronic skin (e-skin). E-skin is a set of artificial electronic devices formed by different materials that, together, mimic the human skin in its sensing abilities, and in its capacity for stretching and bending, benefiting from stretchable sensing systems.

Many ends to e-skin include robotics [28], ambient parameters [29], health monitoring [30] and even, more recently, machine learning in soft robotics [31]. Figure 1.3 shows a circuit printed directly on the human skin that included printed temperature and humidity sensors, and oximeters.

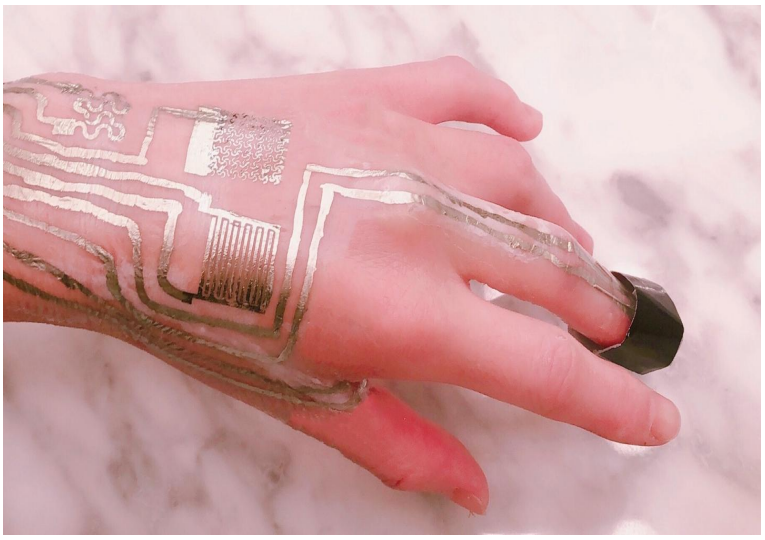

Figure 1.3: Circuit directly sintered on human skin at room temperature [9]

1.3 Printed Batteries: Motivations

Despite the advances accomplished so far, most of the previous implementation are tethered to an external power supply, or use a battery, which represents the bulkiest rigid component of the patch. This presents limitations in several scenarios, especially related with biomonitoring. A good example is a patient in a hospital or at home needing a patch in the chest with an Electrocardiogram (ECG). A rigid, larger battery presents a source of discomfort and motion limitation. Other possibility is to make these devices smaller, but, in most cases, this comes at the cost of reducing the battery's capacity. As such, further investigation on already known materials and discoveries of new materials for thin-film stretchable batteries are needed.

In recent years, research on printable batteries has been directed towards novel architectures [32], and materials for current collectors [33], electrodes [34] and electrolytes [35]. Several fabrication mechanisms, like screen and stencil printing [36], laser patterning [37] and spray coating [38], have also been the subject of numerous studies. As a result, flexible [39], stretchable [35], and thin-film [40] batteries have been developed and applied in practical cases as, for example, an epidermal patch [7].

A family of batteries being used more frequently in miniaturized devices, that includes hearing aids, smart watches and glucose monitors, is the silver oxide – zinc batteries (Ag_2O-Zn). This is mainly due to their high-power density [41], low self-discharge rate and low flammability when compared to lithium-ion batteries (LiBs) [42]. These types of batteries use an aqueous-based electrolyte.

In the past, an investigation project in Instituto de Sistemas e Robótica (ISR), conducted by Cristina Leal, assembled a disposable thin-film sticker with a printed Ag_2O-Zn battery over a thin tattoo paper (around 5 μm) [43], attaining a maximum capacity of 5.10 mAh/cm^2. [43]

Despite these promising results, the current technique for fabricating these batteries required many manual steps, and is still not autonomous, and scalable.

Stretchable energy storage devices are able to follow the motion of the body. They also do not present the size limitations that other rigid power sources do, as they are able to bend and stretch, according to the shape of the substrate. By improving this technology, eventually, every free space in wearables, biomonitoring patches or e-skin in robotics can be used for printing a battery. The enhanced areal dimensions, as a result, increases the capacity of the device and allows for a greater autonomy of the system.

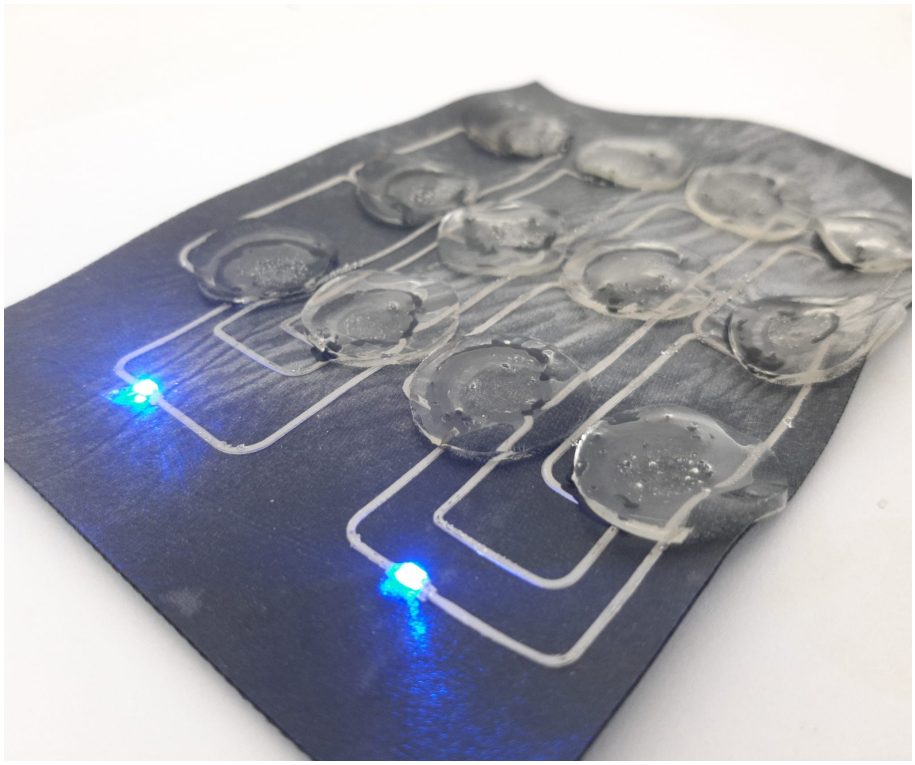

Figure 1.4: Digitally printed stretchable battery

1.4 Objectives

While rapid advances were made in the field of printed and stretchable batteries, including the previous work of [43], at the ISR, methods for fabrications of these batteries were all labor intensive, including many manual steps. Although, the word printing is used in many of these works' titles ([44] [45] [46]), in all cases printing refers to stencil or screen printing, all of which include manual fabrication of the battery's layers.

The main objective of this thesis was then set to explore the possibility of a fully digitally printed stretchable battery. At the time of this dissertation, we don't know any report of fully digitally printed stretchable batteries. This mechanism of assembling the device can provide an excellent set of advantages, including autonomous and scalable fabrication, and the possibility of rapidly tailor making the battery for each application. One can rapidly adjust the size, and shape of the device, based on the available space on the patch or the e-textile, or to print and connect several battery cells to each other with printed interconnects to adjust the output voltage and current, as it will be shown in this work.

In summary, the goal of this dissertation is to develop materials and methods for fully digitally printed stretchable batteries. As the current collector, this work counts on an existing digitally printable stretchable ink that was previously developed in ISR. However, novel digitally printable electrodes needed to be developed, especially regarding the anode. The previous method based on pouring Zn powder over the Current Collector (CC) (see chapter 4) is impractical for scalable fabrication. At the same time, developing a stable zinc composite revealed to be challenging. As such, one of the main objectives of this dissertation was addressing this problem, either by trying to modify the zinc-SIS composite, in order to make it printable, or to come up with an alternative solution. In addition, the CC layers were also optimized for digital printing, as previous works only revealed fabrication methods for stencil printing.

Finally, the printed batteries were characterized by the following parameters:

- **Electrochemical Characterization**: Including maximum areal capacity (mAh/cm^2), areal capacity when electrochemically cycled (rechargeability), and electrochemical performance under different currents.
- **Electromechanical Characterization**: Including maximum strain before failure, and electrochemical performance after strain cycles.
- **Electrochemical performance** when changing the **fabrication technique**

from stencil to digital printing.

By conducting the above-mentioned experiments, this work aims to contribute to the existing State of the Art (SOTA) by introducing a fully digitally printed stretchable battery for the first time and a novel digitally printable gallium-Carbon Black-SIS electrode, subjecting it to characterization.

Chapter 2

State of the Art

This chapter focuses on the SOTA of different energy solutions developed for stretchable and flexible electronics. This includes energy harvesting (RFs, antennas, photovoltaic cells...) and energy storage (SCs and batteries). Their respective working principles are presented, as well as recent technological advances and scientific discoveries displayed in different articles, with the main focus being on stretchable thin-film batteries. Also, in the beginning, an overall review on the materials used for printable inks, substrates and applications in wearable technology and e-textile is presented.

2.1 Recent advances and challenges in biomonitoring

The next generation of soft, stretchable, and thin-film electronics is expected to have a transformation impact in various fields of applications, including electrophysiological data acquisition [47], e-skins for robotics applications [48], e-textiles [8], flexible displays [49], and 3D-transferable electronics [20].

All of this is related to the increased demand in domiciliary hospitalization and constant health monitoring. This is mainly due to several factors, including the increasing average age of the world's population [50] and the rising number of chronically diseases [51].

The rapid advance of IoT has led to the increasing interest in its application towards medical purposes (IoMT). Still, only 7% of the IoT systems are used for medical ends [52] and it is often related to wearable bioelectronics. This includes studies on data processing and the materials used, along with fabrication techniques that allow for conformable and comfortable wearable monitoring [53].

A recent example of developed wearable technology is presented in [54]. This article reports the fabrication of comfortable and affordable e-textile headband used for electroencephalogram (EEG) acquisition. All the electrodes were already integrated in the band, removing the necessity of wiring or electrode placing. The acquired data would be transmitted to the mobile phone a PC.

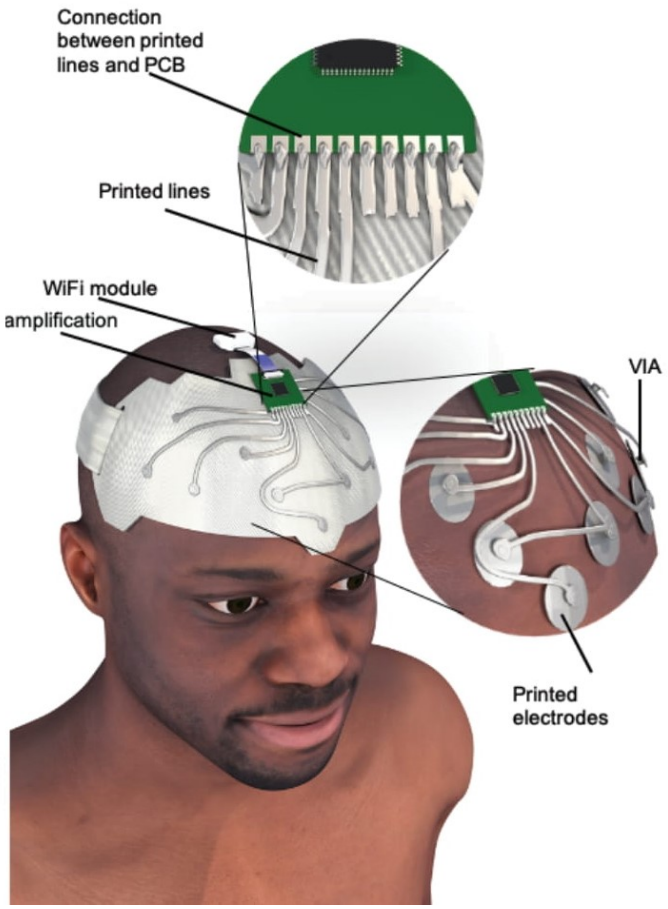

Figure 2.1: Schematic of the wearable presented in [54] with e-textile headband used for EEG acquisition.

Stretchable electronics is used to provide wearables the ability to adapt do different shapes, related with the movements of the human body. This implies using materials that include conductive composites with percolating filler particles that are integrated in soft polymer matrices [55].

Also, different architectures, including micro and nanoparticles, conductive flakes [56] and NanoTubes, embed with silicon- based elastomers [57], are under research.

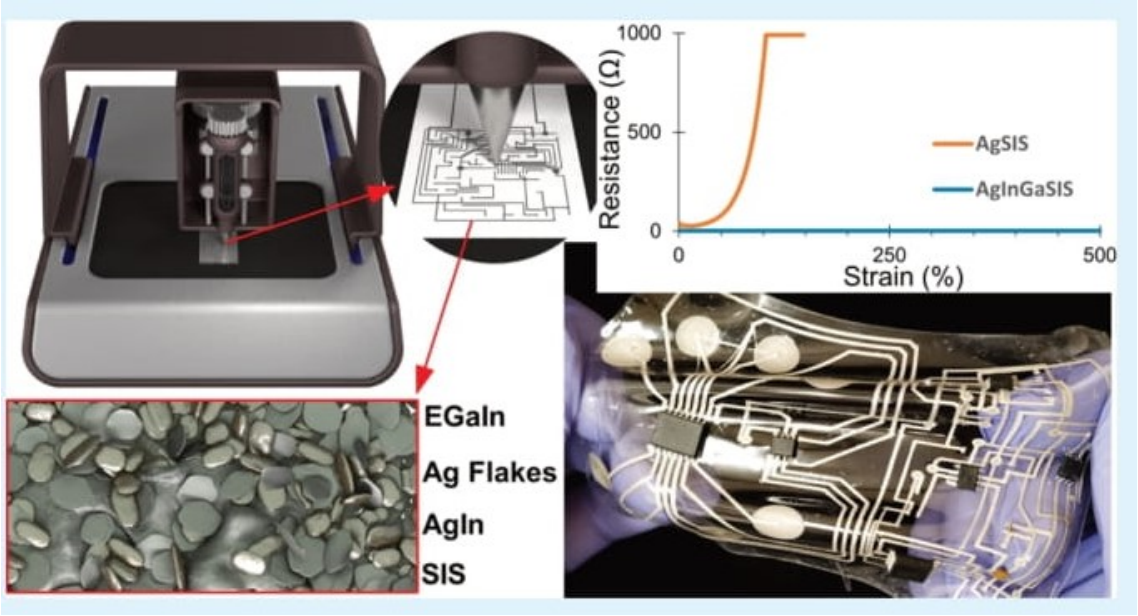

Figure 2.2: Image taken from [55], showing a schematic for digitally printable Bi-Phasic, Ag-In-Ga-Embedded elastomer inks to be applied in stretchable electronics

The materials being used and explored as biocompatible elastomers can also be applied as substrates. PDMS is a good example of a widely used elastomer. It has an elastic modulus of 1-3 MPa and it possesses a stretchability of 160%. Other attractive properties include transparency, hydrophobia, chemical inertia, biocompatibility and also conforming with most surfaces [58]. Other choices for thin and transparent substrates are polycarbonate (PC), polyamide and Polyethylene terephthalate (PET).

Active materials mostly used include semiconductors, NanoWires (NWs) and NanoParticles (NPs), metals (like platinum, copper, zinc, silver) and Carbon NanoTubes (CNTs). A material being explored since before 2010 is graphene, a semiconductor with a zero bandgap. Graphene exhibits exceptional properties that include chemical stability and great thermal and electrical conductivity (250 000 cm^2 V^{-1} s^{-1}) [59]. Other features include its mechanical properties (1TPa Young modulus), high surface area (3000 m^2g^{-1}) and high optical transparency [60], absorbing very little visible light. One can easily comprehend the appealing factor of studying this carbon-based material.

Despite recent advances, one of the main challenge is related to creating an energy autonomy solution for wearable biomonitoring. Usually, to cope with the size demands, miniature coin-sized batteries are the most common approach taken. Still, in order to achieve the ultimate goal of conformal patches for biomnitoring in applications that require long-term usage, there is still the need of resourcing

to rigid and bulky batteries. Chapter 1 has already specified the disavantages of using such solutions regarding applications related to domiciliary hospitalization, biomonitoring patches and wearables. As such, to remove this limitation, research on the field of thin-film stretchable batteries have been developed.

2.2 Energy Harvesting and Energy Storage

When referring to energy supply for e-skin, biomonitoring patches and wearables, one needs to address the two main categories: energy harvesting and energy storage. Working towards flexible and stretchable energy-autonomous solutions, involving these two categories, has been the goal of many scientific studies.

Energy harvesting is a process, or a set of processes, that generates current from an external source. A few cases include solar harvesting (through photovoltaic cells), piezoelectrics, triboelectric, electromagnetic harvesting through near-field coils and far-field antennas, thermoelectrics and biofuel cells.

Energy is gathered in energy storage systems in a certain state (chemical energy, for example) and, when a load is applied to the terminals, it is released as electricity. The main types of energy storage devices are batteries and SCs.

Already there are stretchable energy harvesting and energy storage systems. The main goal is to reach power and energy density values comparable to rigid formats or, at least, sufficient to power flexible and stretchable devices. Figure 2.3 compares the areal power density of thin-film and printed solutions for energy harvesting, and energy storage, based on a recent study [14]. As a reference, the article included coin-cell batteries as well.

As it can be seen, from figure 2.3, according to this source, when comparing energy storage solutions, coin-cell batteries are able to reach around 50 mWh/cm^2. The graphic also demonstrates the potential of thin-film batteries to reach power density in the magnitude of 10 mW/cm^2 , whereas SCs could only present around 1 mWh/cm^2. Also, the energy density in batteries is higher then in SCs.

This shows clearly that the thin-film printed batteries, while still being in their infancy, have a very interesting potential to address the problem of energy supply for IoT systems.

2.2.1 Energy Harvesting

Energy harvesting converts different forms of energy (thermal, solar ...) into electrical current. This mechanism is based on materials that can work as transductors of body motion into electrical energy. This means that they can be used as

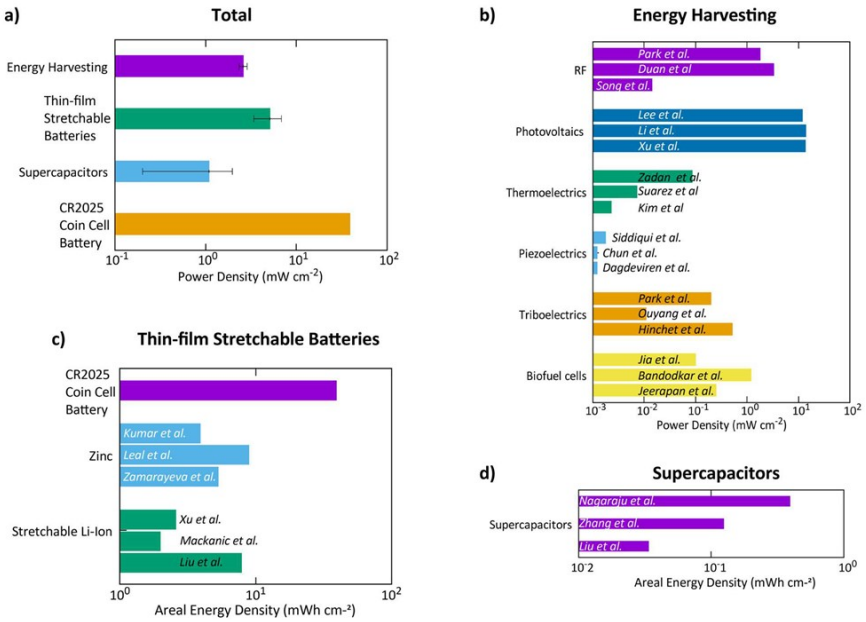

Figure 2.3: a) Comparison of the areal power density of different energy harvesting and energy storage forms; b) Comparison of the areal power density of different energy harvesting systems; c) Comparison of different thin-film stretchable batteries in terms of areal energy density and the comparison with a rigid Coin Cell-type Battery; d) Comparison of the a [14]

stand-alone energy devices. However, they present low power density values, in the range of the $\mu W/cm^2$ (see figure 2.3). Triboelectrics are presenting higher values in this department and have also been applied in e-skin recently [61].

Thermoelectrics convert temperature gradients into electrical energy. This mechanism is relatively simple and it is also showing significant advances. In [62] a thermoelectric generator, composed of liquid metal embedded elastomer (LMEE) composites with up to 100 integrated semiconductor structures, was able to achieve a power density of $86.6\,\mu W/cm^2$ using a temperature gradient of $\Delta 60$ °C. The main disadvantage of thermoelectrics is their low power density when compared to other energy harvesting methods (see figure 2.3). Biofuel cells are also the subject of numerous studies. Some mechanisms are even based on the usage of human sweat. In [63], a set that included an integrated electrode system was built to achieve a power density of $1.2\,mW/cm^2$. This was enough to power a Bluetooth communication module.

The other two energy harvesting mechanisms are RFs and Photovoltaic cells. RFs use radio waves as a source of electrical power. They are made of a transmitter, a harvesting device composed of antennas, and a rectifying circuit. In [64], using a 3 layered Printed Circuit Board (PCB), with metamaterial particles, a metallic ground

and a rectifying circuit, an RF device was capable of obtaining 66,9% of energy conversion efficiency, at 2.45 GHz, reaching a power density of 5 mW/cm^2. Photovoltaics, on the other hand, convert photons into electrons through electrochemical, photothermal and photovoltaic mechanisms. They are exhibiting the higher values of power density. However, their low efficiency and dependence on solar light present limitations when trying to implement them. Applications in this field include moving parts of robotics, machines, textiles, displays and health care [65]. A recent article covered a new solar cells technique for solar applications using Perovskite Solar Cells (PSCs) applied in stretchable substrates. The final result obtained a performance efficiency of 19.15%, a value already comparable to rigid counterparts [66].

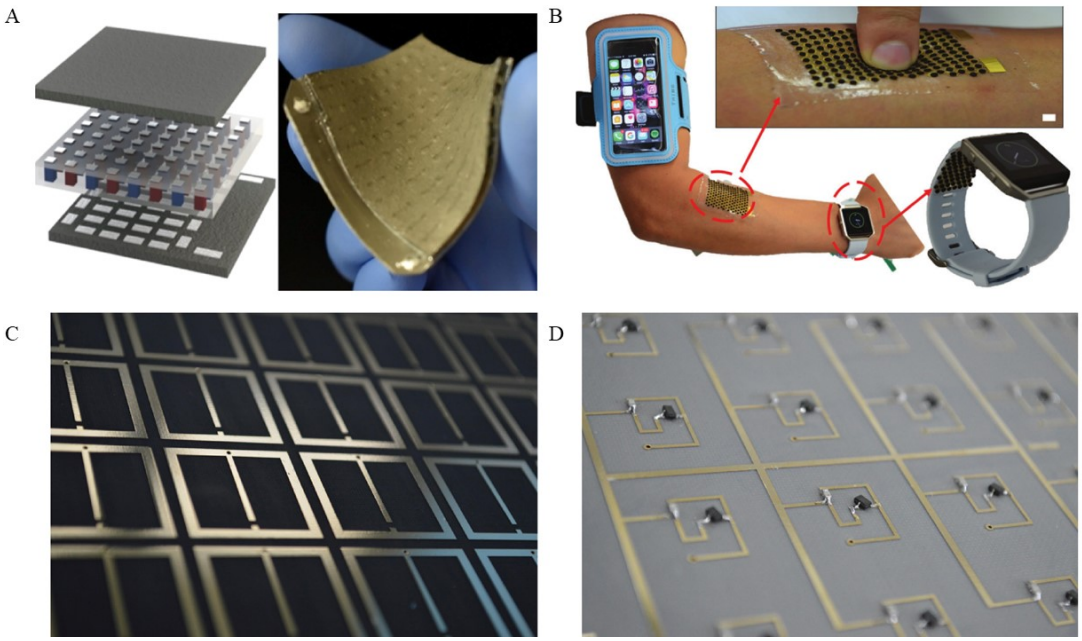

Figure 2.4: Some examples of energy harvesting devices: a) Thermoelectric constructed in [62] ; b) Energy Harvesting based on human sweat [63];c and d) RF system using a 3 layered PCB [64]

2.2.2 Energy Storage

As the name suggests, the principle behind energy storage is the accumulation of charges between two electrodes. Capacitors are an example of this. They are devices consisting of 2 conductive plates with a dielectric medium in between. When voltage between the two terminals is applied, accumulation of charges occurs in the electrodes. The positive charges are accumulated in the cathode and the anode accumulates negative charges. This creates an electrostatic field between the plates, holding the charges in their respective electrodes. When the DC voltage is removed,

the charges are stored in the capacitor. By applying a load in the terminal, current flows through the circuit, discharging the capacitor. The dielectric medium, since it is composed of bipolar molecules that repel the respective charges, affects the capacity of this device.

The principle behind supercapacitors is the same, despite these last ones dealing with ionic charge motion through an electrolyte. The electrons, generated through fast reduction-oxidation reactions (redox), taking place in the electrodes [67], flow through the CCs. The potential, similar to a battery, is ionic potential, which is related to the capability of the active materials giving (or receiving) ions (and electrons).

The capacitance of a capacitor (and of a supercapacitor) is related to the potential applied between the electrodes and the charges accumulated:

$$C[F] = \frac{U[V]}{Q[C]} \tag{2.1}$$

We can also relate the current and the voltage variation with the capacitance:

$$i = C \cdot \frac{dv}{dt} \tag{2.2}$$

The main reason behind the advances being made in flexible and stretchable supercapacitors is the improvement in the knowledge of nanomaterials, graphene,CNTs and fabrication mechanisms that allow more scalability in the design and construction of new SCs [68]. Graphene, in particular, has attracted scientists to explore its properties as an active material for the electrodes and it has been showing promising results [69]. Other types of structures used in electrodes include graphite, metal oxides, quantum dots, CNTs and composite materials.

A recent article, [70], reported a fabrication method of a Hybrid Supercapacitor, with a capacitance of 1.147 F/cm^2 at a current density of 3 mA/cm^2 with power density of 2.353 mW/cm^2 (exhibiting an energy density of 0.392 mWh/cm^2). This SC used a polyester white shirt as a non-conductive substrate and the active material consisted of Coaxial NC LDH NFAs@NSs as the positive electrode and activated carbon as the negative electrode.

The possibilities in wearables and e-skin are plenty for SCs. However, they still present some fabrication challenges. Also, the discharge is a very fast process in these devices, which makes them non-suitable for uses that require higher and stable capacity for long periods of time. They also present lower areal energy density values, when compared to batteries.

Batteries are electrochemical storage devices based on reduction-oxidation reac-

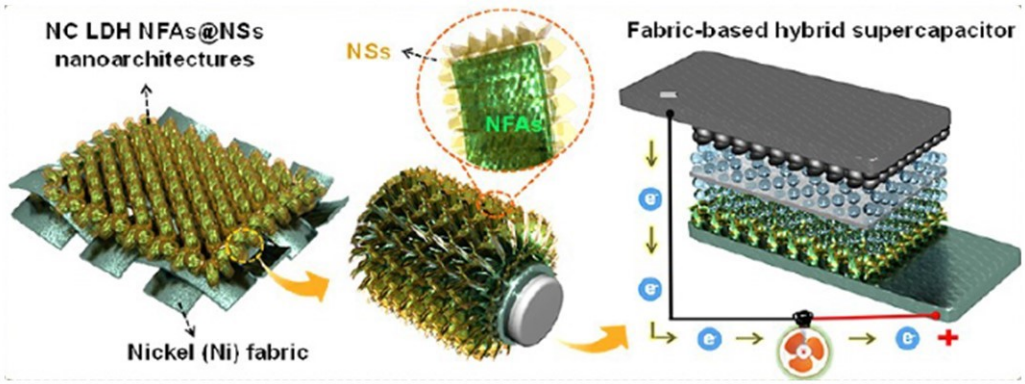

Figure 2.5: Hybrid supercapacitor built on [70]

tions between two metals. The voltage of the battery depends on the active material. The most known battery family is the Lithium-Ion Batteries. These rechargeable batteries use, as the name suggests, lithium ions that go back and forth in the electrolyte between the electrodes [71]. A battery has chemical energy stored inside that, when the redox reactions occur, it is converted into electricity. These reactions happen between the two metals, in which one "gives" the electrons (the anode) and the other "receives" them (the cathode). In the case of rechargeable batteries, or secondary batteries, the reactions are reversible. Therefore, when current is applied on the contrary direction, the opposite reaction takes place, which increases the potential of the battery.

The property of a battery that describes its ability to store energy is its capacity. The capacity of a battery is a reflection of the time it takes to discharge (or charge) when subjected to a current I:

$$C[Ah] = I[A]\Delta t[h] \tag{2.3}$$

The energy stored in the battery is given in Wh, which is the power the battery can supply during a certain time interval.

$$P[Wh] = C[Ah]V[V] \tag{2.4}$$

Besides the already mentioned LiBs, other common types of batteries include the silver-zinc (Ag-Zn) and silver oxide-zinc batteries (AgO-Zn), manganese dioxide-zinc batteries (Zn-MnO2), nickel-zinc batteries and zinc-air batteries. A review article, [72], presented recent advances and challenges in zinc-based batteries. In

recent years, in addition to these more traditional families of batteries, gallium and Liquid Metals have been explored as active materials in gallium-based electrodes [73].

2.2.3 Stretchable Batteries

The emergence of wearables has allowed a growth in the interest of stretchable energy storage devices (see chapter 1), more especifically, the study of new materials that can be applied, different architectures [74] [75], printing techniques [76] [43] and electrolytes (hydrogels being more commonly used to interface with the electrodes [77]). Low power electronics is also emerging. This allows the existence of practical applications for these novel stretchable batteries that are appearing. As we can see in figure 2.3, stretchable batteries are not only the solution with the highest power density, but are also reaching values comparable to their rigid commercial formats. However, more efforts need to be spent in order to make these batteries viable in commercial devices, since coin cells are still the more desirable approach.

Still, a rigid power source presents limitations for a stretchable device. It can lead to failure when the system is put in motion due to mechanical deformations. Those are reasons why stretchable batteries are becoming more and more appealing, as the stretchable electronic market grows. A recent work conducted, [33], presented a fully stretchable water-proof device platform. In this report, a Lithium-ion battery of 1.23 V was developed with a capacity of 9 mAh/g at 100% strain. This battery had a 89.5% capacity retention at 2000 cycles, which was the highest value compared to previous works on LiBs. Nozzle printing was used for the fabrication of the stretchable circuit. The current collector consisted of Ag flakes and Au nanosheets composite and SIS polymer as an elastomer. The anode and cathode were spray-coated on the deposited CCs. EGaIn was the material selected to print the interconnects. Ag/SIS flakes were placed on the top, in order to prevent conductive passivation and the leakage of the Liquid Metal into the surface. The electrodes of the battery, in order to guarantee high mechanical stability under stress and high electrical performance, were exposed to the surface via holes. A pressured sensitive switch was added to this circuit to save energy and control the turning ON and OFF states of the LED. The switch was an insulator in idle state. However, when a small pressure was added (for example, by the touch of a fingertip), the same switch became a conductor turning the LED on.

Although some layers of the CCs were digitally printed, this battery still required other manual processes, such as dipping, and drying the CCs into a Au nano sheet solution. Also, spray coating, which requires preparation and application of stencils.

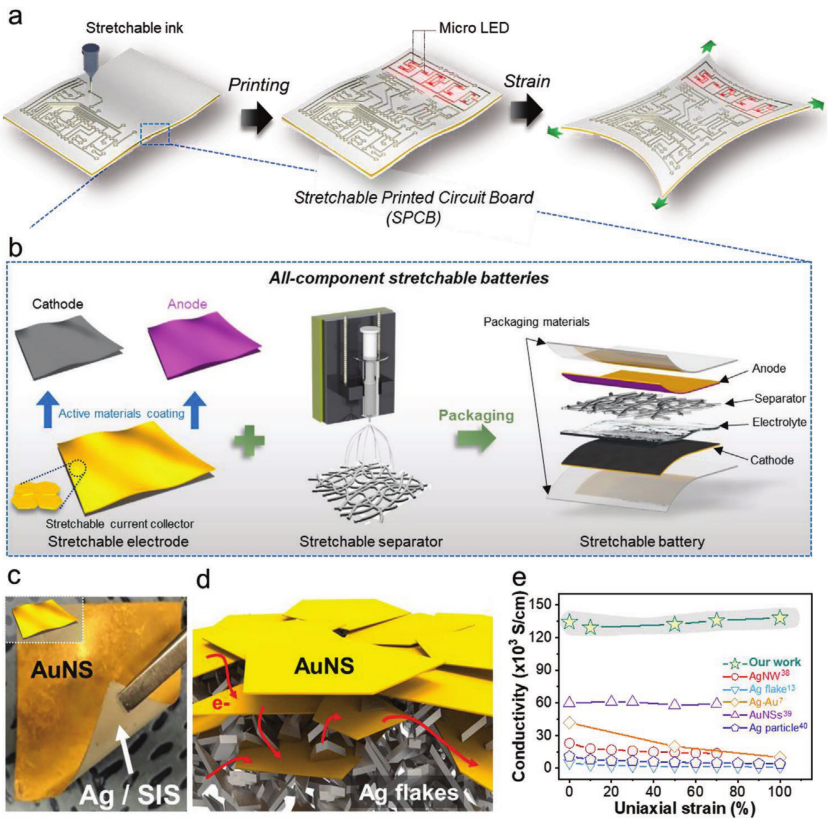

Figure 2.6: a) Nozzle printing the electronic circuit; b) Components of the stretchable battery: The stretchable current collector with the spray-coated active materials on top and the separating membrane; c)Digital schematic of the Current Collector consisted of a gold nanosheet; d) Electron's percolation pathway through the bilayered current collector; e) Conductivity comparison as a function of the strain applied in different electrodes and the current collector. All images were taken from [33]

2.2.4 Silver-Zinc Batteries

This work started by studying silver-zinc batteries and their respective applications on electronic skin and wearables. Already a project made in ISR by Cristina Leal approached these types of batteries [43]. Therefore, research on the State of the Art of this family of batteries was important. In fact, Ag-Zn batteries has been the subject of many research works, mainly due to the following characteristics:

- The low-cost and safety of metallic zinc [72];
- Low flammability compared to LiBs [78];
- Higher theoretical energy density compared to LiBs [79];
- Stable discharging process and high voltage accuracy [72];
- Recyclability, making these batteries environmentally friendly [80];

- Easy and simple fabrication methods, for example, screen printing [81].

The cathode and anode correspond, respectively, to the silver electrode and the zinc electrode. The discharge process consists on the conversion of Ag_2O into metallic silver and zinc into zinc oxide. They have 2 plateau voltages corresponding to the formation of Ag_2O from AgO (at 1.8 V) and Ag from Ag_2O (at 1.5 V). The reactions occurring in the electrodes are reversible, making the batteries rechargeable. The ions travel through an alkaline electrolyte and the electrons are gathered by a current collector providing current flow in the circuit. Since the electrolyte is such an important part of the battery system, studies to compare different Potassium Hydroxide (KOH) concentrations in water-based solutions have been developed. Normally these are very strong alkaline solutions, as their concentration vary between 6 M to 10 M concentrations.

Already articles on the latest results on silver–zinc batteries are reporting promising capacity values, fabrication techniques, life cycles and capacity retention under strain forces. In [35], the development a flexible low-cost battery is described. This battery maintained stability for around 170 cycles and showed capacity retention above 98%. The capacity values obtained were between 1.2 mAh and 1.8 mAh. The most interesting part of this system wasn't the capacity of the battery itself, but its wire-shape geometry, which increased the range of possibilities in terms of applications and studies of different architectures. The authors of the article [32], developed a new mechanical structure of a silver-zinc battery with helical springs and serpentine designs, for mechanical support (see figure 2.7). The results were noteworthy, as this battery showed a capacity of 1.7 mAh, retaining this value over 17000 bending cycles of 0.5 cm. Another article exhibited higher values of capacity, 2.5 mAh at a 3 mA/cm^2 discharging current density, while testing the properties of a hyperplastic binder called SIS [81].

The battery developed by Cristina Leal [43] used EGaIn-Ag-SIS as a first CC, a second CC of Carbon Black and SIS and the two electrodes. Using hydro transferring techniques, the battery was placed in a PDMS substrate, in order to integrate it into a biomonitoring patch. All the layers were deposited via stencil printing, except for the anode. They integrated the battery in a heart monitoring patch, which was interfaced with a battery-free electronic circuit whose purpose was to acquire the signal and perform wireless transmission of data. The capacity values increased from 5.59 mAh/cm^2 to 6.88 mAh/c^2 after stretching, which, according to the hypothesis of the authors, was due to the increase in the exposed active area.

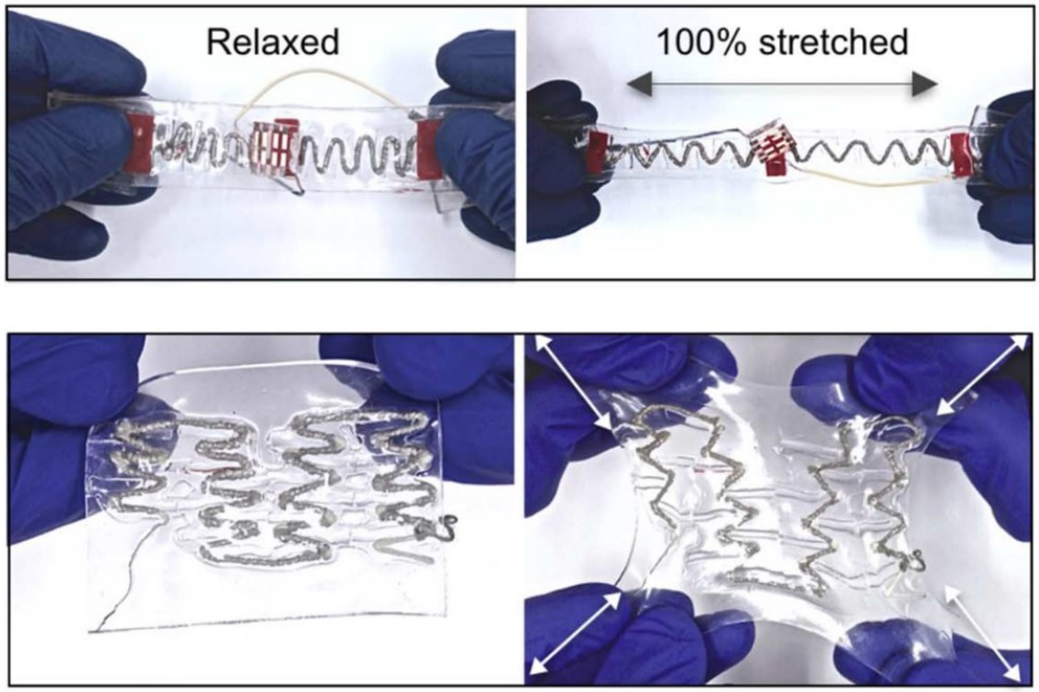

Figure 2.7: Battery developed in [32] with helical springs and serpentine designs. The battery was able to withstand different stretching motions.

Although significant progress has been made on Ag-Zn batteries during the last couple of years, fabrication methods for stretchable batteries are not yet automatic or digital. With the advances of IoT, IoMt systems, and personalized healthcare, it is desired to have solutions that can be easily custom-made and printed using autonomous machines, and without the need for preparation of stencils, or screens. A method of creating conductive digitally printable inks with the right properties is still to be demonstrated. Using the previous example, despite the good results demonstrated in [43], the method to expose the zinc electrode was limited to a manual method, by pouring the particles by hand on top of the second current collector (see chapter 4). This reveals limitations in terms of scalability and fabrication.

Zinc-based batteries still present several other drawbacks. The zinc electrode, when in contact with an alkaline electrolyte, forms dendrites of $Zn(OH)_4$ [72], which disturbs the electrochemical performances of Zn-Ag batteries. These dendrites can also form structures that pass through the separators and lead to an earlier short-circuit, damaging the battery. This results in the death of the device. Zinc oxide accumulation is another problem because it reduces the surface area of the electrode, decreasing its conductivity. Sometimes, in order to address the situation of the dendrite formation, mercury was added to the zinc electrode. However, mer-

cury is highly toxic and, environmentally speaking, it presents several problems as well. To replace mercury, other metals like bismuth, indium or gallium were suggested [82]. Flexible separators also represent an interesting field of research to solve the short-circuit situation generated by the dendrites [83], while maintaining the desired mechanical properties.

A recent study on a Ag-Zn battery showed a very high areal capacity of 12.5mAh/cm^2, albeit the developed battery was not stretchable [84].

Nevertheless, new materials and combinations can have advantages and interesting properties that can prove to be useful. One of these includes the metal gallium.

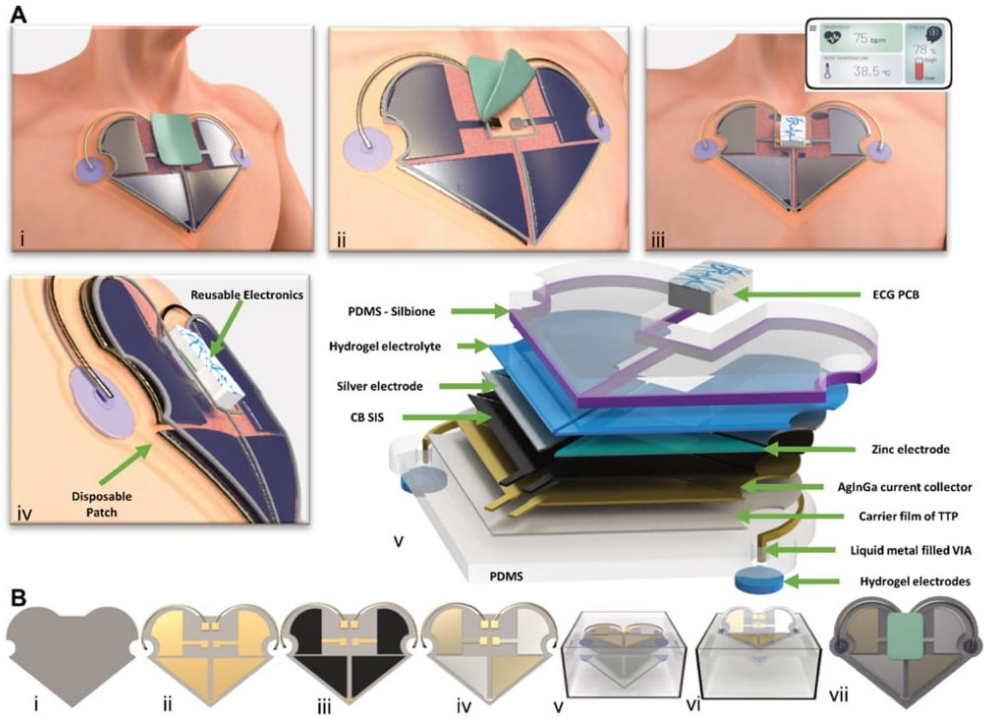

Figure 2.8: a) Application of the Ag-Zn battery integrated in a disposable patch: i) illustration of the disposable biomonitoring patch; ii) protection film layer being removed; iii) schematic of the interface of ECG-PCB board with the patch for data acquisition and wireless transmission to a smartphone; iv) side view of the fabricated patch v) compositions of the different layers of the fabricated patch; b) Different steps for fabricating the battery: i) Transfer Tattoo Paper Substrate; ii) printing the 1^{st} CC and the interconnects; iii) deposition of the 2^{nd} CC; iv) placement of the electrodes; v) hydro-transferring process; vi) battery transferred to a PDMS substrate; vii) application of the electrolyte and PDMS encapsulation layer.

2.2.5 Gallium-based batteries

Gallium is a material that reveals interesting properties that can be used in batteries consisting of gallium-based anodes. These batteries present high ionic motion due

to the low melting point of gallium of 29°C [73]. During charge and discharge, the electrodes suffer volume changes caused by the charges' motion. Gallium and gallium alloys (as EGaIn), allow a self-healing mechanism, resulting in higher cycles stability in some cases. The usage of gallium based cells in LiBs has been explored. In the article [85], the authors took advantage of the self-healing properties of this material to enhance the life cycles of the battery. The results proved to be successful as the device lasted for 4000 cycles without showing any obvious decay in capacity. They also described this material as having good theoretical capacity. Another similar article reported "remarkable cycle durability" and pointed out the enhanced capacity of the lithium-ions when in contact with gallium and indium [86].

Despite the positive impact that gallium brings when applied in different battery families, like zinc, this material also presents low flammability and high theoretical capacity. As such, based on the theoretical proposal of a patent from 1993 ([87]), other works have been exploring gallium-based anodes. Some of them still use indium as protection against corrosion [88] [89].

Different architectures and fabrication mechanisms have also been developed. In [90], a stretchable wire-type EGaIn-air battery was fabricated. The battery was highly elastic, stretching up to 100% and recovering without significant damage. However, the battery's capacity was still low, compared to others (around 3 mAh/cm^2). A PAA-based aquose gel-type electrolyte placed in a 37% KOH alkaline solution was used. By wrapping a carbon fiber around the electrolyte and injecting the liquid metal inside (as we can see in figure 2.8) the wire shape was formed. A more recent article reported the fabrication of a gallium-based battery using MnO_2 as cathode [89]. They reached capacity values of 3.8 mAh/cm^2 and showed a possible application, by inserting it in a strain sensor.

At the end of this chapter, a summary table of the SOTA for stretchable batteries is presented, with the main features including type, capacity at first discharge and maximum strain reported (see table 2.1).

2.2.6 Reduction-Oxidation reactions occurring in the electrodes

The positive electrode chose for this project was silver oxide, in order to compare the results with the ones presented in [43].

The discharging process of the battery consists in the reduction of the cathode and oxidation of the anode. The silver electrode has two discharging (and charging steps). They are the following:

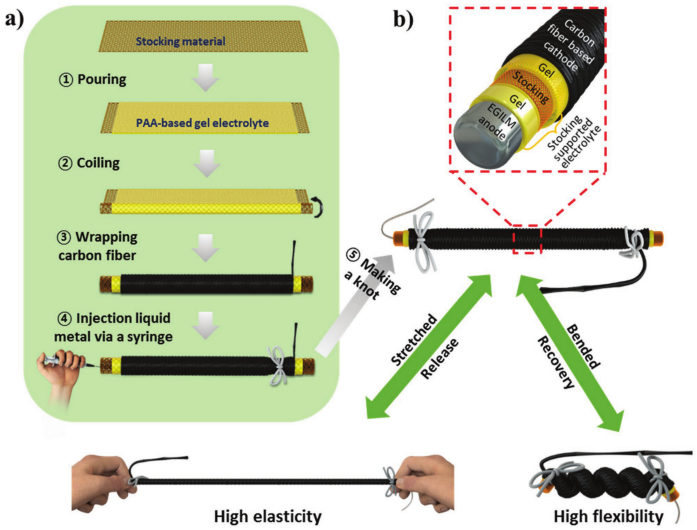

Figure 2.9: Sketch for the cable-shaped eutectic gallium–indium liquid metal-air battery. a) The simple and manoeuvrable preparation process; b) The internal structure, high flexibility, and high stretchability of this cable-shaped liquid metal-air battery [90]

$$2\,AgO + H_2O + 2\,e^- \longrightarrow Ag_2O + 2\,OH^- \tag{2.5}$$

$$Ag_2O + H_2O + 2\,e^- \longrightarrow Ag + 2\,OH^- \tag{2.6}$$

The last equation corresponds to the first discharge in the batteries fabricated in this project (see chapters 3 and 4), as the batteries constructed are Ag_2O-Ga batteries.

For the anode, according to [87] and [89] the reaction is the following:

$$Ga - 3\,e^- + 6\,OH^- \longrightarrow {GaO_3}^{3-} + 3\,H_2O \tag{2.7}$$

This leads to an overall reaction (see full calculation in appendix I):

$$3\,Ag_2O + 2\,Ga + 6\,OH^- \longrightarrow 5\,Ag + 2\,{GaO_3}^{3-} + 3\,H_2O \tag{2.8}$$

The initial open circuit potential of the battery, theoretically, is of 1.75 V. Despite no literature, as far as my knowledge at this moment, presenting a silver oxide-gallium battery, using the Nernest's equation, it was possible to perform the calculations to arrive at this value (see appendix II).

2.2.7 Current challenges

Despite the significant advances mentioned, there are still challenges that flexible and stretchable batteries need to overcome. The nature of these challenges is related to obtaining higher capacity values, stable discharges voltages and, naturally, reaching scalable fabrication methods.

Regarding the silver oxide electrode, the main obstacles to overcome consist mostly in delaying the corrosion mechanism. Silver dissolves in alkaline electrolytes during the charging cycles [72]. $Ag(OH)^{2-}$ is formed, leading to the deterioration of separators and the corrosion of the electrode itself. Techniques that include surface coating this electrode with metals like copper, indium or gold can improve its stability [72].

Reaching higher stability in the life cycle and discharge plateaus of gallium using additives such as Ca^{2+} is also highlighted in [89]. Several gallium alloys and new mechanisms of fabrication still need to be explored.

In spite of the recent articles suggesting new fabrication methods of printable batteries, a low-cost, scalable way of producing these energy storage devices is still to be demonstrated.

Due to the emergence of microelectronics, batteries also need to be built in smaller dimensions, with all of its components being fabricated into a very small device (at the micro and even nanoscale). This represents a major obstacle regarding the fabrication methods and the energy storage capacity of these devices.

In conclusion, improving the materials and fabrication techniques is vital to the battery's performance and its seamless integration in stretchable electronics. The main goal is to reach an automate digital fabrication method that allows digital and automated printing of the battery, along with other elements of the circuits, such as sensors, antennas and interconnects. At the same time, improving the areal capacity, and the resilience of this energy storage device against mechanical strain are other important objectives to be considered.

2.3 Conclusion

In this chapter, the State of the Art on the field of stretchable electronics was presented, with special focus on stretchable energy storage devices. Different research projects on stretchable batteries were analyzed from silver-zinc batteries to gallium-based anodes. It was possible to observe the improved results with different materials, architectures and fabrication mechanisms.

Despite the rapid progress on printed batteries, their fabrication usually relies on manual deposition techniques, or mechanisms that require preparation of stencils or screens. Instead it is interesting to develop methods that allow direct digital printing of stretchable thin-film batteries, which is set as the objective of this dissertation. Therefore, a considerable amount of effort in this work is focused on coming up with a digitally printable and stretchable gallium based anode, its characterization and optimization for maximizing the areal capacity of the battery. This is then followed by optimization of other materials (Current Collectors, and the cathode electrode), and subsequent printing of them. In the end, a fully digitally printed battery is demonstrated.

Table 2.1: Summary of the SOTA different type of batteries

Reference	Type	Capacity	Maximum Strain
[32]	Zn-Ag	1.2 mAh/cm2 - 1.8 mAh/cm^2	100%
[43]	Zn-Ag	5.59 mAh/cm^2	20%
[84]	Zn-Ag	12.5 mAh/cm^2	0%
[90]	EGaIn-air	3 mAh	100%
[89]	EGaIn-MnO_2	3.8 mAh/cm^2	100%

Chapter 3

Materials and Methods

This chapter focuses on the experimental section of the work conducted during this project. As it was mentioned in the previous chapters, the theme of stretchable batteries had already been approached in ISR. Therefore, continuation on this field of study, as well as testing new parameters and types of batteries, are carefully described in this section. The characterization methods of the batteries included electrochemical performance and studies on the effects of stretchability in the capacity of these devices.

Firstly, the materials and equipment used in the different tests are mentioned, including information about the fabricator. Afterwards, the different procedures to assemble a stretchable battery on a Thermoplastic PolyUrethane (TPU) substrate are described, followed by explanations on the different analysis performed.

3.1 Materials

3.1.1 Silver flakes 071 (Ag 071)

This material is distributed by Technic, Inc. It is labelled as "41-071 Silver Flake Material 071". According to the supplier, 95% of the particles measure less than 4.8 μm and 50% less than 1.9 μm with a silver percentage of 99.86%. Silver flakes-based inks, like the ones used in this project, are normally used as conductive fillers. Therefore, they were a key factor in enhancing the conductivity of the battery.

3.1.2 Carbon Black (CB)

Carbon Black presented various endings in this project, as will be explained further on. It was used to provide conductivity to the electrodes and as a primary material in the second current collector. In this project the CB used was from Alfa

Aesar, “Carbon Black, acetylene, 100% compressed, 99,9+%”. Chemical properties presented on the official website indicate a density from 170-230 g/L.

3.1.3 Eutectic Indium Gallium (EGaIn)

Liquid Metals are materials that exhibit metallic properties while being, at the same time, in a liquid state at room temperatures. Their main characteristics include glow and high conductivity. EGaIn is an example of a liquid metal composed of a homogeneous mixture of 75.5 wt% of gallium and 24.5% of indium. To obtain this homogeneity, after weighing, the materials were placed at 60.5°C for 24 hours. The conductivity values of gallium and indium are, respectively, 3.4×10^6 S m^{-1} and 3.5×10^6 S m^{-1} [91]. The melting point of EGaIn is around 15°C [92].

EGaIn was used mainly as a part of the 1^{st} current collector. Several research projects have used EGaIn as active material due to the importance of Indium in protection against corrosion. However, this was not the case in this project as, for starting point, analysing the properties of gallium alone was simpler than using two metals that could interact with the electrolyte.

3.1.4 Zinc Flakes 5 (Zn5)

This product is supplied by Alfa Aesar. The particles are 149μm size or less. It is 99.9% metal basis. Its relative density is 7,14. This material was mainly used at the beginning of the dissertation in order to continue the work of Cristina Leal. It is the main component used to fabricate the anode in an Ag-Zn battery.

3.1.5 Silver Oxide (Ag_2O)

This material is a product of Alfa Aeser, “Silver(I) Oxide”, product number 11407. It is composed of 99.9% of metal basis. Ag_2O was used as the active material for the cathode.

3.1.6 Gallium

The gallium used is a product of "Novaelements", with a 99.995% trace metal basis. Gallium is mixed with carbon and SIS to form a printable ink. It functions as the primary component of the battery's anode. This material possesses interesting properties already briefly mentioned, including self-healing abilities and a low melting point of 29°C.

3.1.7 Polystyrene-block-polyisoprene-block-polystyrene (SIS)

SIS is a hyperelastic binder with elongation up to 1300%. This polymer's elastic properties provide stretchability and flexibility to the several layers of the battery assembled. Also, as the term binder suggests, holds several materials together. However, it presents very low conductivity. As such, its quantities were carefully measured in order that the batteries could present good stretchability and good conductivity at the same time. More on properties of materials like SIS are presented in [81]. The product used during this project is distributed by "SigmaAldrich", product number 432393. The weight in Styrene was 14%.

A solution of 20% (wt) was prepared, by dissolving 4g of SIS in 16g of toluene. SIS was also used to fabricate a different substrate for the battery (see chapter 4). When doing so, the ratio SIS:toluene used was 1:2.

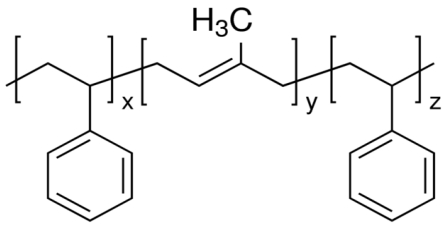

Figure 3.1: Polystyrene-block-polyisoprene-block-polystyren

3.1.8 Electrolyte

The electrolyte represents the medium through which the ions are conducted. They can be conductive composites or polymers. However, using hydrogels is considered a great choice due to their softness, ionic conductivity and reduced electrode-skin impedance. In this project, a stretchable hydrogel was fabricated to function as the alkaline electrolyte (appendix III). This hydrogel was placed in a 35 wt% KOH solution for a day before applying it to the battery, in order to be saturated with the alkaline medium.

3.2 Equipment

The following section describes the several instruments used to fabricate and characterize the batteries. This includes both electrochemical and electromechanical characterization.

3.2.1 Mixer

In order to bind all the materials together various composites produced in this work, a Mixer “Thinky ARE-250” by Intertronics was used.

Figure 3.2: Mixer “Thinky ARE-250”

3.2.2 Electromechanical Characterizer

The "Instron 5943" was utilized in order to perform electromechanical characterization, which will be described in more detail later in this chapter. Its major components are, according to its datasheet, a load frame with an integral controller, a load cell with capacity up to 1 kN, grips for tension testing and table-mounted anvils for compression testing and a computer system. Its accuracy is up to ±0,5%.

Figure 3.3: Instron 5943

3.2.3 Thin-Film Applicator

This instrument allows the fabrication of thin-films from 500 μm to 3000 μm thickness. During the realization of the project, several times, films with very low thickness had to be produced. This included the substrate used for the application

of the battery in the "WoW Belt", which was a SIS substrate.

Figure 3.4: Thin – Film Applicator ZUA-2000

3.2.4 Laser Cutter

In this project, a "VLS3.50 Desktop" by Universal Laser System was utilized. It is a CO_2 laser with a power range from 10 W up to 50 W. The laser cut several materials that included stencil, TPU and different substrates. It allowed the creation stencil of masks of different shapes with accurate dimensions.

3.2.5 Palm Sens4 Potentiostat

One instrument used to perform electrochemical characterization on the batteries was the "PalmSens4" by "Compact Electrochemical Interfaces". This device allowed several modes of characterization and was used especially for the open circuit discharge, constant capacity measurements and internal resistance calculation. Other possible modes include performing cyclic and linear voltammetry and impedance measurements.

3.2.6 Potentiostatic/Galavnostatic System

The disadvantage of using the PalmSens4, despite its accuracy, was the low number of batteries it could characterize (only one at the time). A normal battery would

Figure 3.5: Laser Cutter VLS3.50 Desktop

take 2 to 7 days to perform one single discharge. Therefore, a low-cost solution to perform multiple tests was found, by designing PCBs that were programmed in C (using Cypress and PSoC) in order to supply and control the current and the voltage necessary. As a result, over 100 batteries were tested, with different parameters, exporting the data to log files to be analyzed using a Python script. This system will be referred to as Potentiostat/Galvanostate (PGSTAT). Also, the fabrication of these PCBs allowed the characterization of 10 batteries at the same time. They all were fabricated during the period of time of this dissertation. A brief explanation of its fabrication process and working principle is present on the appendix IV.

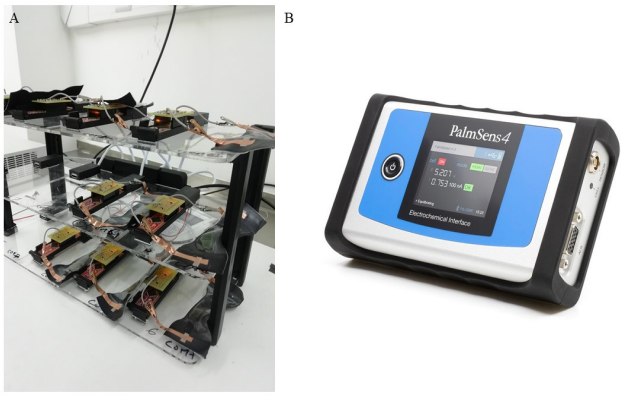

Figure 3.6: a) PGSTAT system developed in ISR characterizing stretched batteries; b) PalmSens4

3.2.7 Voltera V-One Printer

The "V-One Printer", developed by Voltera, is an extrusion printer that is also able to perform drilling or soldering. It is more commonly used to print flexible inks on Printed Circuit Boards but, in this laboratory, it was adjusted to print on top of soft substrates, like polymers or textiles. As a result, there was the need to change some of its settings. The adjustable parameters are explained in the appendix V

Figure 3.7: V-one digital printer

3.2.8 Ultrasonic Processor

This instrument is a product of "Lawson Scientific". It is a mechanical disrupter that uses ultrasonic waves, that travel through a liquid and, through mechanical strength, disperse particles or ruptures materials. It was used to generate gallium microparticles.

Figure 3.8: Ultrasonic Probe

3.3 Fabrication of the battery

After the materials were correctly prepared, the next step was assembling the battery. The fabrication process of the different layers is explained in further detail in the next chapter.

In order to fabricate the batteries, both stencil and digital printing techniques were used. First, stencil printing was approached in order to perform initial feasible tests, and ink formulations. Only when the best methodology was found, we started working on optimization of the ink for digital printing. In this section the fabrication of the batteries for each of the techniques is described.

- **1^{st} CC:** For stencil printing, using the laser cutter, a stencil mask was made with the shape of a square with sides of 1 cm. The square was connected to a pad. Afterwards, using this mask, 2 layers of a Silver and EGaIn (EGaIn-Ag-SIS) based ink were applied on the substrate and left curing at 60°Cfor 30 minutes. The inks where applied using a spatula. For digital printing, the inks were first transferred to cartridge to be used in the extrusion printer. The quantities of each component of this ink changed from stencil to digital printing. The digitally printable ink was made based on [55].

- **2^{nd} CC:** Despite having a conductivity three times lower than the previous layer, the main purpose of the 2^{nd} CC is to protect the 1^{st} CC against contact with the electrolyte.This is mainly to prevent Ag, Ga and In (present in the previous layer) to participate in any redox reaction and alter the results. Carbon has also a good resistance against corrosion and oxidation. Two layers of CB-SIS were applied on top of the 1^{st} CC and subsequently cured at 60°Cfor 5 minutes. Both the stencil and digitally printed composites where synthesized using the same formula.

- **Electrodes:** Lastly, 2 squares of $1 cm^2$ of active material were placed on top of the previous layer. It was very important to maximize the area in contact with the electrolyte. The silver electrode was synthesized using the same quantities of materials present in [43]. However, for the gallium electrode, since there were no reports of gallium-based inks, several attempts were performed, exploring different quantities of gallium and carbon. The results are presented in chapter 4.

- **Electrolyte:** On top of the electrodes, the hydrogel was placed. The hydrogel ought to had been previously kept in a recipient conveniently sealed since it

tends to absorb humidity, reducing the KOH concentration. Afterwards, the voltage observed between the battery's terminals was around 1.7 V, meaning the battery was working and was ready for the electrochemical characterization. This value is near to the theoretical value of 1.75 V. A layer of EcoFlex or Dragon Skin was usually placed on top to protect the hydrogel and guarantee contact between the electrolyte and the electrodes while the battery was under test.

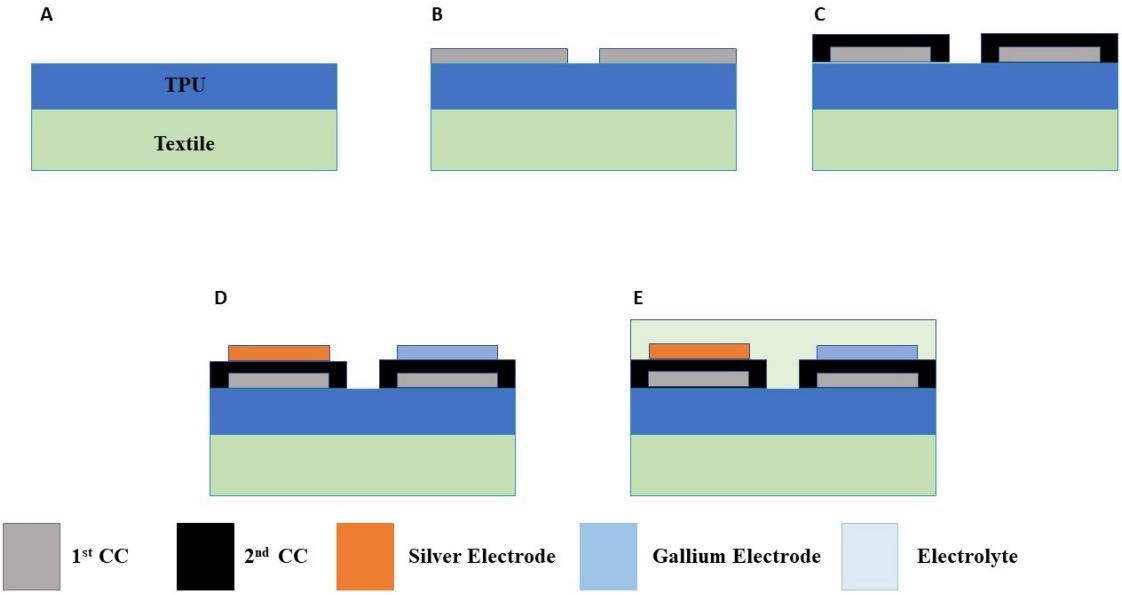

Figure 3.9: Assembly Schematics: a) TPU substrate over textile; b) Placing the 1^{st} current collector; c) Placing the CB-SIS current collector; d) Placing the Electrodes; E) Placing the Electrolyte

3.4 Electrochemical Characterization

A battery is an energy storage device. It works as a warehouse of energy harvested. As such, it is important to know how much energy it can "store". This is given by the capacity of the battery (see chapter 2). The electrochemical tests were performed in order to attain the storage capacity of the printed batteries, and their stability against multiple charging cycles, which was performed by analyzing the charging and discharging cycles of the several batteries fabricated.

According to the electrochemical processes described in chapter 2, while discharging takes place, the current flows from the cathode to the anode. When applying the electrolyte on top of the anode, gallium tends to form gallium (III) oxide, generating

electrons. When an electrical load is placed between the electrodes, the electrons produced in this reaction flow to the cathode. This induces the transformation of silver oxide into metallic silver (see equations 2.7 and 2.8). The mathematical difference between the electrochemical potential of oxidation in the anode, and the reduction in the cathode corresponds to the battery's open circuit potential. Since the reactions are reversible, if one wants to charge the battery, the direction of the current applied should be the opposite.

In order to perform electrochemical characterization, different experiments were conducted. These included obtaining the discharge curve during the first cycle, counting life cycles between 0.8 V and 2.2 V and performing life cycles at constant capacity mode using different currents. The details on every process will be explained in more detail in the following chapter.

The charging rate chosen to perform the tests was also taken into account. Normally it is presented in C-rate nomenclature. As previously mentioned, the capacity (mAh) is the product between the discharge current and the time it takes for the battery to be discharged. Therefore, a battery charged or discharged at C-rate means that it takes 1h to discharge at a current I. For example, if the capacity of a battery is 1Ah, discharging at C-rate means that we are pulling 1A of current, during 1h. If it is at 4C the battery is discharging at 4A for 15 minutes and C/2 means 500 mA for 2h.

The current density chosen to charge and discharge is one of the factors that has influence on the capacity obtained. In fact, when using high current densities for fast charges, a phenomenon can takes place where not all materials are oxidized or reduced. This leads to a lower quantity of active material available to be used in the subsequent discharge, decreasing the capacity. On the other hand, if low current densities are chosen, the existing self-discharge rate, caused by side reactions of the electrodes with the alkaline electrolyte, become predominant. As a result, the charging current applied might not be enough to charge the battery correctly. During the charging and discharging cycles, Ag, Ga, and Zn tend to form certain microstructures, including salts with the shape of crystals,dendrites, and hydroxides as well (due to the reactions with the KOH). These structures reduce the electrode's conductivity and the respective area available. As a result, they are the cause of the batteries' poor performance, reduced capacity over discharging cycles, self-discharging, or even short-circuit between the electrodes.

The current chosen to discharge and charge the electrodes was based on the study made previously by Cristina Leal [43]. She tested different combinations of charge and discharge currents between 200 μA and 600 μA. The best energy storage

capacity and cycle performance were obtained were detected when both currents were equal and with the value of 200 μA. As a result, since this work focused more on the characterization of a new electrode, fabrication techniques and comparison with previous results, there were no further studies on the impact of performing charging cycles at different currents.

The charging and discharging cycles, characterized using the PGSTAT, follow 3 major steps: Discharge at constant current, charge at constant current and charge at constant voltage. Firstly, the batteries are discharged at 200 μm. Once 0.8 V were reached, a charging current is applied until reaching the voltage of 2.2 V. At 2.2 V, the battery is maintained at constant voltage for 2 hours. This process represents a charging cycle.

In this work, instead of performing full cycles to obtain the capacity at the different current, we will approach this matter by changing the range of the battery's charging/discharging current from 200μ to 1mA, and performing several charging and discharging cycles. This is performed for both stencil and digitally printed batteries (see chapter 4).

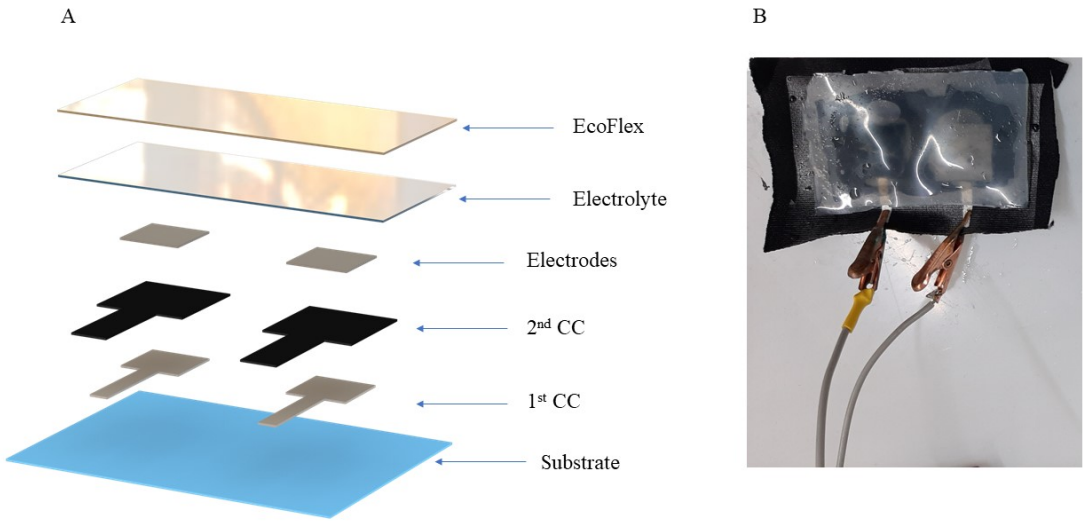

Figure 3.10: a) Schematic presenting the different layers of the battery, which include the substrate, the Current Collectors, the electrodes, the electrolyte and the protective layer; b) Fully printed battery under electrochemical characterization using the PGSTAT.

3.5 Electromechanical Characterization

As these batetries are intended for wearable monitoring sensors, and e-textiles, it is important to make sure they are able to deliver the required function, even when subject to mechanical strain. Within this dissertation, the electromechanical coupling of the developed batteries was characterized, in order to find out their behavior when subject to the mechanical strain.

In order to do so, three tests were performed: First, the maximum strain prior to break was characterized by straining the battery, while discharging it at the same time, using the instron equipment, until there is a mechanical/electrical failure; Second, considering a strain of 20%, the batteries performed 100 cycles until this value. Third, the batteries were stretched until 100% and went back to their initial shape. The capacity was also analyzed. The results are all presented in the next chapter.

The following image, shows an example of a strain test performed over a printed battery, using the instron equipment.

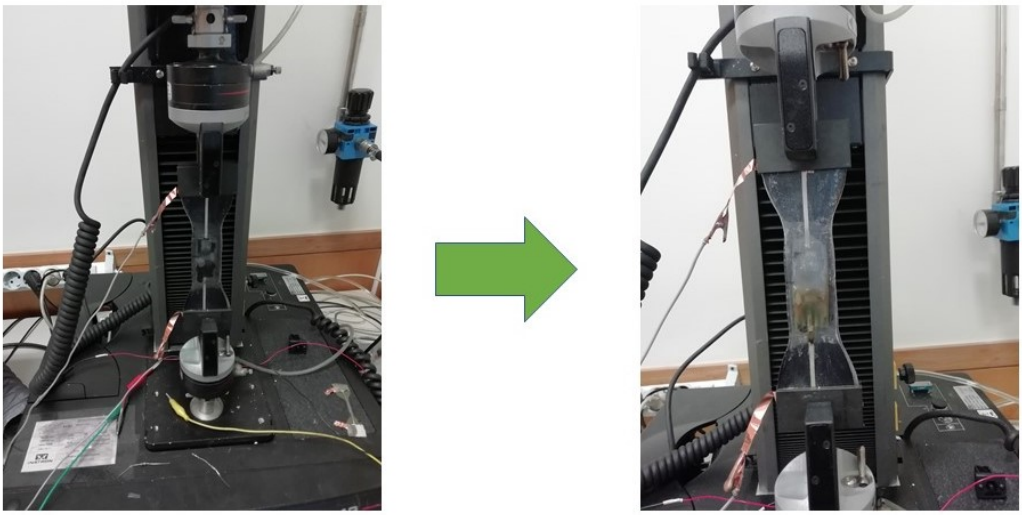

Figure 3.11: Example of a battery under electromechanical characterization

3.6 Fabrication Methods of the Printable Electrodes

The major claim on the novelty behind this dissertation is of a new, scalable method of fabrication that allowed different shapes and sizes to be printed at once, without any manual intervention. As such, it was also important to compare the

batteries produced in the digital printer and the batteries that were produced using stencil printing and analyze the strongest and weakest points of each. Figure 3.12 shows a set of batteries being digitally printed.

The Zn particles used in [43] presented a low surface area to volume ratio. As a result, when mixing them with conductive composites like CB, they tend to be deposited in the bottom. As such, the attempts to create a Zn-SIS electrode, using Carbon Black to enhance the conductivity, were made using Zn flakes (Zn5). These present higher surface area to volume ratio, allowing it to be further exposed. The results are presented in the next chapter.

From the theory of electrochemistry, as mentioned in the previous chapter, the several properties of gallium when compared to zinc, including its higher theoretical capacity, let to the hypothesis that it could be used as an anode.

The main objective of this dissertation, regarding the material for the anode, was to create a digitally printable ink. Gallium has a melting temperature of 29°C, and cannot be directly printed, except if heated to that temperature. Besides, even if printed at high temperatures, although the bulk gallium is deposited, it does not reveal stretchable properties. Therefore, we worked on the creation of a gallium-based printable electrode.

Initial attempts started by synthesis of a gallium-SIS composite. Direct mixing of gallium with SIS did not result in a conductive paste, as the SIS polymer was effectively isolating the gallium microparticles within the composite, thus resulting in a non-conductive electrode. This is similar to what has been reported with Liquid Metal Embedded Elatomers [93]. Although digitally printable, these composites are not conductive right after the deposition, and requires a mechanical pressure, as a method for "sintering" conductive paths.

Therefore, the approach taken to solve this problem, was to use Carbon Black, as the material for percolating between the gallium droplets. Carbon is conductive, and very resilient to strong alkaline electrolytes, which can help in improving the resilience of the electrode.

Therefore, we focused on synthesizing Ga-CB-SIS electrodes, and characterize them in terms of electrical conductivity, printability, and their performance when used as the battery's electrode. Another important factor was how much of the gallium is exposed in the surface, after deposition. This parameter, brought surprising results, and clear advantages when using digital printing, as it will be discussed later on.

Another approach consisted of ultrasonic assisted mixing, via creating gallium microparticles and applying techniques like spray coating to fabricate the electrode.

Three different methods were applied to create electrodes of gallium microparticles combined with carbon, graphene and SIS. The results are presented and discussed in the following chapter.

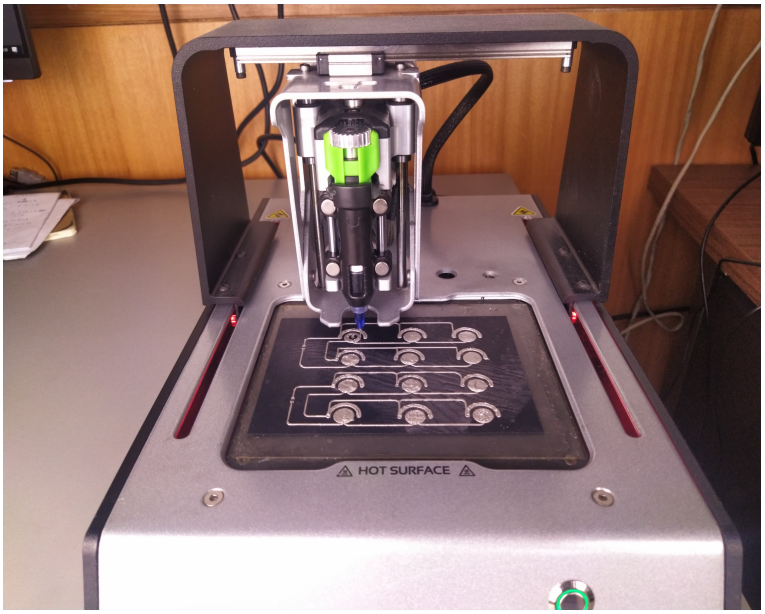

Figure 3.12: Fabricating the EGaIn-Ag-SIS current collector and the interconnect of a multi-cell battery using the extrusion printer "V-one" by Voltera

Chapter 4

Results and Discussion

This chapter presents the results of this dissertation. It includes:

1. Continuation of the study previously conducted by Cristina Leal in [43], on **Ag-Zn Batteries**. It includes an explanation on the different approach taken regarding this project and the positive and negative aspects observed during the several experiments;

2. **Gallium-Carbon-SIS electrons synthesis and characterization**, describing the different methodologies approached to fabricate a digitally printable ink of the Ga-CB-SIS anode. It shows tests related with different quantities and their effects on the electrochemical performance and conductivity;

3. Different attempts for fabricating the gallium electrode by creating **Ga microparticles**. The results are discussed and compared to the ones obtained in the previous section;

4. **Microscopy analysis (SEM)** of the electrodes, and investigation of their changes over the different stage since their fabrication until the death of the battery;

5. **Electrochemical Characterization** of the different batteries, including areal capacity, open circuit discharge, rechargeability, discharging and charging at different currents and internal resistance measurements;

6. **Electromechanical coupling**, including maximum tensile strain prior to failure, and battery performance after being subject to 100 cycles of 20% strain and to 1 cycle of 100% strain;

7. Fabrication and characterization of **digitally printed batteries**;

8. **Case study and Applications**, where it will be shown a digitally printed multi-cell battery, fabricated using the extrusion printer. Also it is demonstrated the application of another digitally printed battery on a wearable monitoring e-textile chest band.

Only the last two section cover tests related with digitally printed batteries. All of the results of the previous electrochemical and electromechanical characterizations are related to stencil printed batteries.

4.1 Silver-Zinc batteries

As mentioned in the second chapter, Ag-Zn stretchable batteries have been explored in several previous works. In this dissertation, and prior to exploring the silver-gallium battery, it was conducted a study on Ag-Zn batteries, by trying to fabricate a digitally printable Zn-SIS electrode.

In [43], the results reported on this type of rechargeable batteries were considered a good improvement of the SOTA, introducing a 2^{nd} current collector composed of carbon black and SIS, combined with an EGaIn-Ag-SIS based 1^{st} current collector.

Despite the good results, the major negative aspect behind this work was related to the fabrication steps, especially regarding the anode. In order to connect the zinc particles to the carbon layer, a pouring mechanism had to be performed. It included the usage of a sticky substrate (in this particular case, a Kapton tape with an adhesive side). After pouring the particles onto the substrate, a CB-SIS thin-film was created on top of the zinc particles and left to dry. Afterwards, the electrode was removed and cleaned with Isopropyl alcohol (to remove the glue), completely exposing the zinc particles. As a final step, once the second current collector was applied, the electrode was immediately placed on top of it, before it had a chance to cure. After drying, the two layers were fully attached to each other.

Figure 4.1, taken from the Supplementary Information of [43], presents a schematic that describes this method of fabricating a zinc electrode:

While promising, this existing method fell short of the ultimate goal of digitally printing a stretchable energy storage device, using widely available production-scale extrusion-based printers. Not only that but it was heavily dependent on a complicated manual-based fabrication process, demanding the electrode to be separately constructed from the rest of the battery, by manually placing the anode on top of the 2^{nd} CC, which isn't a reliable technique.

As a starting point, and in order to learn the fabrication process and working mechanism of stretchable batteries, a different approach was taken. It consisted of

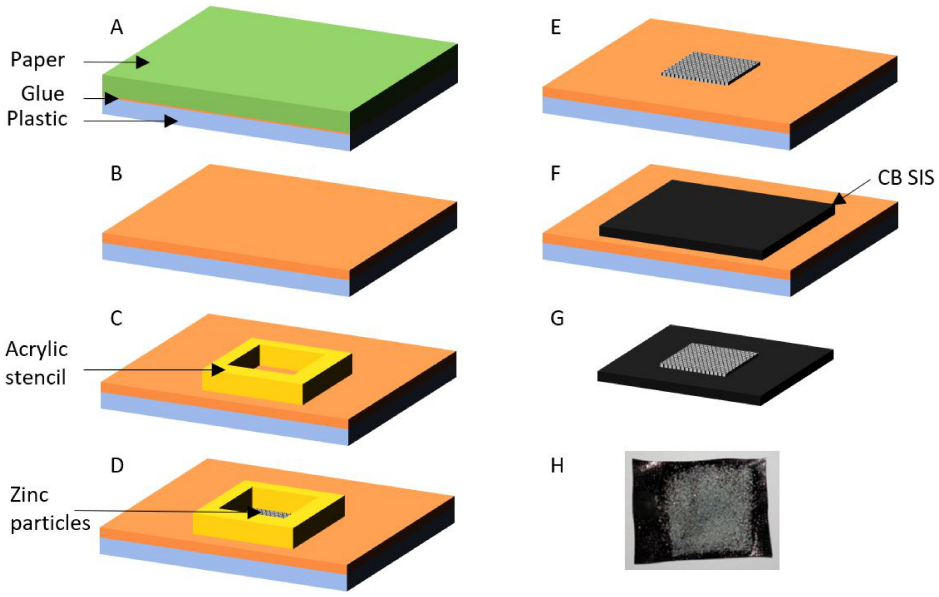

Figure 4.1: Schematic illustration of the preparation of the Zinc electrode. a) 3 layer transfer paper; b) paper layer is removed to expose the glue/sticky layer; c) Acrylic shape with desired shape and area; d) Pouring of zinc particles to the inside of acrylic mold; e) Remove acrylic mold; f) Apply layer of CB-SIS over zinc particles and allow to dry; g) Detach CB-SIS + Zn layer from glue and plastic layer – remaining glue residues removed with Isopropyl alcohol; h) Photo of final Zn-electrode. [43]

fabricating an ink of Zn, CB and SIS and apply it directly on the second CC via stencil printing. By doing so, a printable zinc electrode was able to be created, that eliminated the need for pouring zinc powder over the CB-SIS. The fabrication method behind this technique followed the following steps:

- **EGaIn-Ag-SIS CC:** 1.65 g of Ag '071 flakes were mixed with 1 g of 20% SIS solution and mixed for 3 minutes at 2000 rpm, using the planetary mixer. Afterwards, 0.65 g of EGaIn were added and mixed for 3 minutes at 2000 rpm as well.

- **CB-SIS CC:** 0.2 g of CB were mixed with 2 g of 20% SIS solution and mixed for 3 minutes at 2000 rpm.

- **Ag_2O electrode:** 0.4 g of CB were mixed with 2 g of 20% SIS solution and mixed for 3 minutes at 2000 rpm. Then, 3 drops of toluene were added and mixed for 3 minutes at 2000 rpm. In the end, 1.6 g of Ag_2O was added and mixed, on more time, for 3 minutes at 2000 rpm.

- **Synthesis of a printable zinc-SIS electrode:** Previous attempts on creating zinc-based conductive composite by Cristina Leal were not successful.

The reason for this was the fact that zinc powder was rapidly settling in the SIS solution, not allowing for maintaining the zinc in the surface. In order to address this problem, research of different zinc particles was conducted. Zinc in flake shape (Zn5) was selected. The conductive composite was created by frost mixing 0.6 g of CB with 2g of 20% SIS solution for 3 minutes at 2000 rpm. In the end, 1.6 g of Zn were added and mixed for 5 minutes at 2000 rpm.

The printing method used was stencil printing (see figure 4.2), where each layer was deposited using a spatula, over a laser patterned stencil.

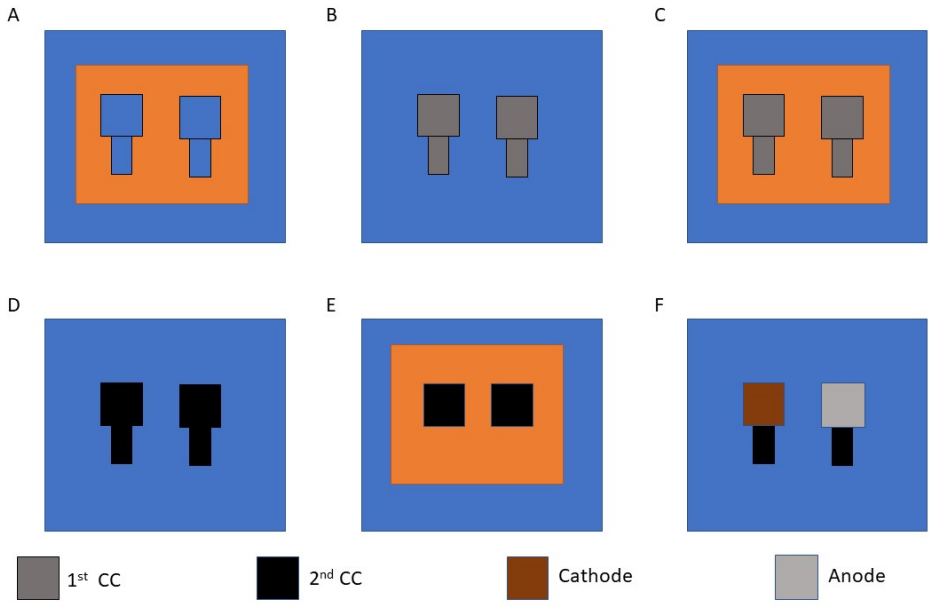

Figure 4.2: Assembly steps: a) Placing 1cm^2 squares with pads; b) Stencil printing the 1^{st} CC; c) Placing the stencil for the 2^{nd} CC; d) Stencil printing the 2^{nd} CC; e) Placing the stencil for the active material; f) Stencil printing the electrodes.

Figure 4.3 presents the results regarding the silver-zinc battery experiment.

The outcome did not reveal to be very promising, especially when comparing it with the experiment by Cristina Leal in [43], where the battery exhibited a capacity of 5.10 mAh/cm^2, performing well for more than 5 cycles. As a result, despite enabling the ability to be fully printed in the extrusion printer "V-One", this battery is not able to deliver a considerable amount of energy and power density.

The reason behind the worst results when comparing both works, regarding the ability to perform electrochemical cycles, could be related to the exposing mechanism of the active material in the anode. As a matter of fact, by using a methodology similar to the first project, if the fabrication is done correctly, the zinc particles should be more directly exposed to the electrolyte leading to an increased capacity.

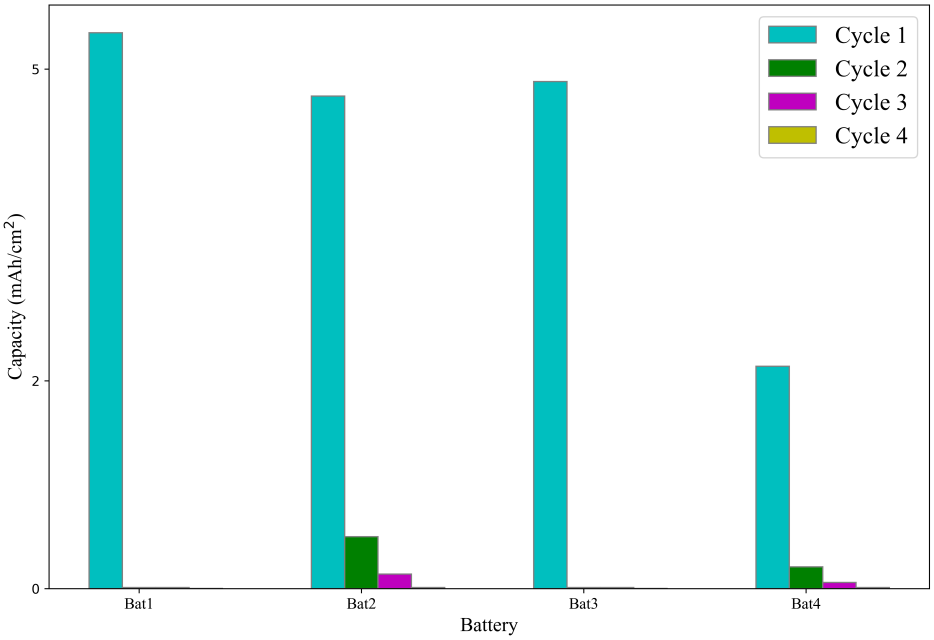

Figure 4.3: Results of the Electrochemical tests performed on stencil printed silver-zinc batteries

In this last scenario, the zinc is homogeneously mixed with the carbon, reducing the exposition area, hence, worsening its performance.

Despite the disappointing results, this first experiment helped to highlight the importance of the exposed area to the electrolyte and the need to explore new materials in order to achieve a digitally printed battery.

4.2 Gallium-Carbon-SIS electrodes synthesis and characterization

As already previously stated during this dissertation, gallium-based anodes have been revealing interesting properties that can benefit stretchable batteries, in terms of fabrication, including its low melting point and high theoretical capacity. Also, its self-healing abilities could lead to an increase in the lifespan of the battery (performing more cycles). However, there were almost no previous studies on the fabrication of printable inks composed of gallium, by the time of the realization of this dissertation. Therefore, different approaches with regards to the quantities of Carbon Black applied in the mixture were studied.

In the silver oxide cathode, the carbon serves as a conductivity enhancer. In order

to analyze the importance of carbon in the gallium electrode, a study was conducted by comparing the composites with different wt% of carbon. These composites, were then applied over a TPU substrate, using stencil masks, and their conductivity were measured. While having a higher conductivity is always appealing, it is important to note that excessive carbon can cover too much the gallium particles, thus resulting in poor electrochemical performance. Figure 4.4 shows the different combinations printed over TPU and textile.

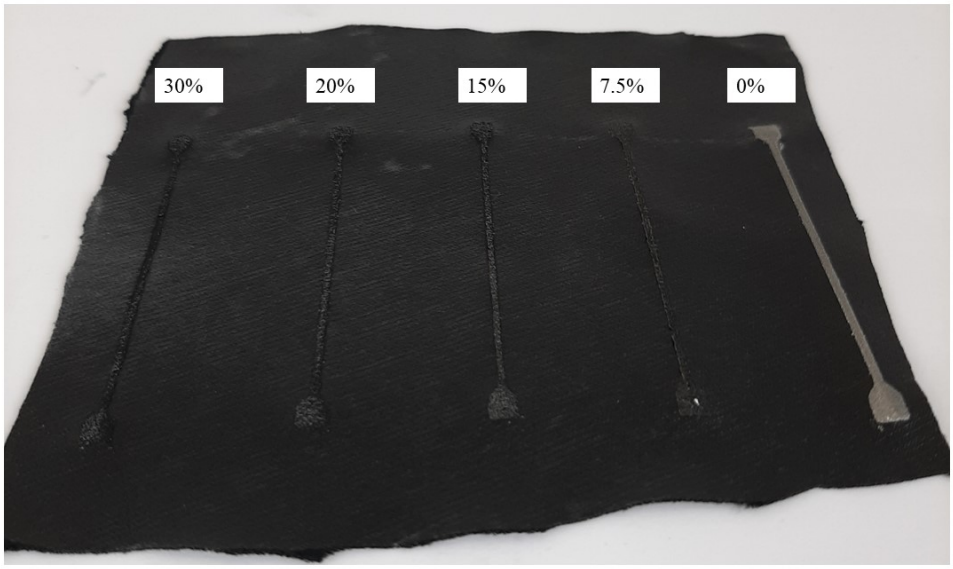

Figure 4.4: Different ratios of CB:Ga printed over a TPU substrate.

The sheet resistance of the different combinations was measured from points in an opposite diagonal in a 1 cm^2 square. The different ratios of carbon:gallium were fabricated using the following technique:

Gallium electrode: 0.6 g of CB were mixed with 2 g of the 20% SIS solution for 3 minutes at 2000 rpm. Afterwards, 1g of toluene was added and mixed for 20 minutes at 2000 rpm. In the end, the different quantities of Ga (see table 4.1), that had been under 60°C, in the liquid state, were added (depending on the ratio tested) and mixed for 3 minutes at 2000 rpm.

Figure 4.5 shows the sheet resistance of different ratios of CB:Ga. As expected, by adding more carbon, the conductivity of the anode increased. This is extremely important to ensure a decrease in the overall internal resistance of the battery fabricated. Nevertheless, the main goal of the battery was to present good energy storage capacity. Subsequently, the electrochemical performance was tested.

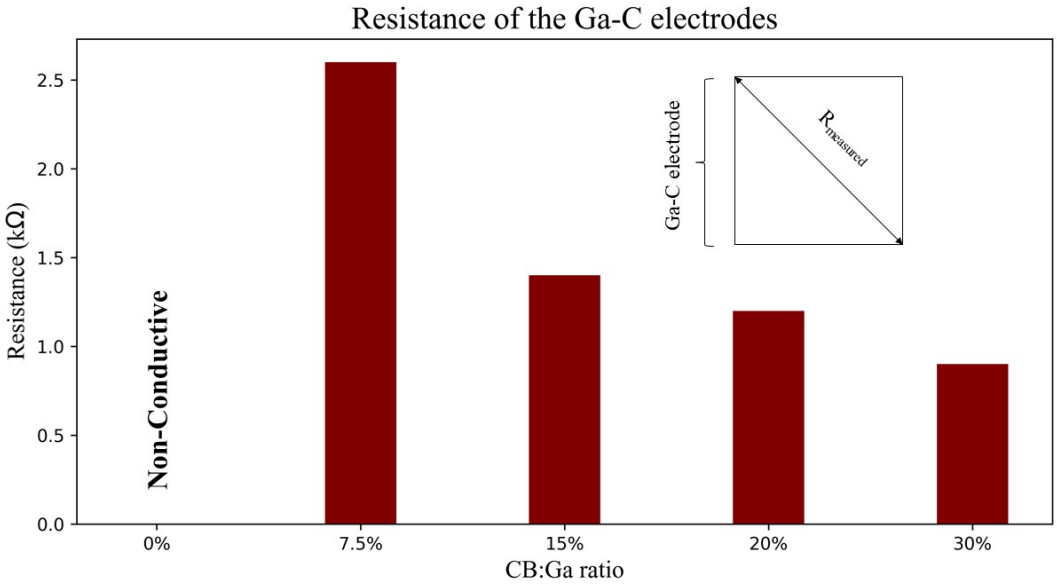

Figure 4.5: Results regarding the sheet resistance of different CB:Ga ratios, when used as anodes for the Ag-Ga battery

Figure 4.6 presents a schematic of the role of carbon in the anode.

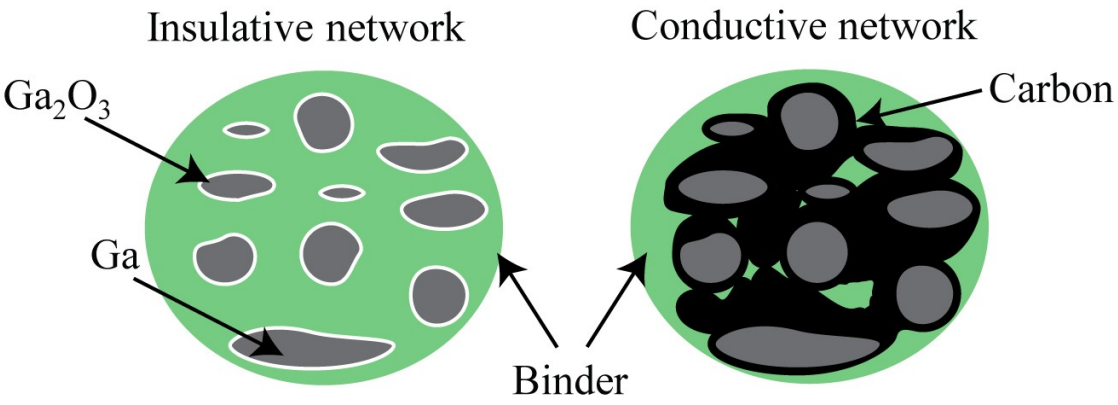

Figure 4.6: The role of Carbon Black in the gallium electrode: Provides a percolating pathway to the electrons making the anode conductive.

There were different tests with different combinations of gallium and CB performed. The batteries were printed over a TPU substrate with thickness of 90.73 μm. This film turns into an adhesive gel, when subject to a temperature of 300°C. This property was exploited in order to transfer the battery into the textile, using a heat transfer machine.

Table 4.1: Different fabrication methodologies analyzed

Materials	Bat1	Bat2	Bat3	Bat4
SIS	0.4g	0.4g	0.4g	0.4g
CB	0.6g	0.6g	0.6g	0.6g
Ga	2g	3g	4g	8g
CB:Ga	30%	20%	15%	7.5%

The main goal was to find an optimal ratio between carbon black and gallium. The capacity values related to the first three cycles, in mAh/cm^2, are presented in table 4.2.

Table 4.2: Capacity obtained for different CB:Ga ratios

Battery	Cycle 1	Cycle 2	Cycle 3
Bat 1	2.5 mAh/cm^2	0.9 mAh/cm^2	0.2 mAh/cm^2
Bat 2	3.0 mAh/cm^2	1.0 mAh/cm^2	0.3 mAh/cm^2
Bat 3	3.5 mAh/cm^2	1.6 mAh/cm^2	1.5 mAh/cm^2
Bat 4	5.49 mAh/cm^2	5.28 mAh/cm^2	2.14 mAh/cm^2

Table 4.3 summarizes the main findings of this section of the dissertation, by comparing the different batteries in terms of the weight of CB , their sheet resistance and their energy storage capacity. Only one battery of each was tested due to the low results of the first 3 batteries.

Table 4.3: Overview of the properties obtained using different methodologies to fabricated Ag-Ga batteries

Battery	CB:Ga ratio	Sheet resistance	Maximum energy storage capacity
Bat 1	30%	0.9 kΩ	2.5 mAh/cm^2
Bat 2	20%	1.2 kΩ	3.0 mAh/cm^2
Bat 3	15%	1.4 kΩ	3.5 mAh/cm^2
Bat 4	7.5%	2.6 kΩ	5.49 mAh/cm^2

We can conclude, from table 4.3, that from batteries 1 to 4, although the conductivity decreased, the energy storage capacity was improved. From batteries 3 to 4, by reducing the CB:Ga from 15% to 7.5%, the capacity values significantly increased. Table 4.2 shows the increase in the number of cycles the batteries were able to perform, mainly, from battery 3 to 4. As such, from this point onward, the formulation presented in battery 4 was used.

Naturally, there were other combinations that could be interesting to analyze, by lowering the ratios even further. Nevertheless, adding more gallium would make the battery more and more expensive. As such, there were no attempts made to further increase the quantities of Ga used.

4.3 Alternative Ga-based electrodes

In this section, 3 other alternative attempts for making gallium-based electrodes using ultrasonic particle generation, and, at the same time, different carbon structures, such as graphene oxide are summarized. While none of these attempts was as successful as the above technique (electrode number 4 in the last section),these composites and their results are briefly reported. Figure 4.7 presents different pictures of the 3 methods used.

Note that, although these results are very preliminary and under explored, these composite may serve as a starting point for further improvement in future works.

- **Method 1 - Lifting Spray Coated Gallium:** 1.6 g of Ga were sonicated in ethanol (without tiol). Afterwards, the resulting colloid was sprayed over the glass at 80°C. Using the thin-film applicator, a layer of 1 mm of CB-SIS covered the sprayed particles. A square of 1 cm^2 was cut and placed over the 2^{nd} CC layer before it dried (similar approach to the one presented in section 4.1);

- **Method 2 - Using Graphene Oxide:** 1 g of EGaIn placed in 20 mL of 0.4% commercial graphene oxide (GO) (Graphenea) and 1 mL of 0.1 M acetic acid were sonicated for 20 minutes and sprayed printed in a similar fashion to method 1. Then, once more, a 1 mm layer of CB-SIS ink was added (see figure 4.7). The sprayed film was then placed under laser irradiation (using the 1064 nm fiber laser from JPT) to reduce the graphene oxide into conductive reduced graphene oxide (rGO) [94].

- **Method 3 - Spray Coated Ga-CB-SIS:** 0.5 g of Ga were sonicated in 10 mL of toluene with 2 mL of tiol and 3 mL of IPA. This mixture was added to an already fabricated ink of 0.2 g of CB and 0.5 g of the 20% SIS solution. The resulting mixture was then sprayed in glass at 80°Cand covered with a 1 mm layer of CB-SIS. A square with the same dimensions as the previous method was cut and placed over the current collector.

The batteries fabricated using all 3 methods were electrochemically characterized using the PalmSens. The results are presented in table 4.4, including the first cycle capacity (C_1) and second cycle capacity (C_2). Due to the poor performance exhibited by the devices, no further experiments were conducted.

Hence, gallium microparticles, as an active material, proved not to be very efficient when compared to bulky gallium, not only due to the low capacity values

Table 4.4: Electrochemical characterization of the batteries fabricated using methods 1,2 and 3

Method	Initial Voltage (V)	C_1 (mAh/cm^2)	C_2 (mAh/cm^2)
1	1.7	0.6	$\ll$0.1
2	1.7	1.0	0.6
3	1.7	0.6	$\ll$0.1

previously shown, but also considering the fact that these processes do not allow for a printable and straight-forward fabrication. In the end, despite the higher exposure (see figure 4.7), it came at the cost of lower quantities of active materials used, which could have led to the worst performance.

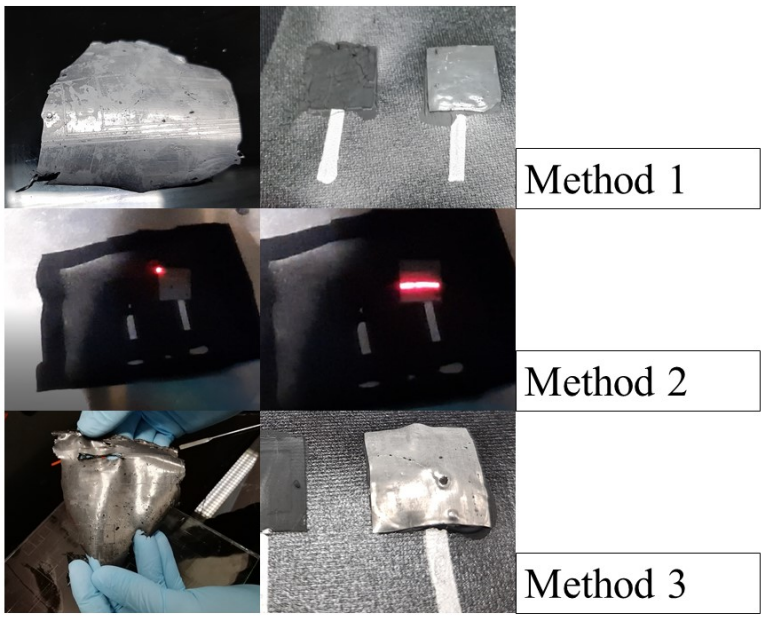

Figure 4.7: Different approaches to create a gallium electrode using gallium particles

4.4 SEM Analysis

Scanning Electron Microscopy (SEM), and Energy-dispersive X-ray spectroscopy (EDS) analysis were performed in order to investigate the constitution and morphology of the electrodes over electrochemical cycles. Figure 4.8 shows this evolution for the anode electrode. All SEM analyses were carried out in the Physic's department of Universidade de Coimbra. A brief explanation of the working principle of Scanning Electron Microscopy (including SE, BSE and EDS) is discussed with greater detail at the end of the dissertation (see appendix VI).

Comparing a fresh electrode, with an electrode exposed to the electrolyte, one can see that, in the last one, more gallium is exposed in the surface. This is confirmed by the elemental intensity maps. After the contact with the electrolyte, gallium particles aggregate at the surface, covering a considerable amount of the surface. This "self-healing", and "self-aggregation" property, improves the performance of the battery, by exposing more gallium at the surface. It is hypothesize that, the solubility of the gallium oxide thin film in the KOH solution, the low melting point of gallium (29°C), and the generated heat during the gallium-KOH reaction, are parameters that contribute to this liquid-like behavior of the gallium particles.

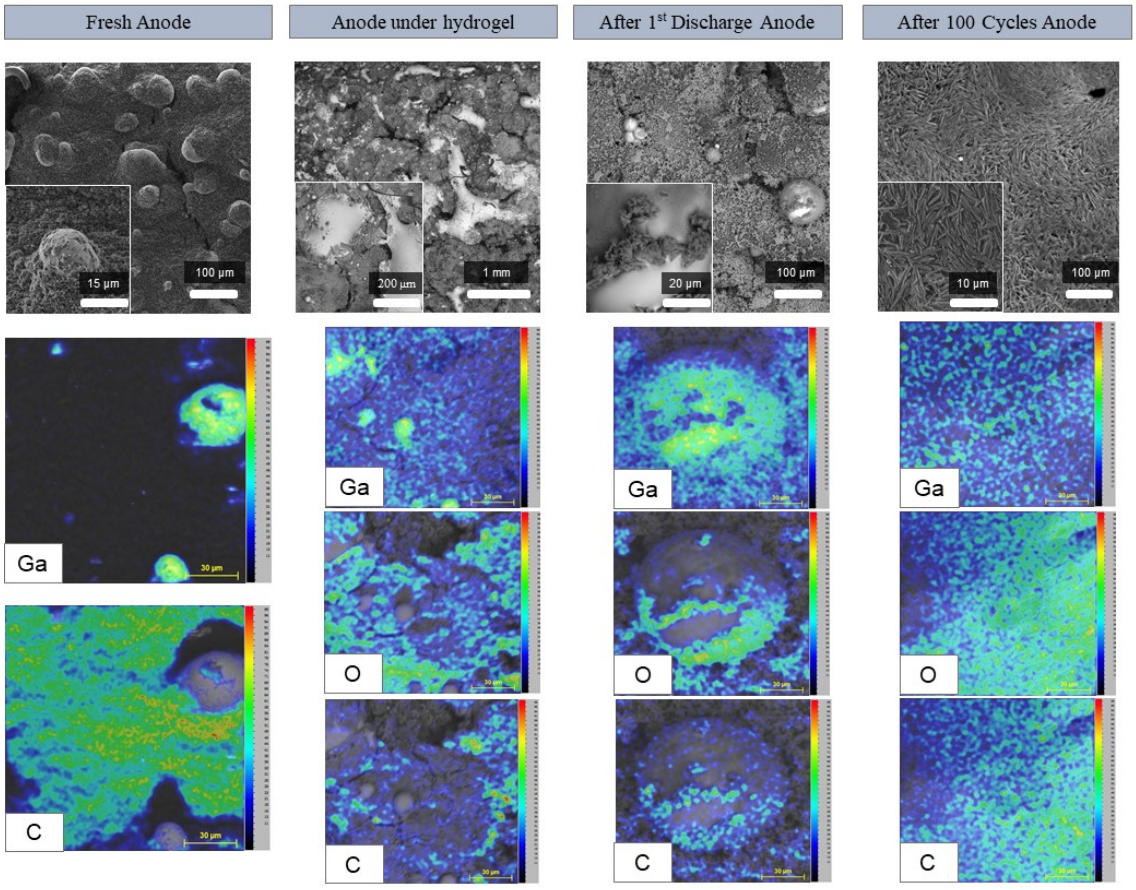

Figure 4.8: SEM analysis of Ga-CB-SIS electrodes under different conditions related to its fabrication process and to the discharging cycles of the battery

It is important to note that the magnification of the intensity maps is different from the SE images. This is because the EDS could only be performed at 1000x magnification.

Figure 4.8 also shows he microstructure of the electrode after discharge and after 100 cycles. The needle like structures are Gallium Oxide (GaO_3^{3-}) that grow over the electrochemical cycles. Figure 4.9, taken from [95], shows the nanostructures of

gallium (III) oxide, presenting the cylindrical shape, similar to the ones detected in our SEM analysis:

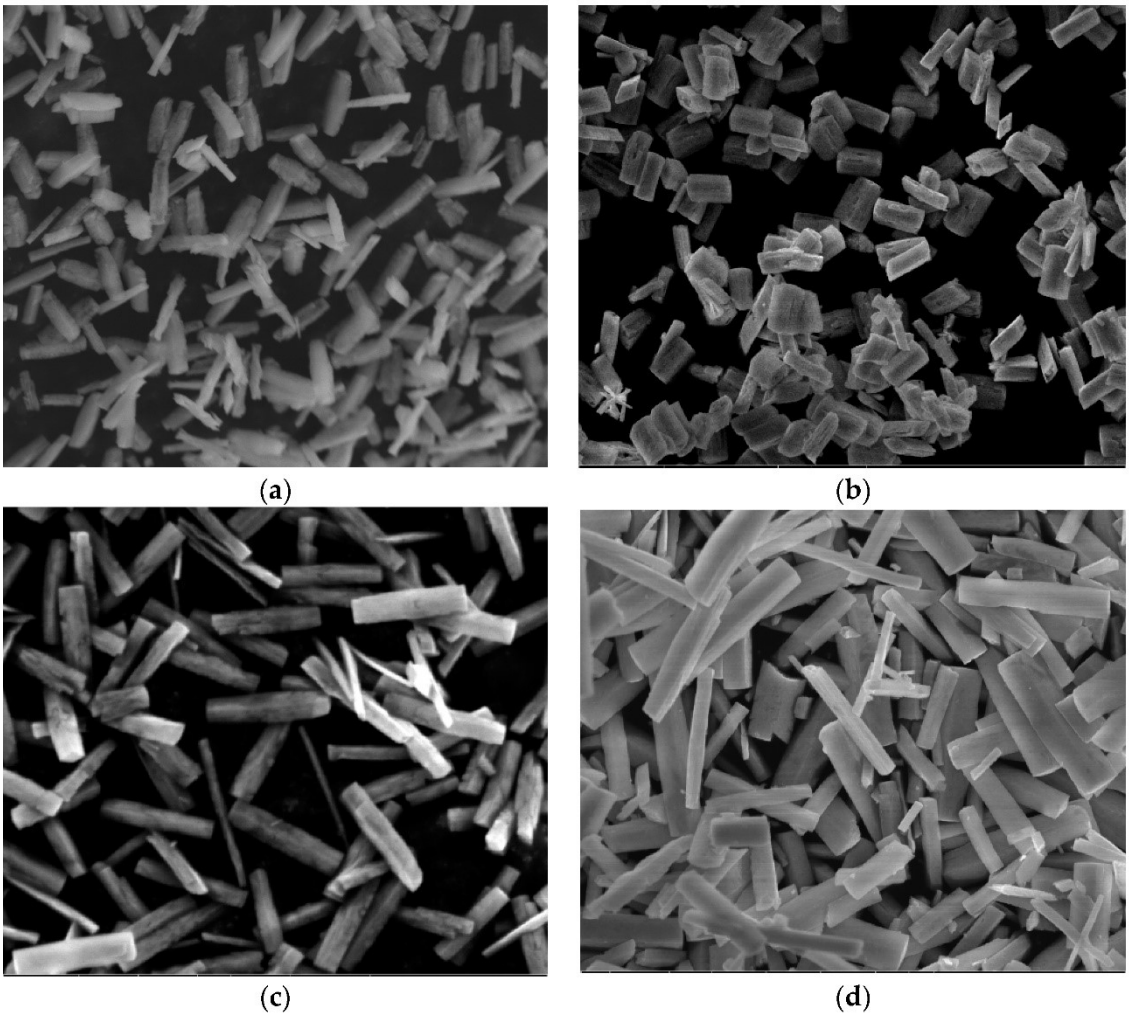

Figure 4.9: Different pictures of gallium oxide taken from [95]

After 100 cycles, only the gallium oxide structures are visible in the electrode, covering the full active area. There is also a strong carbon presence detected.

The SEM analysis allowed to conceive a hypothesis regarding the mechanism of this gallium-carbon electrode: Firstly, the gallium bulks are connected through the carbon particles that not only protect against further oxidation but also form a conductive path inside the electrode. When subjected to the electrolyte, the gallium aggregates at the surface. This is probably due to the low melting point of gallium that allows a biphasic state. As such, it migrates through the cracks until it is in contact with the electrolyte. After the first discharge, the gallium (III) oxide is formed leading to a decrease in the battery's potential. In the end, no more active gallium bulks are present.

The Ag_2O electrode was also analyzed. Still, as it was not the main novelty, and had already been approached in [43], it is not discussed with the same detail. The resulting SEM images are presented in figure 4.10.

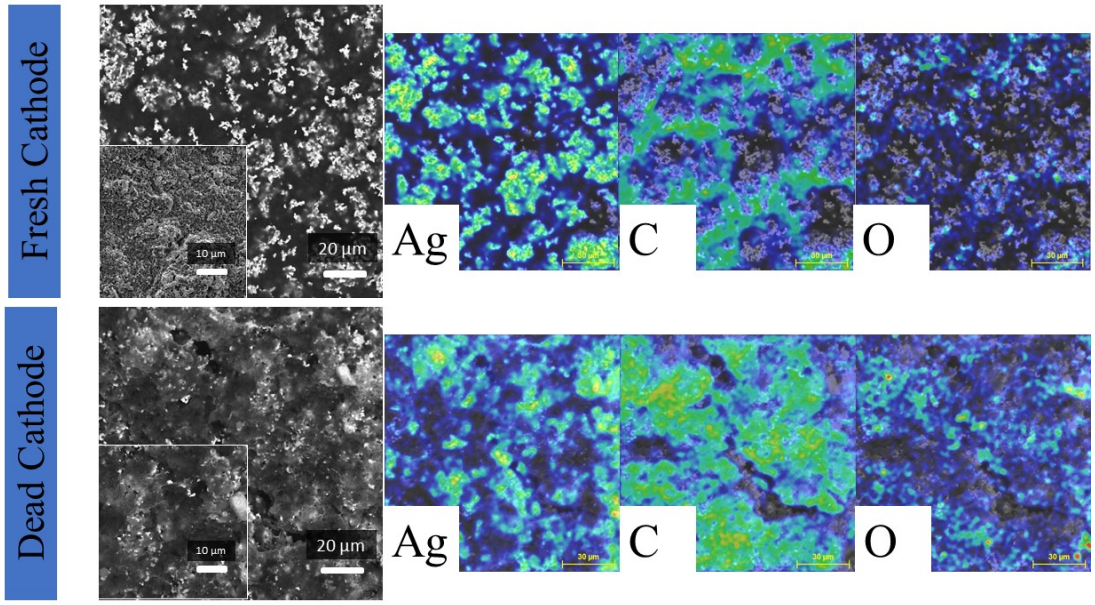

Figure 4.10: SEM analyzes of the cathode in a Ag-Ga battery

The main difference is the increase in the relative quantity of carbon and oxygen at the surface, pointing to the lack of active material exposed in the dead cathode.

4.5 Electrochemical Characterization

The electrochemical performance of batteries produced in this work, were characterized using the PGSTAT system. All batteries were sealed using an ecoflex 30 layer, to protect the hydrogel from changes on the electrolyte concentration, due to evaporation. Capacity values below $0.1\,mAh/cm^2$ were not taken into consideration, as they do not present any valuable significance.

Figure 4.11 presents the results from performing characterization on 6 stencil printed batteries between 0.8 V and 2.2 V. As previously mentioned, all batteries were discharged and recharged at 200 μA. The mean and standard deviation of the capacity in each cycle is shown in table 4.5.

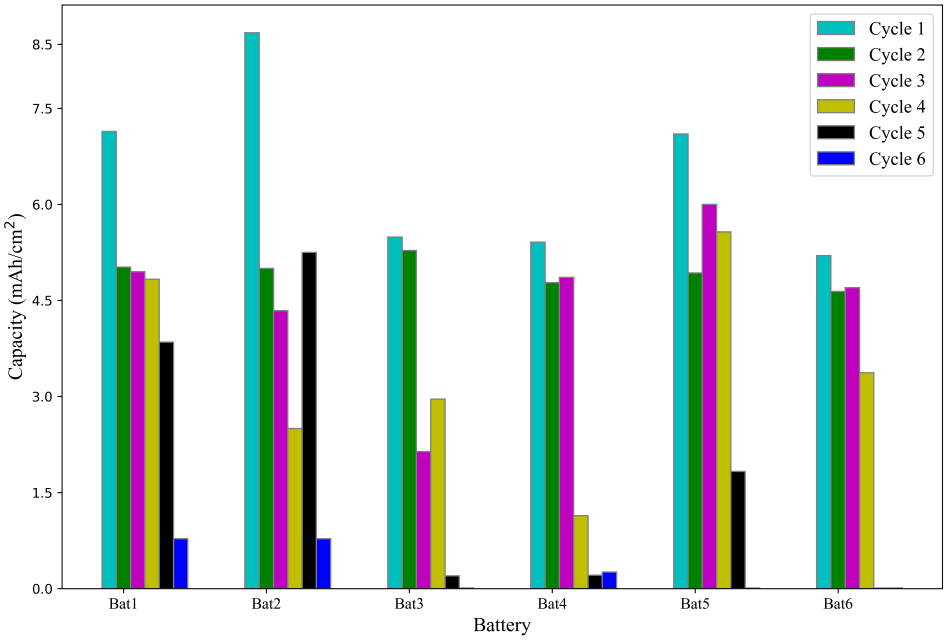

Figure 4.11: Electrochemical results for the silver-gallium battery

Table 4.5: Mean and standard deviation of the energy storage capacity of different cycles performed by the Ag-Ga batteries

Cycle	1	2	3	4	5	6
Mean (mAh/cm^2)	6.50	4.93	4.50	3.39	1.86	0.31
Standard Deviation	1.37	0.22	1.28	1.64	2.20	0.38

The first discharge capacity average obtained was (6.5 $\pm$ 1.37) mAh/cm^2. The batteries in generally obtained capacity values better than previous works in the first 3 cycles. They lasted between 4 to 5 cycles when discharging until very low voltages, which results in the rapid devastation of the battery. Later on it will be shown that, when reducing the charging/discharging time, the batteries can perform a considerably higher amount of electrochemical cycles.

Figure 4.12 shows the first cycle discharge profile, with a stable voltage plateau at around 1.7 V. Figure 4.12, which shows a first disparaging curve for the Ag-Ga battery, reveals an existing flatness in the voltage plateau observed. This is an important parameter, as the voltage of a battery is key to implement it in real life circuits.

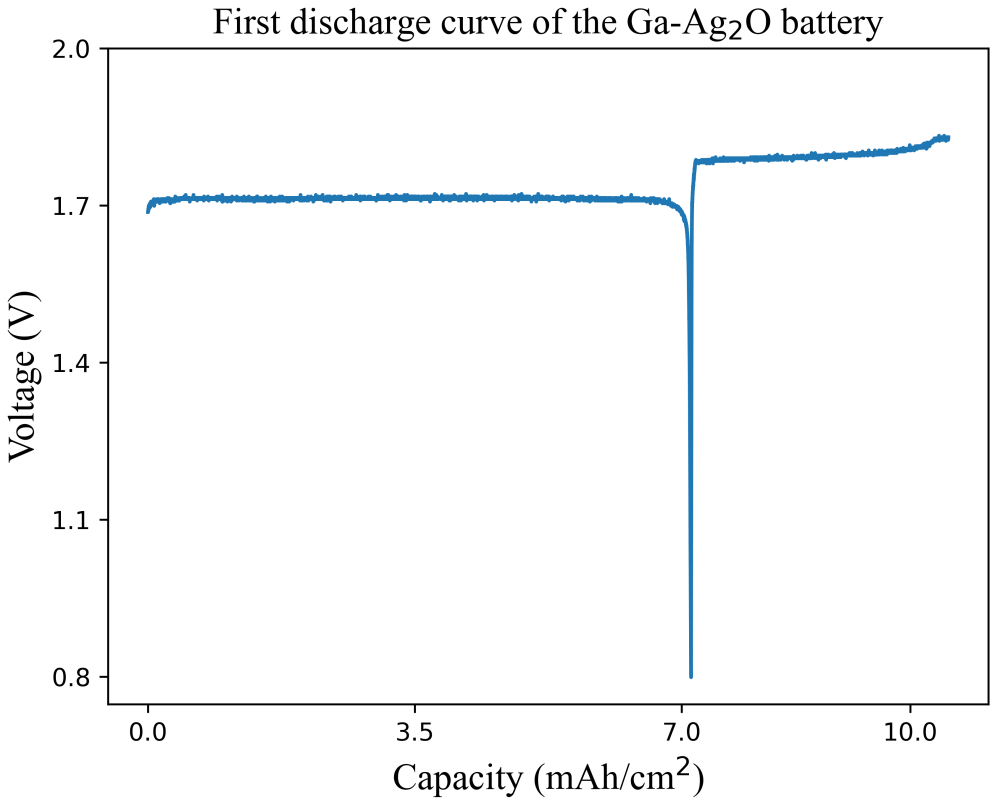

Figure 4.12: 1^{st} discharge curve for a silver-gallium batteries

4.5.1 Discharge at open circuit

After attaining the energy storage capacity, another important aspect to study is the discharging time at open circuit or discharge at zero load. Both gallium and silver, when in contact with the alkaline electrolyte, are exposed to corrosion. This consumes the active materials available, worsening its performance. As such, the self-discharge rate of the battery was studied, by attaining the discharge profile at zero load [96] [72].

In practical terms, this test represents the time that the battery can remain functional after fabrication and before being discharged.

Figure 4.13 exhibits the discharge curve at open circuit. The battery presented a durability of at least 13 days after fabrication. At this time, the battery was still presenting an operational voltage above 1 V. The abrupt decrease in the voltage after 150 hours could be related to some contamination happening in the electrodes.

The results represent a slight improvement on the latest work done in ISR [43], where only a 6 day autonomy was observed.

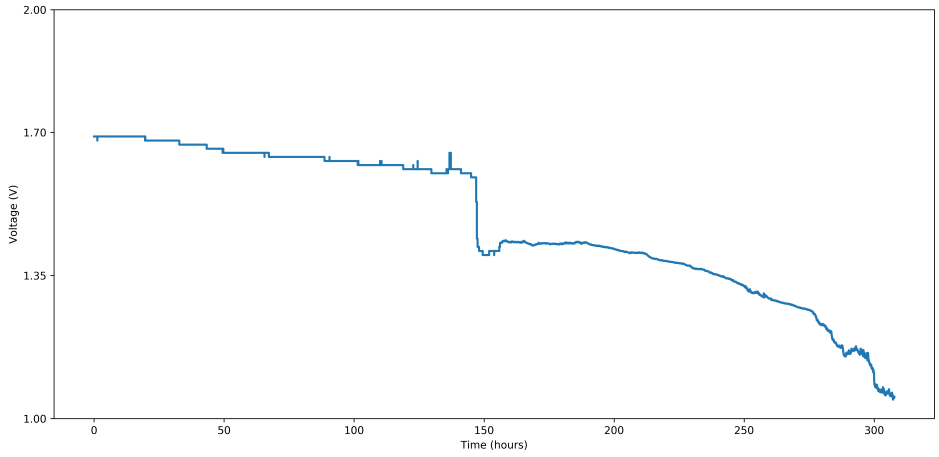

Figure 4.13: Discharge curve at open circuit

4.5.2 Performance at constant capacity mode

From equation 2.3, it is visible that the capacity is a product of the discharge current, and the discharge time interval. In several articles,like in [89], in order to analyze the ability of the battery to be recharged, low voltages as 0.8 V are not achieved. Instead, the batteries are placed under "constant capacity mode", where they are discharged at a constant current during fixed periods of time. For example, a battery that is discharged for 1h at 1 A it is discharging at a constant capacity of 1 Ah. Then, the batteries are charged at the same current during the same period of time.

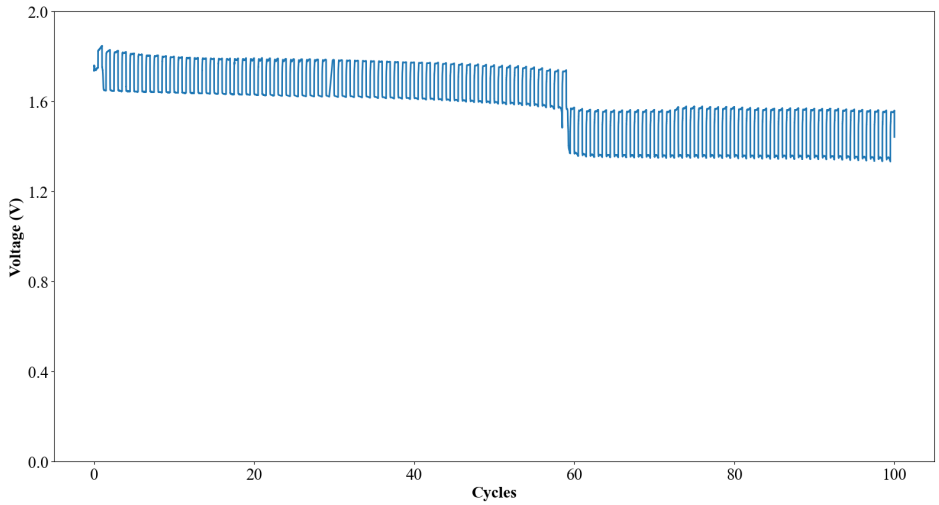

Figure 4.14: Discharge at constant capacity mode at 0.2 mA/cm^2

In order to characterize their rechargeability, and compare it with the SOTA, different batteries were fabricated, using stencil printing techniques, and characterized at 0.2 mA (figure 4.14) or 0.4 mA (figure 4.15) for 100 cycles. The duration of each cycle was of 40 minutes each. These parameters are the same used in [89]. Both batteries were able to perform the 100 cycles which allowed to confirm their rechargeability.

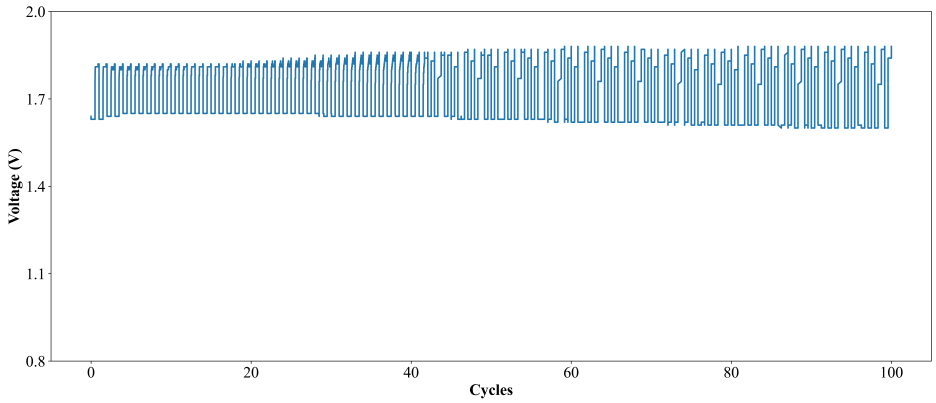

Figure 4.15: Discharge at constant capacity mode at 0.4 mA/cm^2

Another important aspect when characterizing these types of devices is the stability related to the voltage peaks. When applying different currents, the voltage peaks of charge and discharge changes. The smaller the variation, the more stable the battery is. This time, the discharge processes occurred at constant capacity for 40 minutes per cycle, with the current changing every four cycles. Four different currents were analyzed.

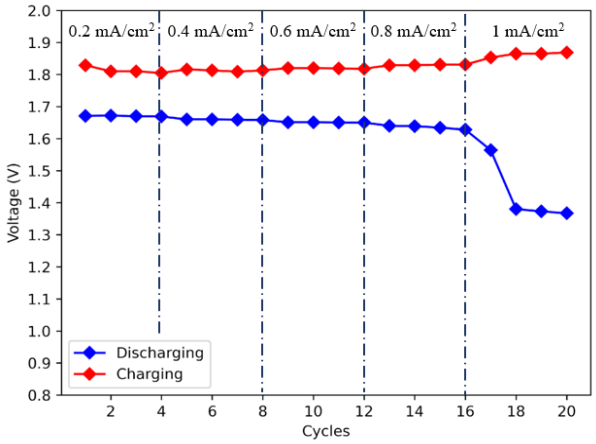

Figure 4.16: Charge and discharge peaks at constant capacity mode, displayed for 4 different currents.

We can see from figure 4.16 that, for stencil printed batteries, only when the current of 1 mA was reached there was an abrupt drop in the respective voltage, indicating the stability presented by the battery. These tests were conducted under small variations of current. The main reason was since the battery was performing more and more cycles, for a higher current than 1 mA, the life span of the battery could start to impact the results as well. The following section deals deeper with the phenomenons taking place at higher currents.

4.5.3 Internal Resistance

In every battery there is a difference when measuring the potential at an open circuit, caused by the chemical potential of both electrodes, and when current is applied. This is due to the internal resistance caused by the materials that constitute the battery.

The equivalent for the internal resistance consists of an external resistor in series with an "ideal battery" (R=0 Ω and V=VOC).

According to Ohm's Law (see figure 4.17a):

$$V = VOC + IR \tag{4.1}$$

Therefore,

$$R = \frac{\Delta V}{I} \tag{4.2}$$

ΔV corresponds to the difference between VOC and V (since the batteries are discharging at I<0).

A method to calculate the internal resistance was conceived in which the discharge current of the device varied from zero (discharge at open circuit) to different values. At every discharge, the tension dropped between the terminals as a consequence, enabling to calculate the internal resistance, following equation 4.4. The discharge current was between 0.2 mA and 10 mA.

The internal resistance of the battery varies between 85 Ω and 250 Ω (see figure 4.17).

4.6 Electromechanical Characterization

The electromechanical characterization was performed utilizing the Instron Machine. The batteries were encapsulated in order to contend the electrolyte. To do so, all the devices were sealed with a TPU layer. A temperature-based sealing method

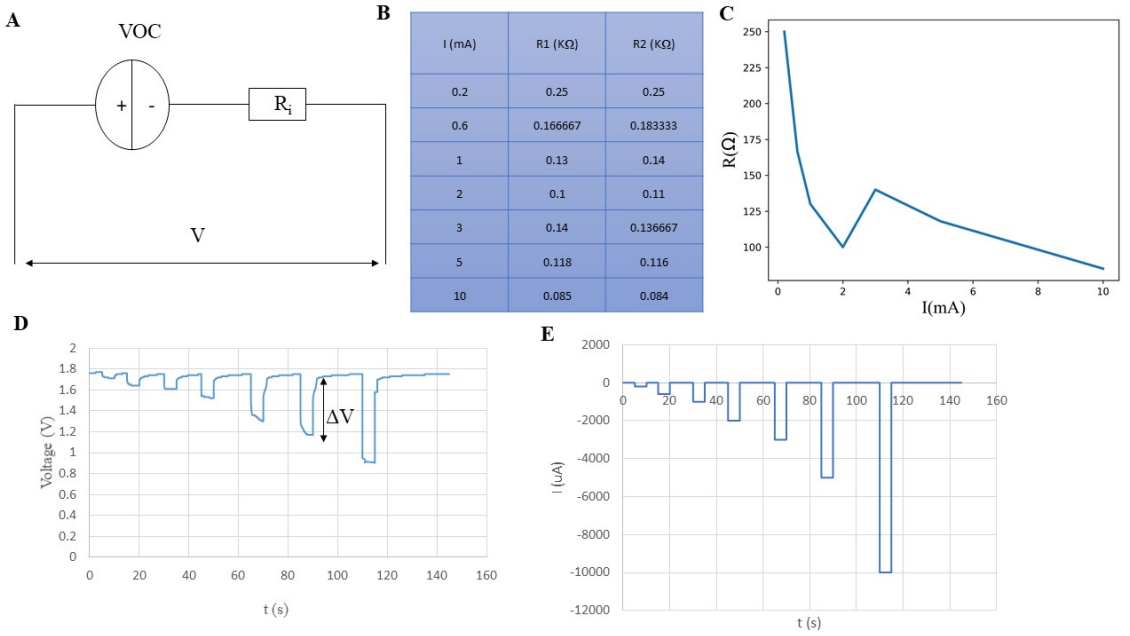

I (mA)	R1 (KΩ)	R2 (KΩ)
0.2	0.25	0.25
0.6	0.166667	0.183333
1	0.13	0.14
2	0.1	0.11
3	0.14	0.136667
5	0.118	0.116
10	0.085	0.084

Figure 4.17: a) Equivalent electric circuit for internal resistance; b) Internal resistance calculated for different currents using eq.4.2; c) Internal Resistance as a function of current; d) Voltage measurements at open circuit and different currents; e) Different discharge current applied as a function of time.

was applied, in which the high temperatures and pressure applied allowed for both TPU layers (sealing and substrate) to connect to each other. The substrates were cut in a dog-bone shape, that is a standard geometry used for electromechanical coupling characterization.

Three major characterizations were performed: Maximum tensile strength before failure, electrochemical characterization after 100 cycles stretching until 20% and electrochemical characterization after stretching until 100% once. The batteries were stretched at 500 mm/min in all experiments.

4.6.1 Maximum Strain Before Failure

In order to characterize the maximum strain prior to failure, a mechanical strain on the dogbone-shape battery was applied, while discharging it under 200μA current, and measuring the voltage between the electrodes. Figure 4.18 shows the results of this experiment. When the connections between the different layers of the battery are broken, the voltage decreases to zero.

As pointed out in figure 4.18 , there are two main points of interest. The first one is at around 50% - 60%, where a drop in the voltage is clear. This can be an indicator of the increase in the internal resistance of the battery. After reaching

133%, the battery fails. It was observed that the hydrogel had broke at this point. As such, my hypothesis is that the strain limitations are related to the maximum stretchability of the hydrogel. We can observe a maximum stretchability of 130%. This value represents an improvement on the SOTA, since most of the references report only values until 100% [89] [90].

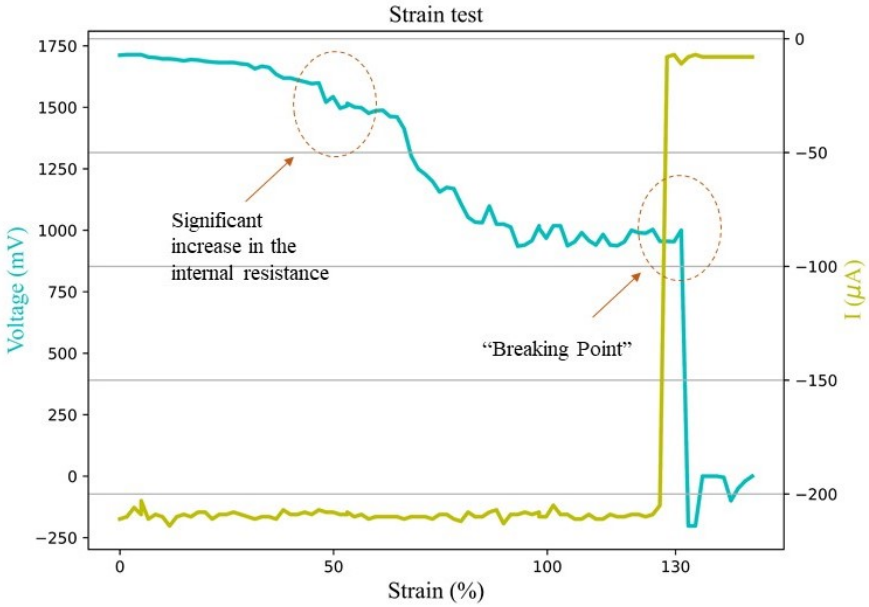

Figure 4.18: Ag-Ga behavior while stretching ad discharging at the same time, until reaching its maximum strain.

The decrease in the internal resistance was noted in a practical example, where a battery with two cells in series was fabricated to light a LED. If there was any voltage drop, the brightness of the LED would decrease, as it is visible in figure 4.19. This was realized when the battery were stretched to 60%, confirming the latest results.

4.6.2 Performing 100 strain cycles until 20%

The battery was first stretched 20% for 100 cycles, and then discharged. The results are presented in figure 4.20. As expected, there are some reduction in the performance of the battery, compared to the pristine battery. This is a little disappointing, due to the fact that some batteries have reported an increase in the electrochemical performance after stretching, [43] [81] and 20% isn't a very high value especially considering the maximum strain of this device.

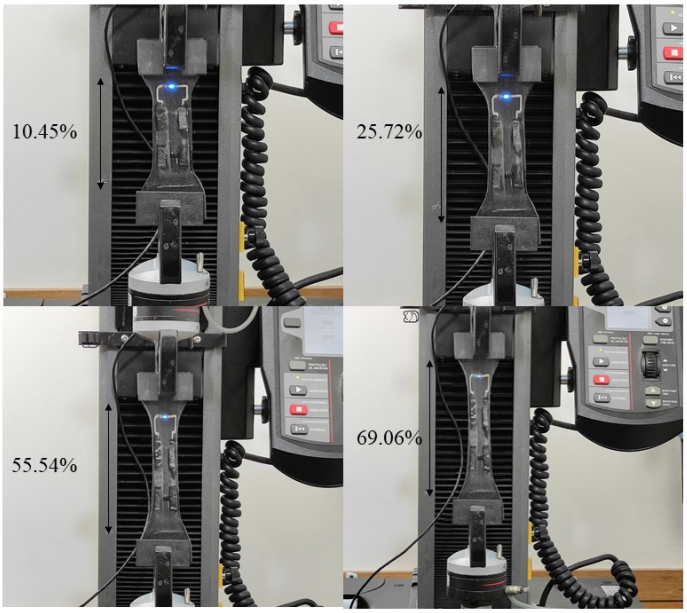

Figure 4.19: Stretching a battery and analyzing the brightness of the LED for each strain value.

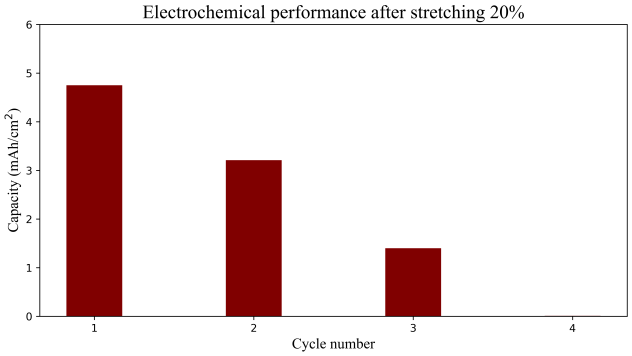

Figure 4.20: Capacity per electrochemcial cycle after stretching to 20%

4.6.3 Stretching to 100% once

The final electromechanical characterization consisted of stretching the battery once at 100%, followed by its performance of charging and discharging electrochemical cycles. Figure 4.21 shows the results of this test.

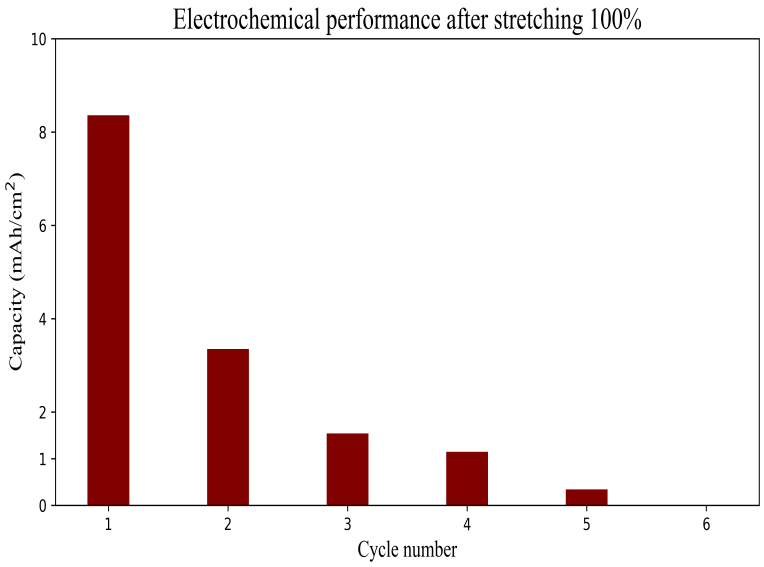

Figure 4.21: Capacity per electrochemical cycle after stretching to 100%

It is clear from these results, the average capacity in the first cycle increased to more than 8 mAh/cm^2. This is an interesting and somehow unexpected result. The improved capacitance of the battery, after large strain has been as well reported by Critina Leal [43]. Two possible reasons for this behavior are:

1. In the EGaIn-Ag-SIS CC, high strains causes the EGaIn droplets to break down, thus releasing more EGaIn into the microstruture.

2. The high strain results in reduced overall thickness of the battery, thus pushing the printed layers, and the electrolyte against each other, thus improving the interface between them.

Figure 4.22 compares both discharging profiles of a pristine battery and a stretched battery.

The same is not happening with 20% strain, maybe because at this strain microcracks are happening on the CC or electrodes, but the strain is not enough to cause any of the positive impacts that were discussed above.

4.7 Digitally printed batteries

Up to this point, all the results obtained only related to stencil printed batteries. Towards the final part of the project, the conducted studies were related with the impact of the fabrication technique (i.e. stencil printing vs. digital printing) on the areal capacity of the battery.

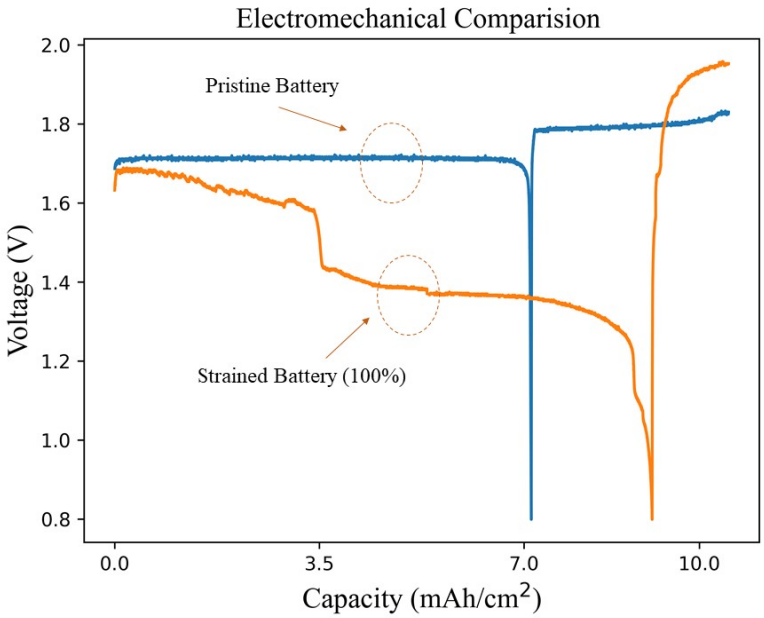

Figure 4.22: Comparison between first discharge curves of a pristine battery and a stretched battery until 100%

The design for the digitally printable batteries was made using the the Eagle Software that produced the Gerber files necessary to print in the Voltera. Figure 4.23 shows printing steps, using this technique.

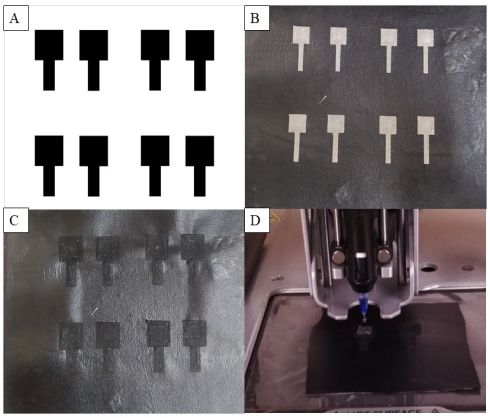

Figure 4.23: Digitally printing the batteries: a) Schematics on Eagle; b) Digitally printed first Current Collector; c) Digitally printed second Current Collector; d) Printing the gallium electrode.

Most of the synthesis of the different materials remained the same. The only change in the synthesis of the materials, consisted in altering the first CC to a formulation more suitable to print due to its physical properties. The new formula was the following:

- **Voltera EGaIn-Ag-SIS CC:** 1.5 g of 25%(wt) SIS solution mixed with 3.09 g of Ag '071 for 3 minutes at 2000 rpm. Afterwards, 6.18 g of EGaIn was added to the mixture and then mixed for 3 minutes at 2000 rpm.

This represented the first fully digitally printed Ag-Ga battery. The batteries were then characterized using the same techniques that were used for stencil printing. At this point, around 80% of the period of time to realize this project had passed, focused mainly on the Ag-Zn batteries and the stencil printed Ag-Ga batteries. As such, there were less tests regarding the characterization of the digitally printed Ag-Ga batteries. Nevertheless, the performed characterizations were enough to draw some important conclusions.

Figure 2.24 shows the capacity of the first discharging cycle of 6 digitally printed batteries. As it can be seen there is a significant increase of over 3 times in the areal capacity of digitally printed batteries, when compared to the stencil printed batteries.

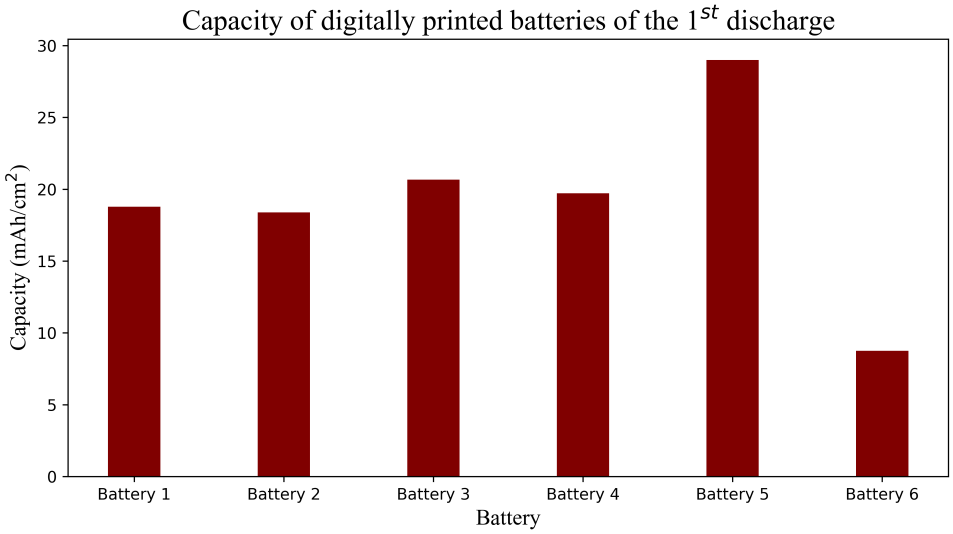

Figure 4.24: Capacity values for the first cycle of digitally printed Batteries

The reason for this difference is clearly observed in figure 4.25. The digitally printed electrode has considerably higher amount of gallium exposed in the surface, whereas the stencil printed electrode has considerably less gallium exposed. The reason for this seems to be related to the deposition procedure. During the stencil printing, a mechanical pressure should be applied to the material using a spatula. Considering that the gallium density is higher than the carbon, the applied pressure contributes to settling the gallium in the lower layers. When the deposition is performed by extrusion printing, the material keeps its homogeneous distribution.

In addition, with digital printing, we are able to print two layers of the electrode, without smearing the ink on the surface, which happened during our attempts for printing multiple layers via stencil printing.

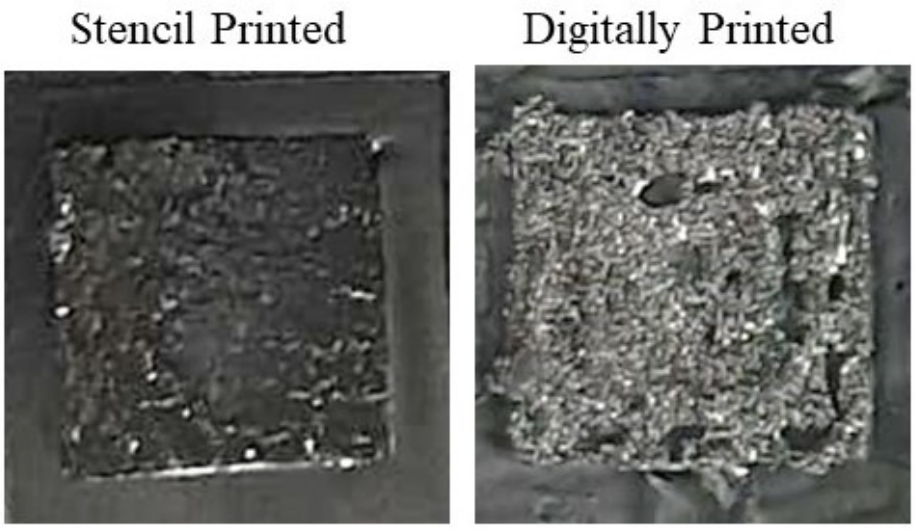

Figure 4.25: Comparison between a stencil and a digitally printed gallium electrode

Once the first discharge was completed, it seems that the battery was not rechargeable anymore. Nonetheless this seems to be related with a deficiency in the cathode electrode, and not the gallium electrode. In order to inspect this, I performed an experiment on a dead battery printed in the Voltera. After completing one cycle, the electrolyte was removed. Then, a new electrolyte was placed connecting a zinc plate (new zinc) to the silver electrode (old silver) and another placed connecting a silver oxide electrode (new Silver) over a conductive textile and the gallium electrode (old gallium). When measuring the potential, the old gallium - new silver combination presented a voltage of 1.6 V and the old silver - new zinc combination presented 0.6 V, revealing that the silver oxide electrode was no longer functional (see figure 4.26).

Also, when adding the total discharge time of both the stencil printed and Voltera printed batteries we can notice that they amount to almost the same. For instance, if we add the total capacitance of all charging and discharging cycles of table 4.5, for stencil printed batteries, we reach to an overall capacity over all cycles of

21.49 mAh/cm^2. In a digitally printed battery, this whole capacity is drained in the first cycle.

All in all, the digitally batteries still present useful functionalities, especially in disposable recyclable patches of one usage only.

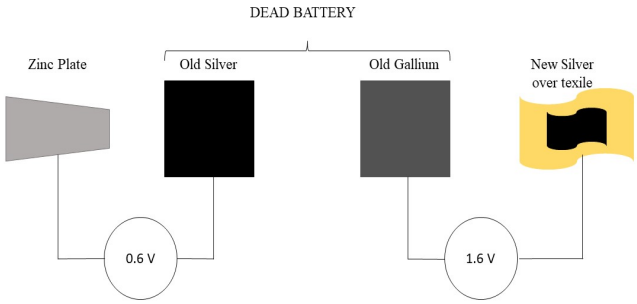

Figure 4.26: Schematic presenting the analysis performed on a discharged digitally printed battery. By fabricating fresh electrodes and connecting them to the battery it is clear that the silver cathode is the first one to lose functionality after one cycle.

Figure 4.27 presents the results of the electrochemical characterization at constant capacity mode (see section 4.5.2), comparing both printing methods at the same time. It is interesting that, when increasing the power, the digitally printed battery shows a more stable behavior compared to the stencil printed battery.

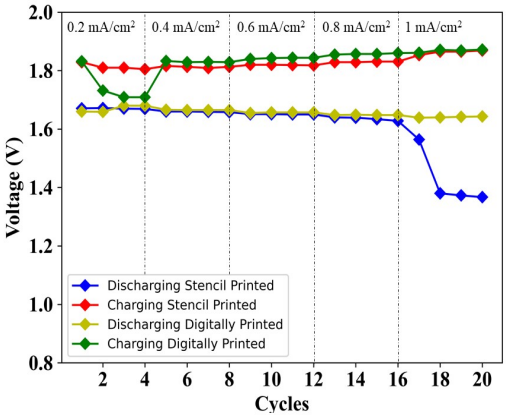

Figure 4.27: Charge and discharge peaks at constant capacity mode, displayed for 4 different currents. Both stencil and digitally printed batteries were included in this graphic.

4.8 Applications - Case Study

As a final section of this chapter, two different applications were conceived in order to show the functionality of the batteries. They focused on two very important practical parameters: Scalability and integration in wearables. At the beginning of this dissertation, these two aspects were highlighted, and several articles on the SOTA of showed the importance of integrating energy storage devices.

4.8.1 Scalability

In order to show the scalable and autonomous fabrication of the printed Ag-Ga battery, and their applications, 2 multi-cells batteries with 6 cells each in series and parallel (Figure 4.28) were designed and printed. As can be seen here, all 4 materials are digitally printed: The two CC layers and the two electrodes. The first CC layer, the EGaIn-Ag-SIS ink, is also used for printing the interconnects between the batteries and the SMD LEDs. In this way, we are able to connect the battery cells in series, and parallel using printed lines, in order to adjust the output power for the required applications. This can be extended to printing electrodes, sensors, and antennas at the same time with the batteries.

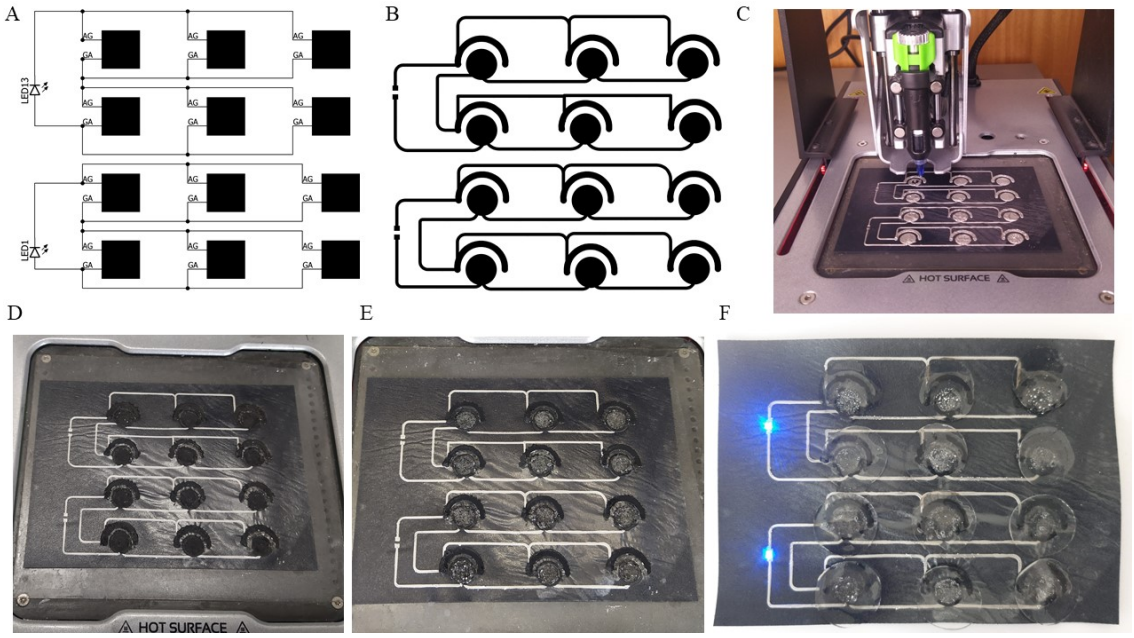

Figure 4.28: a) Schematic of the multi-cell battery (designed in Eagle); b) Design with the shape of the multi-cell battery and the interconnects; c) Digitally printing the first current collector; d) Digitally printed second current collector; e) Digitally printed electrodes; f) Application of the hydrogel revealing that the multi-cell battery was operational.

Figure 4.29 shows the battery under different motions like stretching or bending. The LED stayed turned on during the different mecanhical deformation movements, meaning the batteries were able to sustain morphology deformation.

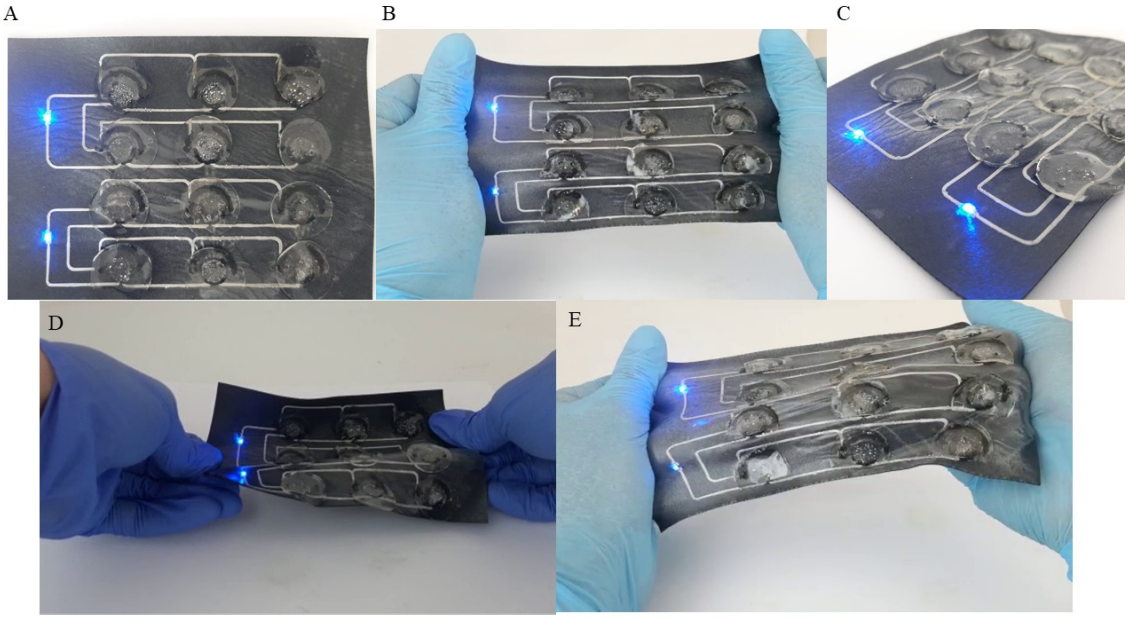

Figure 4.29: Different stretching motions applied on the battery:a) Pristine Battery; b) Stretching; c) Different viewing angle; d) Bending; e) Random morphology applied in the battery by stretching the battery with high strength.

4.8.2 The Wow Belt

The Wow Belt is a solution being developed in ISR for measuring biopotentials in patients. It possesses an ECG, a temperature and a breathing sensor. Despite having all of these sensing capabilities, for this experiment, only the ECG was used. The circuit requires at least 2 V to function. The final objective of this device is to be used in hospital scenarios, allowing a constant monitoring of the vital signals of the patient without any discomfort.

In order to meet such energy requirements, two batteries in series were fabricated. This time, a much simpler design was made. There was a question on how to transfer the battery to the belt. Initially, since the belt was printed over TPU and textile, it seemed that the most obvious solution would be to print the battery directly onto the belt. Despite being the least complicated one, this method could present a disadvantage: If there was to be a problem in the fabrication of the battery, it would not be easy to remove it and redo it. One would have to fabricate a new belt every time a new battery was fabricated. As such, the energy storage system should

Figure 4.30: Schematic presenting end of the "WoW Belt"

be fabricated separately and transferred to the belt.

The procedure implemented was to print the battery in a polyvinyl alcohol (PVA) composite substrate over a PC layer.

The battery was printed "backwards": First the electrodes, secondly, the CB-SIS CC and, in the end, the EGaIn-Ag-SIS CC and the interconnects were printed. Afterwards, a SIS substrate was applied on top using the thin-film applicator. The SIS substrate was fabricated by mixing SIS with toluene with a weight ratio of 1:2 (see chapter 3).

After the SIS substrate was cured, the PVA was detached from the PC and placed over water for 3 hours. Since PVA is soluble in water,this layer was removed and the active material was exposed.

The integration of the battery on the belt was assisted via a transfer method, using Transfer Tatoo Papper (TTP). The TTP was, firstly, attached to the top of the TPU, gently pressed and peeled off right after, leaving a layer of glue on its surface. Next, the battery was put onto this layer interfacing the belt. Finally, the hydrogel was placed on top of the electrodes and a layer of tegaderm was used as sealing mechanism, sticking to the SIS substrate. In the end, the terminals of the battery were connected with the ECG's, using a small stencil to print the interconnects. Figure 4.31 shows the different steps to fabricate this battery and its respective integration in the belt.

After sealing the battery, the belt was attached to the chest and gather signals of heart rate for 10 minutes. The results prove to be a success, as the Bluetooth modulus functioned well, communicating with the mobile phone, as we can see in figure 4.31.

Afterwards, the battery was kept working, as the belt was collecting data for around 22h. While this period of time is quite an interesting energy autonomy, in fact, based on our calculations, the battery had to provide enough energy for around

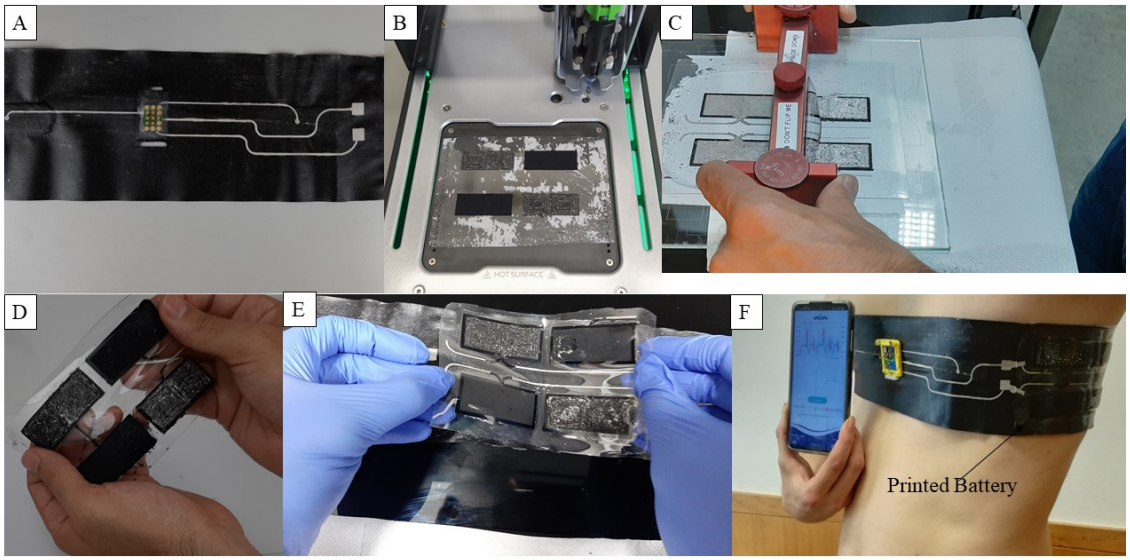

Figure 4.31: A very practical application of stretchable batteries: a) The fabricated WoW Belt; b) Digitally printing the battery; c) Placing the SIS substrate using the thin-film applicator; d) Battery after dissolving the PVA in water; e) Placing the battery on the Wow Belt; f) Operational WoW Belt functioning using a digitally printed Ag-Ga battery.

around 200 hours of operation, since the area of the electrodes was 10 cm^2. In order to investigate the reasons for the reduced capacity, the literature was studied, and we found that the problem was initiated from putting two batteries in series. As also explained in [97], when putting two batteries in series, both batteries should have a perfect matching internal resistance. Otherwise, one battery can "consume the charges of the other battery". As a matter of fact, even when connecting industrial batteries in series, it is important to be of the same fabricator, since factors like capacity, voltage, age and others, need to be balanced in order to ensure a normal discharge.

Nonetheless, despite not being optimized, the battery set still worked for a decent amount of time, already implementable for these belts, which are meant to work for 1 day. Another important aspect demonstrated is the versatility in terms of the different substrates in which the battery can be printed, other than TPU over textile. The fact that the battery was also made separately from the belt and could be removed once it was no longer functional, showed the practical aspect of the fabrication method, as a battery can be replaced without needing to fabricate a new belt.

4.9 Summary of the Results

This chapter focused on the results obtained during the investigation on stretchable batteries. In the beginning, in order to learn the working process, fabrication, and characterization of the batteries, the previous work made by Cristina Leal was reproduced. With the goal of attaining a fully printable battery, attempts towards fabricating a zinc-based conductive composite were put into work. However, they did not prove to be successful. As a result, the properties of gallium were explored.

When starting to study the usage of this new material as anode for a battery, various composites of gallium and carbon were synthesized and characterized. The increase of carbon quantities seemed to increase the conductivity of the electrode but resulted in a lower capacity. When no carbon was applied the electrode did not conduct any current.

Afterwards, the comparison between using gallium bulks or particles was explored. The first ones proved to be more successful. After the SEM analysis on this new electrode, the behavior of gallium became more clear. After contact with KOH there was an increase in the exposure of the active material to the surface, that was being turned into gallium oxide during the charge and discharge process until no more active material was available.

During the electrochemical and electromechanical characterization, the stencil printed batteries exhibited an average capacity of 6.5 mAh/cm^2 on the first cycle, a maximum stretchability of 133% and internal resistance of 85 Ω-250 Ω. The tests of cycle performance showed that the battery was able to perform 100 cycles both at 0.2 mA and 0.4 mA. After stretching 100 times until 20%, the capacity seemed to decrease. However, when stretching until 100% for 1 time, the reverse effect took place and the battery's capacity increased. Digitally printed batteries, on the other hand, showed a very high first discharging capacity of 19.22 mAh/cm^2 but did not show any sign of rechargability. Still, this was not due to the gallium electrode. Instead, the Ag_2O cathode was not functional after the electrocehmical cycle.

Finally, two applications were demonstrated. The first application was a simple demonstration of a multi-cell printed battery, interfaced with some LEDs. Using digital printing, one can tailor-make the required current/voltage by freely connecting printed battery cells in parallel or serial configuration together. After bending and stretching the batteries still worked, confirming the stretchability of the digitally printed devices. The second application revealed an end of the printed batteries for wearable biomonitoring and e-textiles, by implementing them in a wearable called the "Wow belt", that collected vital signals using an ECG. Both cases showed the

advances and importance of making a digitally printable stretchable battery.

Chapter 5

Conclusions and Future Work

The main objective of the work was to continue the previous study from the team on stencil printed Ag-Zn batteries [43], and improve it in terms of fabrication by moving towards digital printing. However, during the dissertation a new idea was suggested, which consisted in replacing the zinc with gallium as the anode. Theoretically, Ga-based anodes should present a higher energy storing capacity compared to the Zn electrode, and the low melting temperature of gallium could be exploited for improved functionality. Therefore, there was focus given to the synthesis of a printable gallium-based conductive composite, which resulted in the synthesis of the Ga-CB-SIS electrode. This, combined with digitally printable current collectors (EGaIn-Ag-SIS and CB-SIS) and an Ag_2O-SIS electrode, resulted in the fabrication of a fully digitally printed stretchable battery, which, to the best of our knowledge is the first report of such implementation. By attempting different methodologies and fabrication techniques, it was possible to achieve the goal of this project.

Figure 5.1 compares the results obtained during this project with the SOTA on printed stretchable thin-film batteries. Note that none of the previous works in this graph are digitally printed, and only our work is fully stencil-free and digitally printed. It is clear that, despite some improvements being needed, the data obtained looks promising.

The power density per area (in Wh/cm^2) of the battery can be achieved by multiplying the average capacity and the voltage. For stencil printed batteries it equals $6.5 \times 1.7 = 11.05$ mWh/cm^2, whereas for digitally printed batteries, assuming a discharging plateau of 1.2V (see appendix VII), it corresponds to $19.22 \times 1.2 =$ 23,06 mWh/cm^2. Both results, when comparing with the values from figure 2.3, represents a step closer to the commercial coin cells (50 mWh/cm^2).

In summary, during this project I was able to discover a method of creating a conductive Ga-CB-SIS composite that can be used as an anode for a Ag-Ga bat-

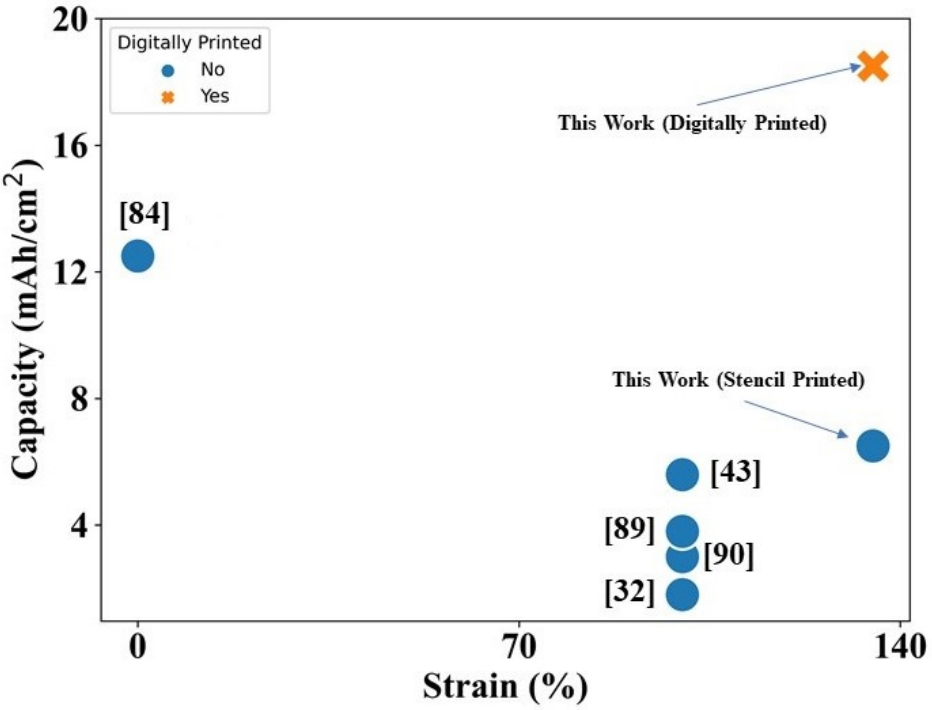

Figure 5.1: Position of the battery compared to the State of the Art

tery. The batteries can be printed using both stencil printing (presenting an energy storage capacity of 6.5 mAh/cm^2) and digitally printed (increasing the energy storage capacity up to 19.22 mAh/cm^2). The battery is rechargeable and was able to perform 100 cycles at 0.4 mA/cm^2. The electromechanical characterization revealed a maximum strain of 130%.

5.1 Future Works

In this section, I summarize possible improvements and studies that are interesting to explore, but weren't possible to perform within the time frame of this dissertation;

- **Constitution of the electrodes:** Throughout this project, several references were made regarding the corrosion mechanisms in the electrodes, especially the silver electrode. One article has addressed this problem, for the gallium electrode, by using gallium alloys, claiming also higher stability. [89] had already used indium as well, claiming it helps delaying the corrosion. Calcium chloride was studied to further improve the stability of the anode and the battery. Regarding the silver oxide electrode, since it is the first one to lose functionality, special focus should be given to it. As previously mentioned, attempts

to integrate copper and gold particles can lead to better results;

- **Optimized Electrolytes:** This dissertation used the same electrolyte for both electrodes. However, in the SOTA most of the batteries use different electrolytes for each electrode. For the gallium electrode especially, different KOH concentrations could be studied.

- **Architecture:** A vertical assembly could be experimented. Sandwiched structures could improve the results, as the distance travelled by the ions is reduced.

- **Digital Fabrication:** As we were able to see in the latest part of this dissertation, there is still further work needed when exploring digitally printed batteries. This project only briefly approached it as a demonstration, but work on optimizing the different printing parameters still needs to be addressed. Also, exploring and characterizing in greater detail these batteries could give further insight into the different electrochemical results (for example, by means of performing SEM analysis).

- **Different cell combinations:** As seen in the example with the WoW belt and in the SOTA, applying batteries in series can prove to be a challenge. Exploring mechanisms to improve and optimize these combinations can be interesting and useful. However, this seems a difficult task, as already commercial batteries are dealing with this situation.

In conclusion, this dissertation showed for the first time, a fabrication method for a digitally printable novel silver-gallium battery with two current collectors. This battery was stretchable and presented good energy storage capacity numbers compared with the existing SOTA, combined with new fabrication techniques.

As a result, since this represented a first attempt at fabricating a gallium-based battery in ISR, the work performed can be considered successful and can lead to further investigation moving forward.

Appendix I

The calculations for the overall reaction of the battery

This section is meant to give a justification for equation 2.9, having as a starting point equations 2.7 and 2.8.

For the cathode half reaction, multiplying by 3 equation 2.7:

$$3\,Ag_2O + H_2O^+ + 6\,e^- \longrightarrow 6\,Ag + 6\,OH^- \tag{I.1}$$

Finally, the half reaction of the anode, multiplying by 2 the equation 2.8:

$$2\,Ga + 12\,OH^- \longrightarrow 2\,{GaO_3}^{3-} + 6\,H_2O + 6\,e^- \tag{I.2}$$

By adding both equations, we arrive at equation 2.9:

$$3\,Ag_2O + 2\,Ga + 6\,OH^- \longrightarrow 6\,Ag + 2\,{GaO_3}^{3-} + 3\,H_2O \tag{I.3}$$

Appendix II

Thermodynamic equilibrium state of open circuit potential (OCV)

This section contains the theoretical explanation for the voltage measured between the terminals. A battery's voltage represents the difference between the electrochemical potential of the cathode and the anode. In order to calculate them, using the Nerst equation one needs to use the Gibbs formation energy and the standard potential of both reactions.

Table II.1, taken from Factsage 7.3 (Education Version), presents the Gibbs formation energy for every molecule present in the discharging process.

Table II.1: Gibbs formation energy

	GaO_3^{3-}	Ga	OH^-	e^-	H_2O	Ag	Ag_2O
ΔG_f(J/mol)	-603803	-12176	-226744	-4.8×10^9	-342180	0	-11210

$$\Delta G^o_{anode} = \Delta G^o_{products} - \Delta G^o_{reactant} \tag{II.1}$$

$$\Delta G^o_{anode} = \Delta G_f(GaO^{3-}-3)+3\Delta G_f(e^-)+3\Delta G_f(H_2O)-[\Delta G_f(Ga)+6\Delta G_f(OH^-)] \tag{II.2}$$

Hence, by replacing the values with the ones presented in table VII.1:

$$\Delta G^o_{anode} = -401703 J/mol \tag{II.3}$$

Since,

$$E^o = -\frac{\Delta G^o}{nF} = \frac{401703}{3\times 66485} = 1.38 \tag{II.4}$$

According to the Nerts Equation:

$$E_{anode} = E^o + \frac{RT}{nF} \times ln(10) \times log\frac{[GaO_3^{3-}]}{[OH^-]^6} \tag{II.5}$$

$$E_{anode} = 1.38 + \frac{8.314 \times 298.15}{3 \times 96485} \times ln(10) \times log\frac{[GaO_3^{3-}]}{[OH^-]^6} \tag{II.6}$$

$$E_{anode} = 1.38 - 0.1182pH + 0.0197log([GaO_3^{3-}]) = 1.38 - 1.773 + 0 = -0.39 \tag{II.7}$$

Note that

$$POH = 14 - pH = -log[OH^-] = 14 - (-1) = 15 \tag{II.8}$$

Also:

$$log\frac{[GaO_3^{3-}]}{[OH^-]^6} = log([GaO_3^{3-}]) - 6log([OH^-) \tag{II.9}$$

This was calculated for 10 M concentration of KOH.

For the cathode the calculations followed exactly the same process:

$$\Delta G^o_{cathode} = \Delta G^o_{products} - \Delta G^o_{reactant} \tag{II.10}$$

$$\Delta G^o_{cathode} = 2\Delta G_f(Ag) + 2\Delta G_f(OH^-) - [\Delta G_f(Ag_2O) + 2\Delta G_f(e^-) + \Delta G_f(H_2O)] \tag{II.11}$$

$$\Delta G^o_{cathode} = -4098 J/mol \tag{II.12}$$

$$E^o = 0.0212 \tag{II.13}$$

$$E_{cathode} = 0.0212 + \frac{8.314 \times 298.15}{2 \times 96485} \times ln(10) \times log[OH^-]^2 \tag{II.14}$$

$$E_{cathode} = 0.0212 + 0.05913pH = 0.90815 \tag{II.15}$$

In order to normalize the equation, there is the need to multiply this value by the ration between electrons consumed and produced in the reaction:

$$E_{cathode} = \frac{N_{electrons}(anode)}{N_{electrons}(cathode)} \times E_{cathode} = \frac{3}{2} \times E_{cathode} = 1.3622 \tag{II.16}$$

Finally, we arrive at the battery's voltage (at open circuit):

$$E_{total} = E_{cathode} - E_{anode} = 1.3622 - (-0.39) = 1.75V \tag{II.17}$$

Appendix III

Fabrication of the Hydrogel

The fabrication of the electrolyte was based on a previous dissertation conducted in ISR by Tatiana Patrício called "Hydrogel-PDMS conjunctions for Biomonitoring Patches". In this section, the process to make the hydrogel is briefly explained.

Firstly, 30 mL of water were placed in a glass with a magnetic stirrer. 0.732 g of sodium alginate were added. Once it was completely dissolved, 0.006 g of Methylenbisacrylamide (BIS) and 4.5 g of acrylamide were added and dissolved completely as well.

The second step consisted of placing the resulting solution in a vacuum with the stirrer underneath. The main goal was to remove the air bubbles. Once there were little to no bubbles, the stirrer would be turn off. At the end, when the final bubbles had burst, the solution was removed from the vacuum.

Afterwards, separately, 0.0492g of irgacure and 0.0646g of calcium sulfate were weighed and placed on a syringe with 1mL of water. In a separate syringe, 20 mL of the previous solution were removed without air (as much as possible).

Using a proper adaptor, the materials were transferred from one syringe to the other without any air entering the mixture.

In the end, the final result was deposited in a glass with a PDMS or a Dragon Skin mould and pressed using another glass.

After being one day under UltraViolet (UV) light, the final product was placed in the KOH solution. The following image shows the final result:

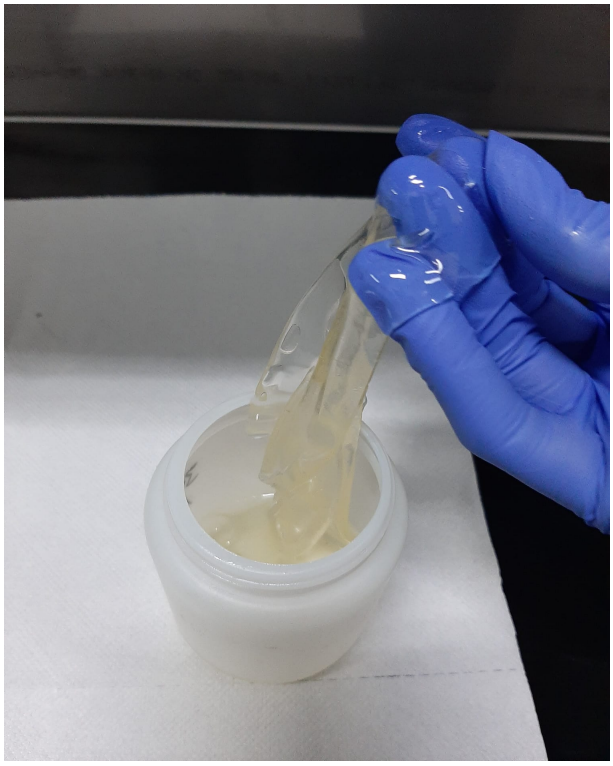

Figure III.1: End result of the fabrication of the Hydrogel

Appendix IV

Hardware explanation: Potentiostat/Galvanostat characterization system - PGSTAT

During the realization of this project, an instrument to characterize the batteries was developed. Although the PalmSens4 was able to perform this task, only one battery at the time could be characterized. As such, in order to perform tests on several batteries, the PGSTAT system was developed in ISR. A potentiostat controls the voltage and a Galvanostat controls the current.

Based on an article, [98], using a Programmable System on Chip from Cypress Semiconductor Corporation, the PGSTAT was fabricated. Despite the article mentioning a reference electrode, at the beginning of this project, only 2 electrodes were being used and the reference was considered the ground. The processor has an Analog to Digital Converter (ADC) that needs a 5 V voltage to function. In order to do so, a board with a chip that provided 5 V from a USB port was utilized. Despite improving the capacity of characterizing several batteries at once, some optimizations still were needed.

As we can see in figure II.1, taken from Cristina Leal's dissertation, the reference voltage of 5 V was external to the boards and common to all of them. This presented two problems. The first one was related to space and practical utilization. Every time a new board was added, new wires and soldering created more confusion in the setting. For around 4 PCBs it would be rather easy to function, but for 12 boards, more complicated and "messy" systems would be an issue. Secondly, it was observed that if any one of the batteries would have a problem, or a different code was applied, it could affect the performance of the other PCBs as well.

To solve these issues, a new design was conceived that directly placed an indi-

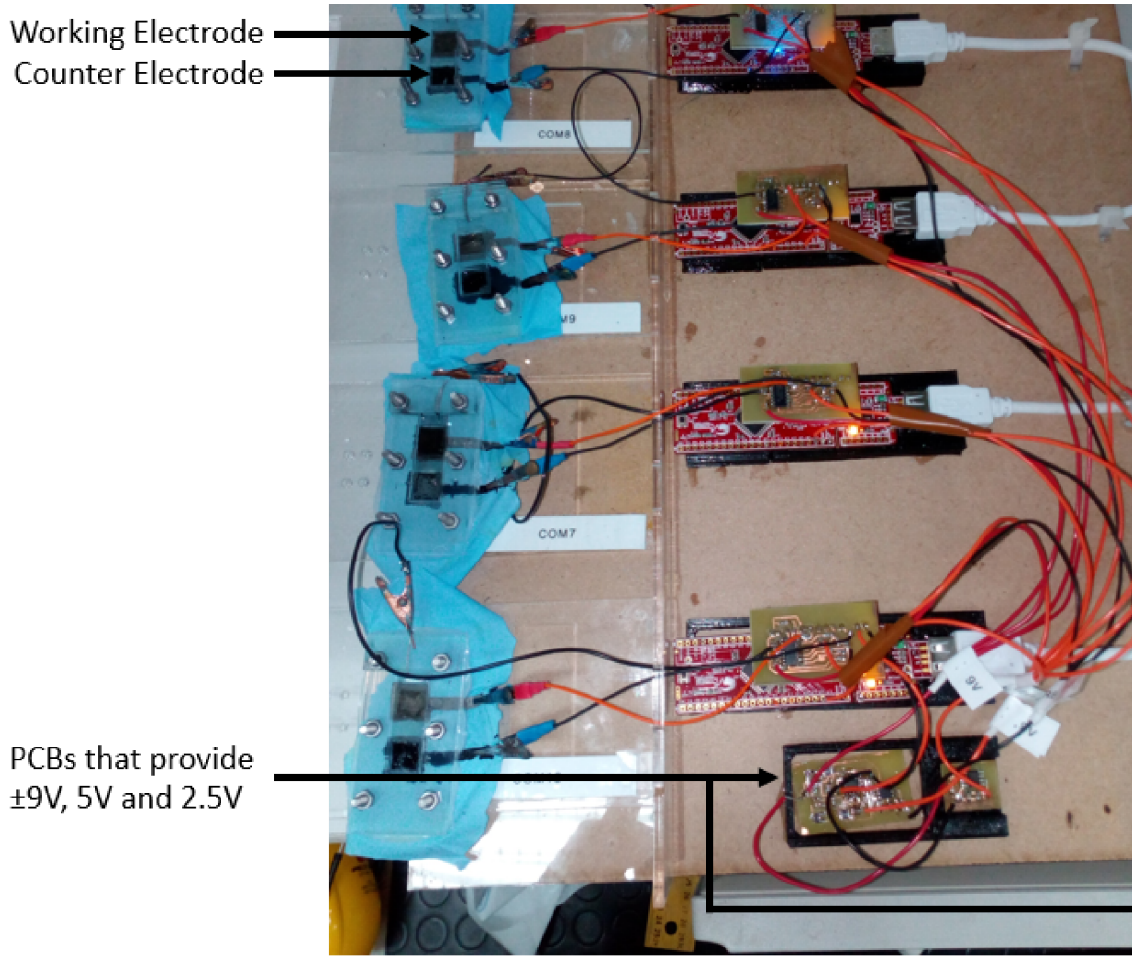

Figure IV.1: An image taken from Cristina Leal's dissertation, "Stretchable silver-zinc based Battery - A Novel Fabrication Method", from the initial PGSTAT system

vidual reference voltage on top of every board (see figure II.2). The new PCBs were designed using Eagle software.

The system read the voltage between the electrodes and, using a current generator, the firmware allowed to control the value and direction of the current in the range of 0-618 μA. This was key in the constant current charging and discharging. For the constant voltage charging a control variable was used, which would control the distance and value of the current, according to the difference between the voltage of the battery and the constant voltage set value.

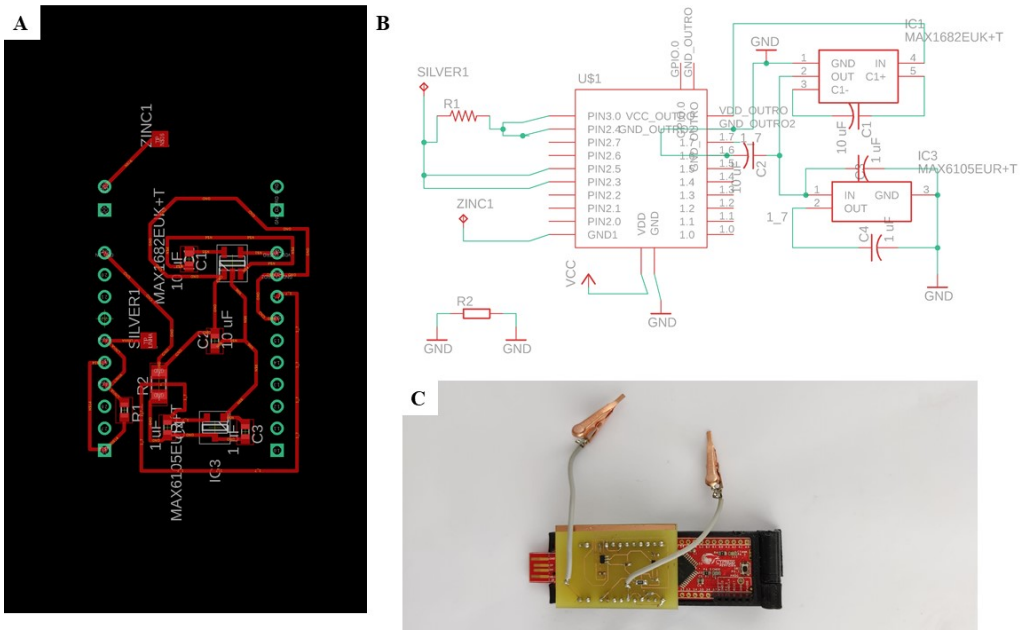

Figure IV.2: a) Board of the optimized PGSTAT System (from Eagle); b) Schematic of the optimized PGSTAT System (from Eagle); c) Optimized PGSTAT System

The code exported the values of the variables with the voltage, current and cycles, among others, to a log file that were analyzed in a python script created to retrieve automatically the capacity values for each cycle.

The following image presents the state machine of the PGSTAT:

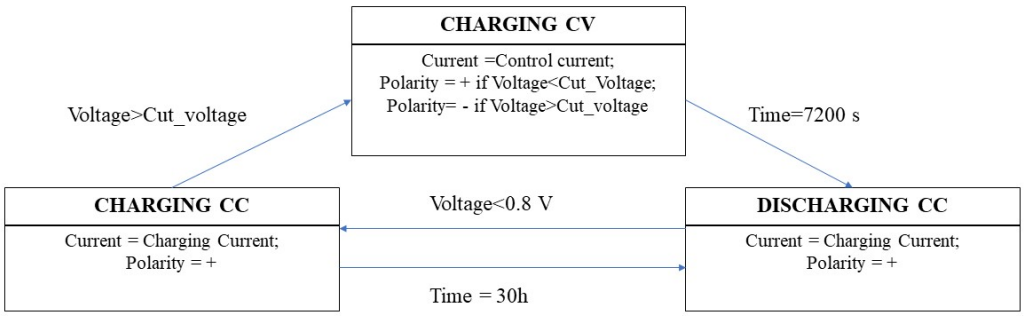

Figure IV.3: State Machine for the PGSTAT system

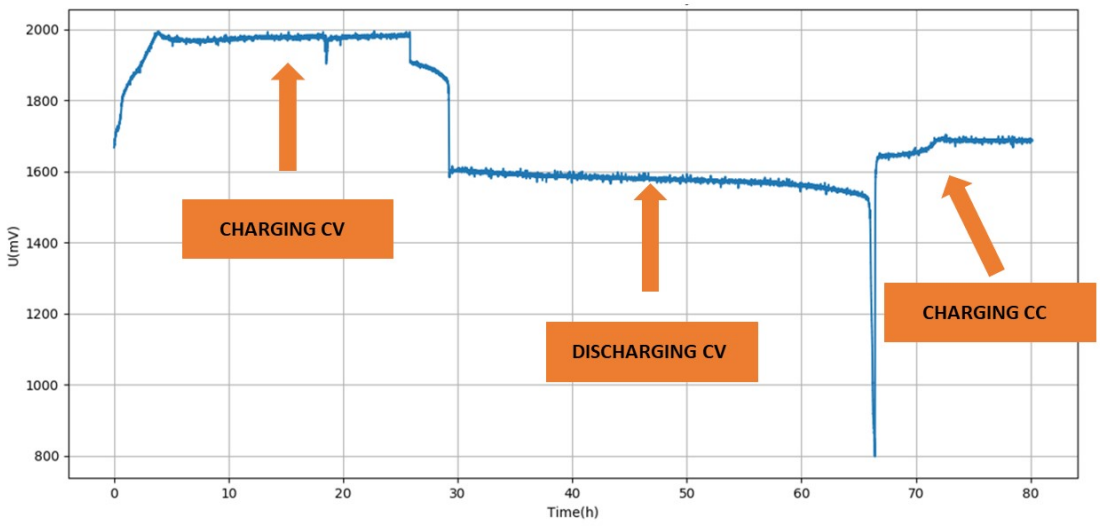

Figure IV.4: Characterization steps in a silver-zinc battery

Appendix V

Voltera Parameters

In this project, all the inks utilized in fabricating the digitally printed batteries had different physical properties. These characteristics were hard to accurately study. Nevertheless, they influenced the settings of the Voltera.

An experimental procedure was conducted, by printing several times and adjusting the parameters, until the best set was achieved (so far). This section gives a brief explanation of this matter and reveals the used settings of the Voltera printer.

The following list contains the different features that are adjustable to each ink:

- **Trim Length:** The voltera prints in line segments. This parameter corresponds to the size of the line the voltera prints in a row, without reapplying pressure. By reducing this value, the amount of ink it deposits is increased for small lines. By increasing the value, the amount of ink it deposits is reduced, making longer lines.

- **Feedrate:** Corresponds to the distance travelled per revolution. In other words, it defines the speed at which the voltera provides ink onto the substrate.

- **Kick:** This is one of the most important parameters. It controls the distance the piston travels when applying pressure at the beginning of each line. For fluids with higher viscosity, a larger kick is required, whereas, for less viscous fluids, the opposite effect takes place.

- **Soft start and soft stop ratio:** The properties of the inks and the mechanical features create a delay between the kick and when the ink starts printing a line correctly. These parameters are used to compensate for it.

- **Rheological setpoint:** This parameter controls the compensation of the printer for the flow rate over time.

- **Pass spacing:** Controls the distance between printed lines.
- **Trace penetration:** This is a parameter not very important to this work. It is used to ensure the connections between traces and pads, by controlling the distance a trace goes into a pad.
- **Anti-Stringing distance:** Certain fluids tend to be attached to the nozzle instead of the board, forming a string. In order to prevent the string to break while moving forward, the voltera travels back over the feature to break the string over it.
- **Dispense height:** Height of the piston while printing. It is adjusted during printing.

The following table shows the final parameters used to improve the printing quality for the 4 used inks:

Ink	AgGaIn	CB-SIS	Ag_2O	Ga-CB-SIS
Pass spacing	0.27	0.37	0.27	0.37
Dispense height	Adjustable	Adjustable	Adjustable	Adjustable
Feedrate	500	500	500	500
Trim length	150	150	100	100
Trace penetration	1.00	1.00	1.00	1.00
Anti-string distance	0.1	0.8	0.4	0.8
Kick	0.25	0.25	0.25	0.25
Soft start ratio	0.01	0.01	0.01	0.01
Soft stop ratio	1.00	0.05	0.05	0.05
Rehological setpoint	0.30	0.45	0.45	0.55

Table V.1: Voltera Parameters for the inks used

Appendix VI

Scanning Electron Microscopy

Scanning Electron Microscopy (SEM) is a mechanism to produce images based on the detection of different electrons that scatter throughout the sample's surface. Since electrons have a wavelength much smaller than visible light, this type of technology allows for a better resolution.

The electrons with high kinetic are produced via an electron gun and are focused with electromagnetic lenses (resourcing to electromagnetic fields). The detector is sensitive to the electrons (instead of visible light).

The different interactions result in electrons with different energy. When the beam hits the sample, some electrons are produced due to the excitation of the atoms caused by the energy of the incident electrons. They are called the **Secondary electrons**. These have lower energy and provide information on the topography of the sample. The **Backscatterd electrons** provide information on the different materials. Materials with higher atomic numbers backscatter more electrons. As such, they appear brighter on the images, whereas the rest look darker [99].

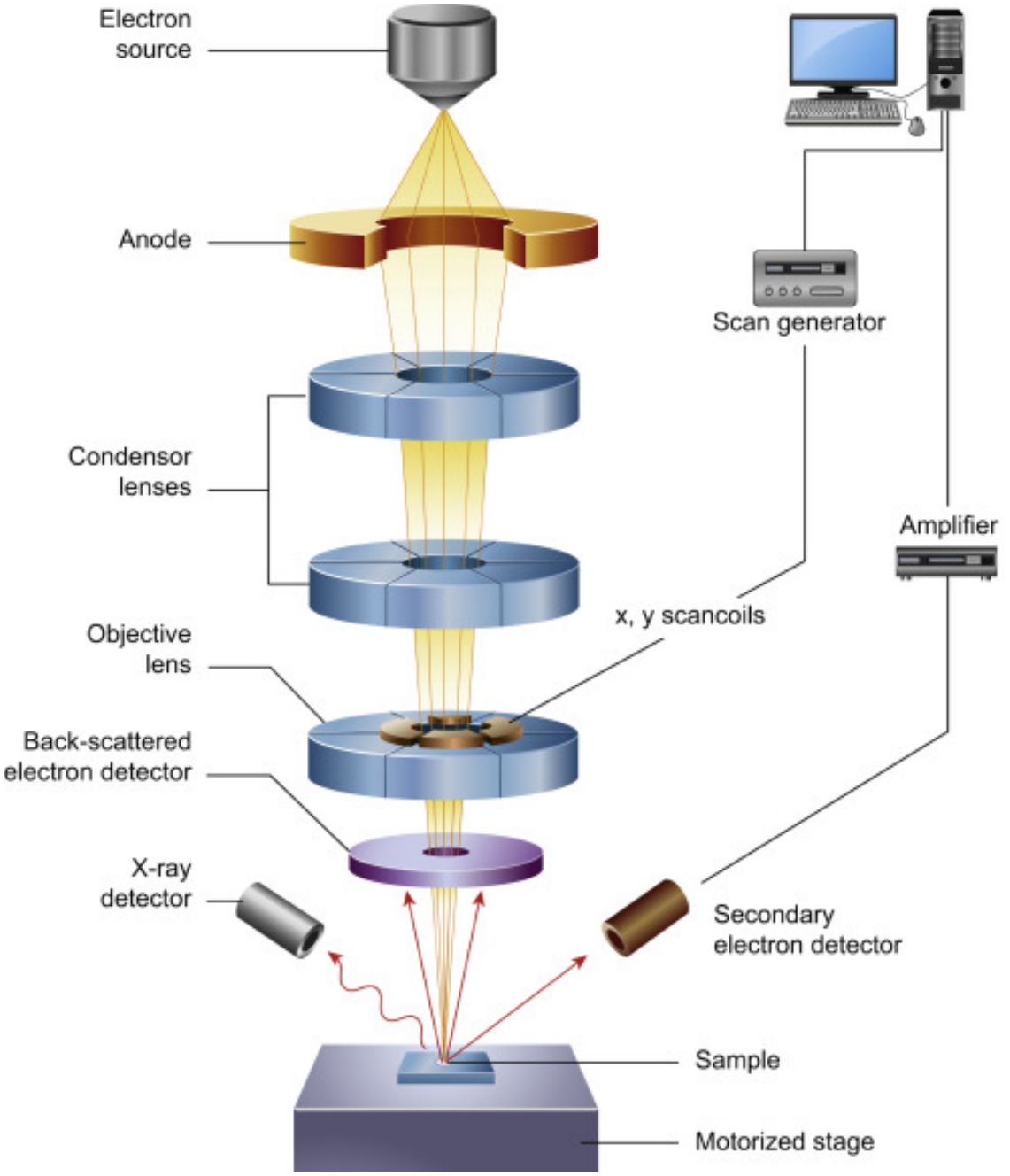

Figure VI.1: Schematic of a SEM microscope, taken from [100]

Vacuum is necessary in SEM, in order not to scatter the electrons in gas molecules.

Energy Dispersive X-Ray Spectroscopy (EDS) is used for identifying different elements in a sample. The atoms on the surface are excited and produce x-rays, that is later detected. By analyzing the wavelengths of the different beams, the materials can be identified [101] [102]. It is used to create colour and intensity maps of the different elements.

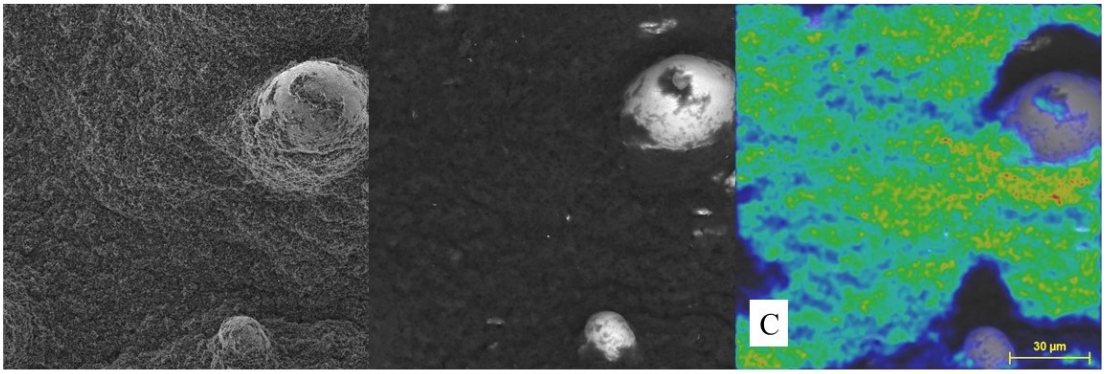

Figure VI.2: From left to right: SE image from gallium and carbon electron; BSE image from gallium and carbon electrode; EDS colour mapping of the carbon element in the same image

Appendix VII

Discharging profile of digitally printed Ag-Ga battery

Figure VII.1 presents the discharging profile of a digitally printed Ag-Ga battery, compared with a stencil printed one.

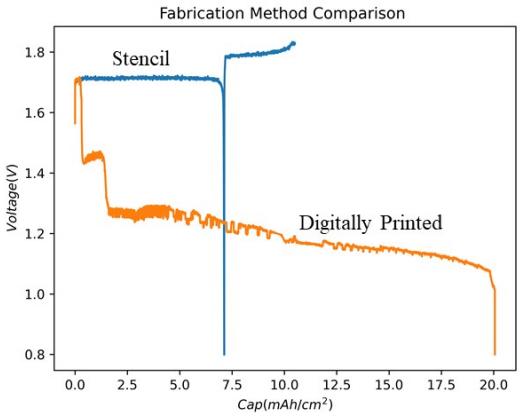

Figure VII.1: Discharging profiles of a digitally printed Ag-Ga battery and a stencil printed Ag-Ga battery.

The strange profile was noted but no justification was found at the time of this dissertation. We assume that further optimization of parameters and printing mechanism should be made.

Bibliography

[1] M Dyson and K Ghaffarzadeh. Flexible hybrid electronics 2020–2030: Applications, challenges, innovations and forecasts. *IDTechEX.[(accessed on 9 October 2020)]*, 2020.

[2] Yutong Jiang, Lulu Xu, Kewen Pan, Ting Leng, Yi Li, Laith Danoon, and Zhirun Hu. e-textile embroidered wearable near-field communication rfid antennas. *IET Microwaves, Antennas & Propagation*, 13(1):99–104, 2019.

[3] Vy Le, Ulrich Lemmer, and Elke Mackensen. Analysis of miniaturized printed flexible rfid/nfc antennas using different carrier substrates. *IEEE Journal of Radio Frequency Identification*, 4(4):428–437, 2020.

[4] Hyo-Ryoung Lim, Hee Seok Kim, Raza Qazi, Young-Tae Kwon, Jae-Woong Jeong, and Woon-Hong Yeo. Advanced soft materials, sensor integrations, and applications of wearable flexible hybrid electronics in healthcare, energy, and environment. *Advanced Materials*, 32(15):1901924, 2020.

[5] Ge Tong, Zhou Jia, and Joseph Chang. Flexible hybrid electronics: review and challenges. In *2018 IEEE International Symposium on Circuits and Systems (ISCAS)*, pages 1–5. IEEE, 2018.

[6] Dirk Schaefer and Wai M Cheung. Smart packaging: Opportunities and challenges. *Procedia CIRP*, 72:1022–1027, 2018.

[7] André F Silva, Hugo Paisana, Tânia Fernandes, Joana Góis, Arménio Serra, Jorge FJ Coelho, Aníbal T de Almeida, Carmel Majidi, and Mahmoud Tavakoli. High resolution soft and stretchable circuits with pva/liquid-metal mediated printing. *Advanced Materials Technologies*, 5(9):2000343, 2020.

[8] Sumit Majumder, Tapas Mondal, and M Jamal Deen. Wearable sensors for remote health monitoring. *Sensors*, 17(1):130, 2017.

[9] Ling Zhang, Hongjun Ji, Houbing Huang, Ning Yi, Xiaoming Shi, Senpei Xie, Yaoyin Li, Ziheng Ye, Pengdong Feng, Tiesong Lin, et al. Wearable circuits sintered at room temperature directly on the skin surface for health monitoring. *ACS Applied Materials & Interfaces*, 12(40):45504–45515, 2020.

[10] Yongseok Joseph Hong, Hyoyoung Jeong, Kyoung Won Cho, Nanshu Lu, and Dae-Hyeong Kim. Wearable and implantable devices for cardiovascular healthcare: From monitoring to therapy based on flexible and stretchable electronics. *Advanced Functional Materials*, 29(19):1808247, 2019.

[11] Yuhao Liu, Matt Pharr, and Giovanni Antonio Salvatore. Lab-on-skin: a review of flexible and stretchable electronics for wearable health monitoring. *ACS nano*, 11(10):9614–9635, 2017.

[12] Yinji Ma, Yingchao Zhang, Shisheng Cai, Zhiyuan Han, Xin Liu, Fengle Wang, Yu Cao, Zhouheng Wang, Hangfei Li, Yihao Chen, et al. Flexible hybrid electronics for digital healthcare. *Advanced Materials*, 32(15):1902062, 2020.

[13] Wei Shi, Yunlong Guo, and Yunqi Liu. When flexible organic field-effect transistors meet biomimetics: a prospective view of the internet of things. *Advanced Materials*, 32(15):1901493, 2020.

[14] André F. Silva and Mahmoud Tavakoli. Domiciliary hospitalization through wearable biomonitoring patches: Recent advances, technical challenges, and the relation to covid-19. *Sensors*, 20(23), 2020.

[15] Taewoo Ha, Jason Tran, Siyi Liu, Hongwoo Jang, Hyoyoung Jeong, Ruchika Mitbander, Heeyong Huh, Yitao Qiu, Jason Duong, Rebecca L Wang, et al. A chest-laminated ultrathin and stretchable e-tattoo for the measurement of electrocardiogram, seismocardiogram, and cardiac time intervals. *Advanced Science*, 6(14):1900290, 2019.

[16] Shiran Shustak, Lilah Inzelberg, Stanislav Steinberg, David Rand, Moshe David Pur, Inbar Hillel, Shlomit Katzav, Firas Fahoum, Maarten De Vos, Anat Mirelman, et al. Home monitoring of sleep with a temporary-tattoo eeg, eog and emg electrode array: a feasibility study. *Journal of neural engineering*, 16(2):026024, 2019.

[17] Laura M Ferrari, Sudha Sudha, Sergio Tarantino, Roberto Esposti, Francesco Bolzoni, Paolo Cavallari, Christian Cipriani, Virgilio Mattoli, and Francesco Greco. Ultraconformable temporary tattoo electrodes for electrophysiology. *Advanced Science*, 5(3):1700771, 2018.

[18] Nargess Nourbakhsh, Fang Chen, Yang Wang, and Rafael A Calvo. Detecting users' cognitive load by galvanic skin response with affective interference. *ACM Transactions on Interactive Intelligent Systems (TiiS)*, 7(3):1–20, 2017.

[19] Aleksandra Przegalinska, Leon Ciechanowski, Mikolaj Magnuski, and Peter Gloor. Muse headband: Measuring tool or a collaborative gadget? In *Collaborative Innovation Networks*, pages 93–101. Springer, 2018.

[20] Mahmoud Tavakoli, Mohammad H Malakooti, Hugo Paisana, Yunsik Ohm, Daniel Green Marques, Pedro Alhais Lopes, Ana P Piedade, Anibal T de Almeida, and Carmel Majidi. Egain-assisted room-temperature sintering of silver nanoparticles for stretchable, inkjet-printed, thin-film electronics. *Advanced Materials*, 30(29):1801852, 2018.

[21] Sacha Noimark, Richard J Colchester, Ben J Blackburn, Edward Z Zhang, Erwin J Alles, Sebastien Ourselin, Paul C Beard, Ioannis Papakonstantinou, Ivan P Parkin, and Adrien E Desjardins. Carbon-nanotube–pdms composite coatings on optical fibers for all-optical ultrasound imaging. *Advanced Functional Materials*, 26(46):8390–8396, 2016.

[22] Gerard Cummins and Marc PY Desmulliez. Inkjet printing of conductive materials: a review. *Circuit world*, 2012.

[23] James Wissman, Tong Lu, and Carmel Majidi. Soft-matter electronics with stencil lithography. In *SENSORS, 2013 IEEE*, pages 1–4. IEEE, 2013.

[24] Arya Tabatabai, Andrew Fassler, Claire Usiak, and Carmel Majidi. Liquid-phase gallium–indium alloy electronics with microcontact printing. *Langmuir*, 29(20):6194–6200, 2013.

[25] Tong Lu, Lauren Finkenauer, James Wissman, and Carmel Majidi. Rapid prototyping for soft-matter electronics. *Advanced Functional Materials*, 24(22):3351–3356, 2014.

[26] Xiaojing Su, Hongqiang Li, Xuejun Lai, Zhonghua Chen, and Xingrong Zeng. Highly stretchable and conductive superhydrophobic coating for flexible electronics. *ACS applied materials & interfaces*, 10(12):10587–10597, 2018.

[27] B Arda Gozen, Arya Tabatabai, O Burak Ozdoganlar, and Carmel Majidi. High-density soft-matter electronics with micron-scale line width. *Advanced materials*, 26(30):5211–5216, 2014.

[28] William Taube Navaraj, Carlos García Núñez, Dhayalan Shakthivel, Vincenzo Vinciguerra, Fabrice Labeau, Duncan H Gregory, and Ravinder Dahiya. Nanowire fet based neural element for robotic tactile sensing skin. *Frontiers in neuroscience*, 11:501, 2017.

[29] Ting Wang, Yunlong Guo, Pengbo Wan, Han Zhang, Xiaodong Chen, and Xiaoming Sun. Flexible transparent electronic gas sensors. *Small*, 12(28):3748–3756, 2016.

[30] Wenting Dang, Libu Manjakkal, William Taube Navaraj, Leandro Lorenzelli, Vincenzo Vinciguerra, and Ravinder Dahiya. Stretchable wireless system for sweat ph monitoring. *Biosensors and Bioelectronics*, 107:192–202, 2018.

[31] Benjamin Shih, Dylan Shah, Jinxing Li, Thomas G Thuruthel, Yong-Lae Park, Fumiya Iida, Zhenan Bao, Rebecca Kramer-Bottiglio, and Michael T Tolley. Electronic skins and machine learning for intelligent soft robots. *Science Robotics*, 5(41), 2020.

[32] Alla M Zamarayeva, Aminy E Ostfeld, Michael Wang, Jerica K Duey, Igal Deckman, Balthazar P Lechêne, Greg Davies, Daniel A Steingart, and Ana Claudia Arias. Flexible and stretchable power sources for wearable electronics. *Science advances*, 3(6):e1602051, 2017.

[33] Woo-Jin Song, Minsik Kong, Sunghwan Cho, Sangyeop Lee, Jimin Kwon, Hye Bin Son, Jun Hyuk Song, Dong-Gue Lee, Gyujin Song, Sang-Young Lee, et al. Stand-alone intrinsically stretchable electronic device platform powered by stretchable rechargeable battery. *Advanced Functional Materials*, 30(50):2003608, 2020.

[34] Wei Liu, Zheng Chen, Guangmin Zhou, Yongming Sun, Hye Ryoung Lee, Chong Liu, Hongbin Yao, Zhenan Bao, and Yi Cui. 3d porous sponge-inspired electrode for stretchable lithium-ion batteries. *Advanced materials*, 28(18):3578–3583, 2016.

[35] Alla M Zamarayeva, Abhinav M Gaikwad, Igal Deckman, Michael Wang, Brian Khau, Daniel A Steingart, and Ana Claudia Arias. Fabrication of a high-performance flexible silver–zinc wire battery. *Advanced Electronic Materials*, 2(5):1500296, 2016.

[36] Robert Kay and Marc Desmulliez. A review of stencil printing for microelectronic packaging. *Soldering & Surface Mount Technology*, 2012.

[37] Y Zheng, Z An, P Smyrek, HJ Seifert, T Kunze, V Lang, A-F Lasagni, and W Pfleging. Direct laser interference patterning and ultrafast laser-induced micro/nano structuring of current collectors for lithium-ion batteries. In *Laser-based Micro-and Nanoprocessing X*, volume 9736, page 97361B. International Society for Optics and Photonics, 2016.

[38] Lakshman K Ventrapragada, Stephen E Creager, Apparao M Rao, and Ramakrishna Podila. Carbon nanotubes coated paper as current collectors for secondary li-ion batteries. *Nanotechnology Reviews*, 8(1):18–23, 2019.

[39] Christine C Ho, Kazuhiro Murata, Daniel A Steingart, James W Evans, and Paul K Wright. A super ink jet printed zinc–silver 3d microbattery. *Journal of Micromechanics and Microengineering*, 19(9):094013, 2009.

[40] Hanwen Liu, Yuqin Zou, Li Tao, Zhaoling Ma, Dongdong Liu, Peng Zhou, Hongbo Liu, and Shuangyin Wang. Sandwiched thin-film anode of chemically bonded black phosphorus/graphene hybrid for lithium-ion battery. *Small*, 13(33):1700758, 2017.

[41] Jae Myeong Lee, Changsoon Choi, Ji Hwan Kim, Mônica Jung de Andrade, Ray H Baughman, and Seon Jeong Kim. Biscrolled carbon nanotube yarn structured silver-zinc battery. *Scientific reports*, 8(1):1–8, 2018.

[42] Chaowei Li, Qichong Zhang, E Songfeng, Taotao Li, Zezhou Zhu, Bing He, Zhenyu Zhou, Ping Man, Qiulong Li, and Yagang Yao. An ultra-high endurance and high-performance quasi-solid-state fiber-shaped zn–ag 2 o battery to harvest wind energy. *Journal of Materials Chemistry A*, 7(5):2034–2040, 2019.

[43] Cristina Leal, Pedro Alhais Lopes, Arménio Serra, Jorge FJ Coelho, Aníbal T de Almeida, and Mahmoud Tavakoli. Untethered disposable health monitoring electronic patches with an integrated ag2o–zn battery, a aginga current collector, and hydrogel electrodes. *ACS applied materials & interfaces*, 12(3):3407–3414, 2019.

[44] Zari Tehrani, Tatyana Korochkina, S Govindarajan, DJ Thomas, J O'Mahony, Jeffrey Kettle, TC Claypole, and DT Gethin. Ultra-thin flexible screen printed rechargeable polymer battery for wearable electronic applications. *Organic Electronics*, 26:386–394, 2015.

[45] Andreas Willert, Carmen Meuser, and Reinhard R Baumann. Printed batteries and conductive patterns in technical textiles. *Japanese Journal of Applied Physics*, 57(5S):05GB02, 2018.

[46] M Hilder, B Winther-Jensen, and NB Clark. based, printed zinc–air battery. *Journal of power Sources*, 194(2):1135–1141, 2009.

[47] José Alberto, Cristina Leal, Cláudio Fernandes, Pedro A Lopes, Hugo Paisana, Aníbal T de Almeida, and Mahmoud Tavakoli. Fully untethered battery-free biomonitoring electronic tattoo with wireless energy harvesting. *Scientific reports*, 10(1):1–11, 2020.

[48] Rui Pedro Rocha, Pedro Alhais Lopes, Anibal T De Almeida, Mahmoud Tavakoli, and Carmel Majidi. Fabrication and characterization of bending and pressure sensors for a soft prosthetic hand. *Journal of Micromechanics and Microengineering*, 28(3):034001, 2018.

[49] J Yoon, Y Joo, B Lee, E Oh, H Cho, and Y Hong. Stretchable active-matrix light-emitting diode array using printed electric components on plastic and elastomer hybrid substrate. In *Digest of Technical Papers-SID International Symposium*, volume 49, pages 1925–1927, 2018.

[50] Hossein Ahmadi, Goli Arji, Leila Shahmoradi, Reza Safdari, Mehrbakhsh Nilashi, and Mojtaba Alizadeh. The application of internet of things in healthcare: a systematic literature review and classification. *Universal Access in the Information Society*, 18(4):837–869, 2019.

[51] Kalliopi Megari. Quality of life in chronic disease patients. *Health psychology research*, 1(3), 2013.

[52] Siba Kumar Udgata and Nagender Kumar Suryadevara. Covid-19, sensors, and internet of medical things (iomt). In *Internet of Things and Sensor Network for COVID-19*, pages 39–53. Springer, 2021.

[53] Tran Quang Trung and Nae-Eung Lee. Flexible and stretchable physical sensor integrated platforms for wearable human-activity monitoringand personal healthcare. *Advanced materials*, 28(22):4338–4372, 2016.

[54] Manuel Reis Carneiro, Aníbal T de Almeida, and Mahmoud Tavakoli. Wearable and comfortable e-textile headband for long-term acquisition of forehead eeg signals. *IEEE Sensors Journal*, 20(24):15107–15116, 2020.

[55] Pedro Alhais Lopes, Daniel Félix Fernandes, André F Silva, Daniel Green Marques, Aníbal T de Almeida, Carmel Majidi, and Mahmoud Tavakoli. Bi-phasic ag–in–ga-embedded elastomer inks for digitally printed, ultra-stretchable, multi-layer electronics. *ACS Applied Materials & Interfaces*, 13(12):14552–14561, 2021.

[56] Yong-Lae Park, Carmel Majidi, Rebecca Kramer, Phillipe Bérard, and Robert J Wood. Hyperelastic pressure sensing with a liquid-embedded elastomer. *Journal of micromechanics and microengineering*, 20(12):125029, 2010.

[57] Joseph T Muth, Daniel M Vogt, Ryan L Truby, Yiğit Mengüç, David B Kolesky, Robert J Wood, and Jennifer A Lewis. Embedded 3d printing of strain sensors within highly stretchable elastomers. *Advanced materials*, 26(36):6307–6312, 2014.

[58] Marc P Wolf, Georgette B Salieb-Beugelaar, and Patrick Hunziker. Pdms with designer functionalities properties, modifications strategies, and applications. *Progress in Polymer Science*, 83:97–134, 2018.

[59] Konstantin S Novoselov, VI Fal, L Colombo, PR Gellert, MG Schwab, K Kim, et al. A roadmap for graphene. *nature*, 490(7419):192–200, 2012.

[60] Jonathan K Wassei and Richard B Kaner. Graphene, a promising transparent conductor. *Materials today*, 13(3):52–59, 2010.

[61] Xu-Zhou Jiang, Yi-Jing Sun, Zhiyong Fan, and Tong-Yi Zhang. Integrated flexible, waterproof, transparent, and self-powered tactile sensing panel. *ACS nano*, 10(8):7696–7704, 2016.

[62] Mason Zadan, Mohammad H Malakooti, and Carmel Majidi. Soft and stretchable thermoelectric generators enabled by liquid metal elastomer composites. *ACS applied materials & interfaces*, 12(15):17921–17928, 2020.

[63] Amay J Bandodkar, Jung-Min You, Nam-Heon Kim, Yue Gu, Rajan Kumar, AM Vinu Mohan, Jonas Kurniawan, Somayeh Imani, Tatsuo Nakagawa, Brianna Parish, et al. Soft, stretchable, high power density electronic skin-based biofuel cells for scavenging energy from human sweat. *Energy & Environmental Science*, 10(7):1581–1589, 2017.

[64] Xing Chen and Lin Zhou. A metamaterial electromagnetic energy rectifying surface with high harvesting efficiency. *AIP Advances*, 6(12):125020, 2016.

[65] Darren J Lipomi and Zhenan Bao. Stretchable, elastic materials and devices for solar energy conversion. *Energy & Environmental Science*, 4(9):3314–3328, 2011.

[66] Xiangchuan Meng, Zhi Xing, Xiaotian Hu, Zengqi Huang, Ting Hu, Licheng Tan, Fengyu Li, and Yiwang Chen. Stretchable perovskite solar cells with recoverable performance. *Angewandte Chemie International Edition*, 59(38):16602–16608, 2020.

[67] Nannan Wu, Xue Bai, Duo Pan, Binbin Dong, Renbo Wei, Nithesh Naik, Rahul Rangrao Patil, and Zhanhu Guo. Recent advances of asymmetric supercapacitors. *Advanced Materials Interfaces*, 8(1):2001710, 2021.

[68] Jingyuan Zhao and Andrew F Burke. Review on supercapacitors: Technologies and performance evaluation. *J. Energy Chem*, 59:276–291, 2021.

[69] Syeda Wishal Bokhari, Ahmad Hassan Siddique, Peter C Sherrell, Xiaoyu Yue, Kariappa Maletira Karumbaiah, Shanghai Wei, Amanda V Ellis, and Wei Gao. Advances in graphene-based supercapacitor electrodes. *Energy Reports*, 6:2768–2784, 2020.

[70] Goli Nagaraju, S Chandra Sekhar, L Krishna Bharat, and Jae Su Yu. Wearable fabrics with self-branched bimetallic layered double hydroxide coaxial nanostructures for hybrid supercapacitors. *ACS nano*, 11(11):10860–10874, 2017.

[71] H Qiao and Q Wei. Functional nanofibers in lithium-ion batteries. In *Functional Nanofibers and their Applications*, pages 197–208. Elsevier, 2012.

[72] Chenxuan Xu, Yu Zhang, Naiqing Zhang, Xiaoyu Liu, Jin Yi, Xiaoqing Liu, Xihong Lu, Qiang Ru, Hao Lu, Xinwen Peng, et al. 2020 roadmap on zinc metal batteries. *Chemistry–An Asian Journal*, 15(22):3696–3708, 2020.

[73] Wenjin Yang, Xianghua Zhang, Huiteng Tan, Dan Yang, Yuezhan Feng, Xianhong Rui, and Yan Yu. Gallium-based anodes for alkali metal ion batteries. *Journal of Energy Chemistry*, 55:557–571, 2021.

[74] Yunyun Wu, Sara S Mechael, Yiting Chen, and Tricia Breen Carmichael. Velour fabric as an island-bridge architectural design for stretchable textile-based lithium-ion battery electrodes. *ACS Applied Materials & Interfaces*, 12(46):51679–51687, 2020.

[75] Keyu Xie and Bingqing Wei. Materials and structures for stretchable energy storage and conversion devices. *Advanced Materials*, 26(22):3592–3617, 2014.

[76] Pedro Alhais Lopes, Hugo Paisana, Anibal T De Almeida, Carmel Majidi, and Mahmoud Tavakoli. Hydroprinted electronics: ultrathin stretchable ag–in–ga e-skin for bioelectronics and human–machine interaction. *ACS applied materials & interfaces*, 10(45):38760–38768, 2018.

[77] Pedro Alhais Lopes, Davide Vaz Gomes, Daniel Green Marques, Pedro Faia, Joana Góis, Tatiana F Patrício, Jorge Coelho, Arménio Serra, Aníbal T de Almeida, Carmel Majidi, et al. Soft bioelectronic stickers: selection and evaluation of skin-interfacing electrodes. *Advanced healthcare materials*, 8(15):1900234, 2019.

[78] Alain Mauger and CM Julien. Critical review on lithium-ion batteries: are they safe? sustainable? *Ionics*, 23(8):1933–1947, 2017.

[79] Kyle Theunis Braam. *Development of an air-stable, high energy density printed silver oxide battery for printed electronics*. University of California, Berkeley, 2014.

[80] Michael J Smith and Fiona M Gray. Batteries, from cradle to grave. *Journal of Chemical Education*, 87(2):162–167, 2010.

[81] Rajan Kumar, Jaewook Shin, Lu Yin, Jung-Min You, Ying Shirley Meng, and Joseph Wang. All-printed, stretchable zn-ag2o rechargeable battery via hyperelastic binder for self-powering wearable electronics. *Advanced Energy Materials*, 7(8):1602096, 2017.

[82] Wolfgang Glaeser. Alkaline batteries containing a zinc powder with indium and bismuth, August 31 1993. US Patent 5,240,793.

[83] Myoungsoo Shin, Woo-Jin Song, Hye Bin Son, Seungmin Yoo, Sungho Kim, Gyujin Song, Nam-Soon Choi, and Soojin Park. Highly stretchable separator membrane for deformable energy-storage devices. *Advanced Energy Materials*, 8(23):1801025, 2018.

[84] Jonathan Scharf, Lu Yin, Christopher Redquest, Ruixiao Liu, Xueying L Quinn, Jeff Ortega, Xia Wei, Joseph Wang, Jean-Marie Doux, and Ying Shirley Meng. Investigating degradation modes in zn-ago aqueous batteries with in situ x-ray micro computed tomography. *Advanced Energy Materials*, page 2101327, 2021.

[85] Yingpeng Wu, Lu Huang, Xingkang Huang, Xiaoru Guo, Dan Liu, Dong Zheng, Xuelin Zhang, Ren Ren, Deyang Qu, and Junhong Chen. A room-temperature liquid metal-based self-healing anode for lithium-ion batteries with an ultra-long cycle life. *Energy & Environmental Science*, 10(8):1854–1861, 2017.

[86] Xuelin Guo, Yu Ding, Leigang Xue, Leyuan Zhang, Changkun Zhang, John B Goodenough, and Guihua Yu. A self-healing room-temperature liquid-metal anode for alkali-ion batteries. *Advanced Functional Materials*, 28(46):1804649, 2018.

[87] Takashi Onoue, Kiyoshi Araki, Noriya Ishida, Toshiya Kitamura, Yasuhiko Niitsu, Makiko Yanagisawa, Ryo Sakamoto, and Fumihiro Sato. Gallium based active material for the negative electrode, a negative electrode using the same, and batteries using said negative electrode, October 31 1995. US Patent 5,462,821.

[88] Qingfeng Zhai, Fuwei Xiang, Fang Cheng, Yongjiang Sun, Xiaoping Yang, Wen Lu, and Liming Dai. Recent advances in flexible/stretchable batteries and integrated devices. *Energy Storage Materials*, 33:116–138, 2020.

[89] Dongye Liu, Laisuo Su, Jiahe Liao, B Reeja-Jayan, and Carmel Majidi. Rechargeable soft-matter egain-mno2 battery for stretchable electronics. *Advanced Energy Materials*, 9(46):1902798, 2019.

[90] Guicheng Liu, Ji Young Kim, Manxiang Wang, Jae-Young Woo, Lei Wang, Dechun Zou, and Joong Kee Lee. Soft, highly elastic, and discharge-current-controllable eutectic gallium–indium liquid metal–air battery operated at room temperature. *Advanced Energy Materials*, 8(16):1703652, 2018.

[91] Daniel Félix Fernandes, Carmel Majidi, and Mahmoud Tavakoli. Digitally printed stretchable electronics: A review. *Journal of Materials Chemistry C*, 7(45):14035–14068, 2019.

[92] Yi Zheng, Zhi-Zhu He, Jun Yang, and Jing Liu. Personal electronics printing via tapping mode composite liquid metal ink delivery and adhesion mechanism. *Scientific reports*, 4(1):1–8, 2014.

[93] Michael J Ford, Dinesh K Patel, Chengfeng Pan, Sarah Bergbreiter, and Carmel Majidi. Controlled assembly of liquid metal inclusions as a general approach for multifunctional composites. *Advanced Materials*, 32(46):2002929, 2020.

[94] Alexandre Chambel, Afsaneh L. Sanati, Pedro Alhais Lopes, Timur Nikitin, Rui Fausto, Aníbal T. de Almeida, and Mahmoud Tavakoli. Laser writing of eutectic gallium–indium alloy graphene-oxide electrodes and semitransparent conductors. *Advanced Materials Technologies*, n/a(n/a):2101238.

[95] Javishk Shah, Paul Ratnasamy, and Maria L Carreon. Influence of the nanostructure of gallium oxide catalysts on conversion in the green synthesis of carbamates. *Catalysts*, 7(12):372, 2017.

[96] T. Hurlen. Anodic dissolution of liquid gallium in alkaline solutions. *Electrochimica Acta*, 9(11):1449–1452, 1964.

[97] Yao C Hsieh, Su P Chou, and Chin S Moo. Balance discharging for series-connected batteries. In *2004 IEEE 35th Annual Power Electronics Specialists Conference (IEEE Cat. No. 04CH37551)*, volume 4, pages 2697–2702. IEEE, 2004.

[98] Thomas Dobbelaere, Philippe M Vereecken, and Christophe Detavernier. A usb-controlled potentiostat/galvanostat for thin-film battery characterization. *HardwareX*, 2:34–49, 2017.

[99] KD Vernon-Parry. Scanning electron microscopy: an introduction. *III-Vs Review*, 13(4):40–44, 2000.

[100] BJ Inkson. Scanning electron microscopy (sem) and transmission electron microscopy (tem) for materials characterization. In *Materials characterization using nondestructive evaluation (NDE) methods*, pages 17–43. Elsevier, 2016.

[101] Daisuke Shindo and Tetsuo Oikawa. Energy dispersive x-ray spectroscopy. In *Analytical electron microscopy for materials science*, pages 81–102. Springer, 2002.

[102] Leslie J Allen, Adrian J DÁlfonso, Bert Freitag, and Dmitri O Klenov. Chemical mapping at atomic resolution using energy-dispersive x-ray spectroscopy. *MRS bulletin*, 37(1):47–52, 2012.